Dissertation

submitted to the

Combined Faculty of Natural Sciences and Mathematics

of the Ruperto Carola University Heidelberg, Germany

for the degree of

Doctor of Natural Sciences

Presented by

Taishi Kanamaru, M.Sc.

Born in: Kanagawa, Japan

Oral examination: 27 July 2021

Balancing the distal tip length of primary cilia is essential for keeping their signaling function in mammalian cells

Referees: Prof. Dr. Gislene Pereira

Prof. Dr. Michael Knop

Summary

Sensing signals from the extracellular environment is one of the most important and fundamental biological processes. Primary cilia are highly conserved antenna-like organelles, which are perceiving chemical and biological molecules for signal transduction. Primary cilia are required for several signalling pathways such as Sonic hedgehog (Shh), Wnt, and mTOR. Thus, defective mutations of cilia component affect signal transduction, causing severe body developmental errors that are categorized as genetic diseases called ciliopathies. Previous studies have shown that abnormally extended primary cilia in ciliopathy patient cells result in lower signalling response. That is why, controlling the cilia length is essential for maintaining their signalling function, but this mechanism is still not completely understood yet.

In my PhD study, I would like to propose one of the reasons why over-elongated cilia in mammalian cells drop the ability of signal transduction. I observed that the middle/distal cilia segmentation is conserved in mammalian cells as the same as the lower eukaryotes. It is known that the middle segment stabilizes cilia structure and the distal segment contributes as the ciliary signalling scaffold. After the small-scale loss of function screening, I have identified Septin as a negative regulator of the distal segment growth. Septin is a fibre-like protein localizing at cilia to regulate the formation of the transition zone, which is a protein complex at the base of cilia passing the cilia-building blocks to cilia selectively like a gatekeeper. A functional transition zone allows transferring a ciliary capping kinesin KIF7 at the cilia tip to suppress the distal segment growth. Moreover, over-elongated distal segment lost the ability of constant cilia length maintenance that leads to a high incidence of cilia excision. The cilia excision event reduces the amount of intermediate Shh pathway factors such as Sufu and Glis at the distal cilia tip. Therefore, cells with over-elongated distal segments fail to upregulate Shh signal transduction.

Finally, I strongly believe that this study opens up the cilia field by elucidating the link between primary cilia segmentation and signalling function in mammalian models.

Zusammenfassung

Die Wahrnehmung von Signalen aus der extrazellulären Umgebung ist einer der wichtigsten und grundlegendsten biologischen Prozesse. Primärzilien sind hochkonservierte antennenartige Organellen, die chemische und biologische Moleküle zur Signaltransduktion wahrnehmen. Primäre Zilien sind für verschiedene Signalwege wie Sonic hedgehog (Shh), Wnt und mTOR erforderlich. Daher beeinträchtigen defekte Mutationen der Zilienkomponente die Signaltransduktion und verursachen schwere Fehler in der Körperentwicklung, die als genetische Krankheiten, die sogenannten Ziliopathien, kategorisiert werden. Frühere Studien haben gezeigt, dass abnorm verlängerte primäre Zilien in Zellen von Ziliopathie-Patienten zu einer geringeren Signalantwort führen. Deshalb ist die Kontrolle der Zilienlänge essentiell für die Aufrechterhaltung ihrer Signalfunktion, aber dieser Mechanismus ist noch nicht vollständig verstanden.

In meiner PhD-Studie möchte ich einen der Gründe vorschlagen, warum überlange Zilien in Säugetierzellen die Fähigkeit zur Signaltransduktion verringern. Ich habe beobachtet, dass die mittlere/distale Ziliensegmentierung in Säugetierzellen genauso konserviert ist wie bei den niederen Eukaryonten. Es ist bekannt, dass das mittlere Segment die Zilienstruktur stabilisiert und das distale Segment als Signalgerüst für die Zilien dient. Nach dem Screening auf Funktionsverlust im kleinen Maßstab habe ich Septin als negativen Regulator des Wachstums des distalen Segments identifiziert. Septin ist ein faserartiges Protein, das an Zilien lokalisiert ist, um die Bildung der Übergangszone zu regulieren. Die Übergangszone ist ein Proteinkomplex an der Basis der Zilien, der wie ein Pförtner die Zilienbausteine selektiv an die Zilien weitergibt. Eine funktionelle Übergangszone ermöglicht die Übertragung eines ciliären Capping-Kinesins KIF7 an der Cilienspitze, um das Wachstum des distalen Segments zu unterdrücken. Darüber hinaus verliert das distale Segment, wenn es überdehnt ist, die Fähigkeit die Zilienlänge konstant zu halten, was zu einer hohen Inzidenz von Zilienexzision führt. Das Ereignis der Zilienexzision reduziert die Menge der intermediären Shh-Weg-Faktoren wie Sufu und Glis an der distalen Zilienspitze. Daher können Zellen mit überdehnten distalen Segmenten die Shh-Signaltransduktion nicht hochregulieren.

Abschließend bin ich der festen Überzeugung, dass diese Studie das Zilienfeld öffnet, indem sie die Verbindung zwischen Ziliensegmentierung und Signalfunktion in Säugetiermodellen aufklärt.

Table of Contents

1. Introduction

1.1 Cilia

"*Ta Panta Rhei*" words from Heraclitus, who is a philosopher in ancient Greece, mean that everything is changing in nature. The extracellular environment is also always changing thus cells have to sense and react to tons of different kinds of signals for survival such as temperature, pressure, brightness, wavelength, fluid, humidity, chemicals, biological molecules, etc. Cilia are one of the specialized organelles that perceive fluid movement and chemical/biological molecules.

Cilia are antenna-like organelles that are generated at the mother centriole of the centrosome, a microtubule-organizing center, and are mainly composed of microtubules, lipids and ciliary proteins (Ishikawa and Marshall 2011; Peter Satir and Christensen 2007). Interestingly, this bio-antenna organelle is observed in a wide range of eukaryotes from Chlamydomonas to human and both structure and function are highly conserved. It is known that cilia are divided into two types: motile cilia and primary cilia (Figure. 1).

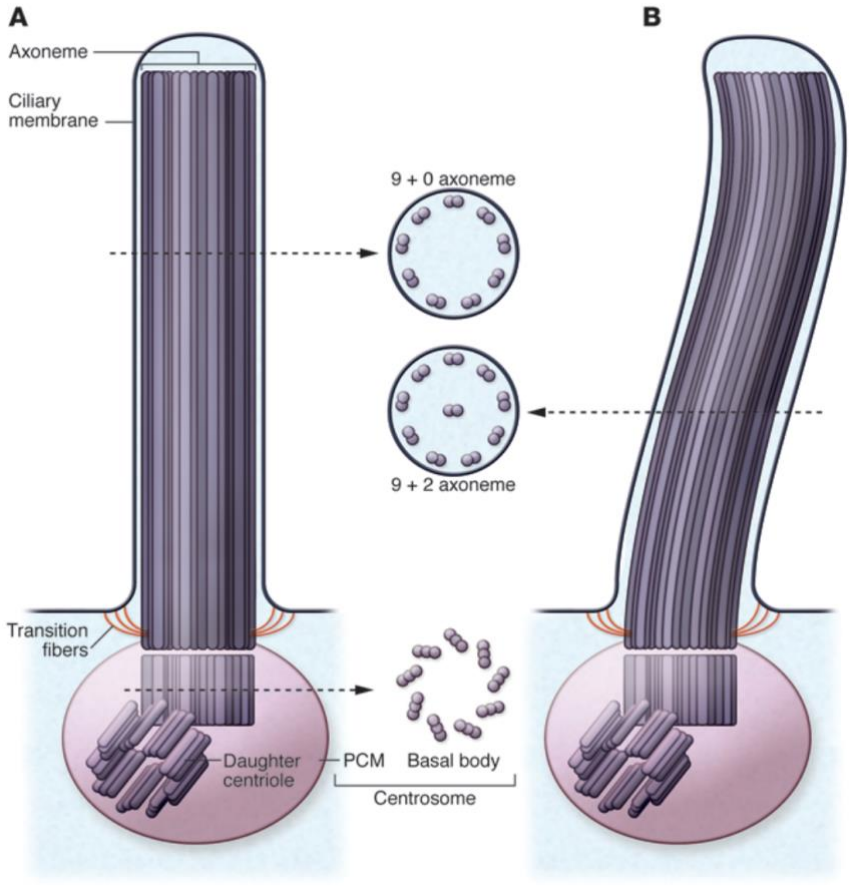

Figure. 1: Primary and motile cilia.

A. The model image of primary cilia. The structure is very similar to motile cilia, but primary cilia lose the central microtubule domain (9 + 0) thus they are unable to move by themselves. **B.** The model of motile cilia. Their microtubule structure highly resembles flagella and sperm tail (9 + 2), therefore they can move and produce locomotion. This figure is adapted from (Saudou 2012).

1.1.1 Motile cilia

Motile cilia are able to move by themselves, producing locomotion, and cells can generate both single to multiple motile cilia (Peter Satir 2017). Motile cilia possess the same axonemal microtubule structure (9+2) thus they have an ability to move by themselves (Figure. 2B). They are mostly observed on epithelial cells in mammals, where they function to sweep small particles from the surface and control the extracellular fluid flowing via their movement ability (Peter Satir 2017; Saudou 2012). The other role of motile cilia, they can sense sodium ions using an epithelial sodium channel (Nachury 2014; Peter Satir and Christensen 2007).

1.1.2 Primary cilia

On the other hand, Primary cilia are generated singularly within cells and extend from the cell surface, exposed to the extracellular environment. The structure is similar to a flagellar in Chlamydomonas and to a sperm tail. However, primary cilia lack the central pair of microtubules as indicated by their so-called 9 + 0 structure, thus they cannot produce moving forces (Gluenz et al. 2010; Sánchez and Dynlacht 2016) (Figure. 1A). Of course, their role does not consist of only drifting through the extracellular environment like a willow; primary cilia can perceive chemical and biological molecules as ligands and transduce these signals into cells.

It is widely acknowledged that almost all multi-cellular organisms are capable of generating primary cilia and also that both the structure and function of primary cilia is highly conserved from worm to human (Blacque et al. 2006; Lee, Chung, and Doo Chung 2015; Mukhopadhyay et al. 2008; Overgaard et al. 2009; Rupik 2013) (Figure. 2). Mammalian primary cilia are observed in many different parts of the body such as eyes, kidneys, neurons, osteoblasts, chondrocytes, and fibroblasts. Moreover, whilst the length of primary cilia is strictly regulated, the average length of cilia differs between tissues (Besschetnova et al. 2010; Kurtulmus et al. 2018; Miyoshi et al. 2014; Qiu et al. 2012; Wann and Knight 2012) (Table. 1).

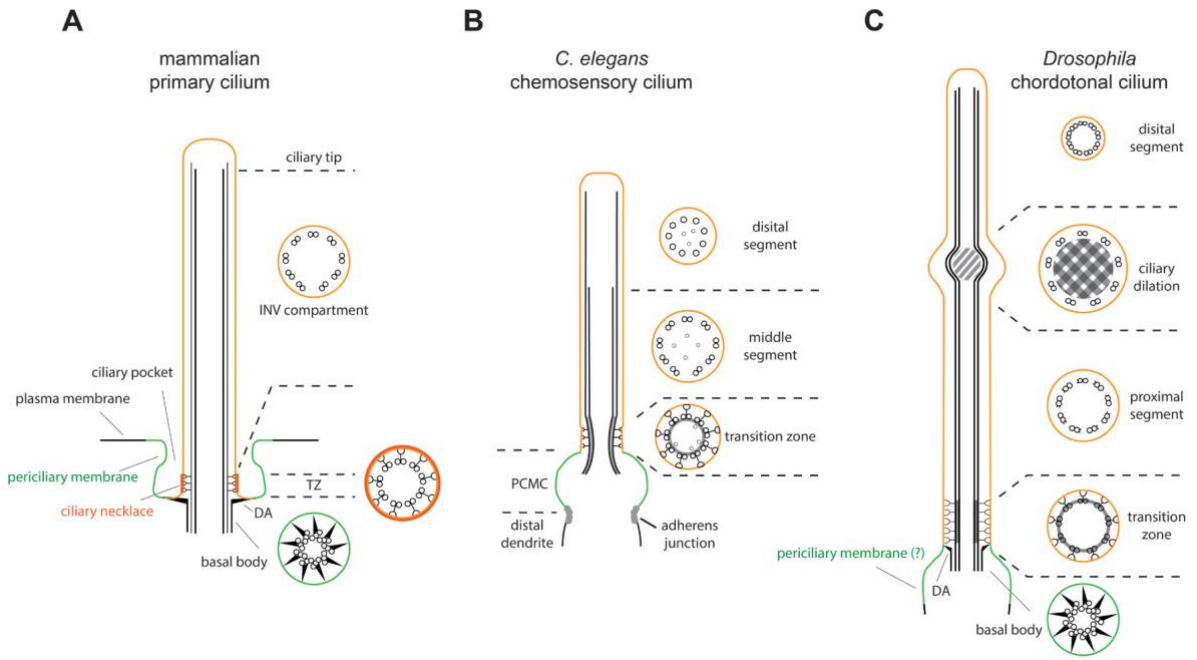

Figure. 2: The structurally similarities of primary cilia between a wide range of animals. Model images represent the overview structure of **A.** mammalian primary cilium, **B.** worm chemosensory cilium and **C.** fly chordotonal cilium. The picture is adapted from (Lee, Chung, and Doo Chung 2015).

Cell type	Average cilia length (μm)
Retinal epithelial cells	3
Kidney epithelial cells	4-5
Neurons	9
Osteoblasts	3-4
Chondrocytes	2
Fibroblasts	3

Table. 1: Average length of cilia in different mammalian tissues. Data is adapted from (Besschetnova et al. 2010; Kurtulmus et al. 2018; Miyoshi et al. 2014; Qiu et al. 2012; Wann and Knight 2012).

1.2 The structure of primary cilia

Primary cilia are multi-organized organelles, constructed from more than 100 different proteins and can be briefly categorized into five parts: Basal body, Transition zone, Axoneme, Intraflagellar transport (IFT) and Ciliary tip (S. Kim and Dynlacht 2013; Pedersen and Akhmanova 2014; P. Satir, Pedersen, and Christensen 2010; Peter Satir and Christensen 2007; Xiaoyu Shi et al. 2017). Here, I introduce the structure of primary cilia in each domain.

1.2.1 Basal body

The basal body is the proximal domain of primary cilia. Structurally speaking, there is no difference between the basal body and the matured mother centriole, but people in the cilia field call this the basal body instead of the mother centriole. The basal body is composed of 9-triplet microtubules that are named A-, B- and C-tubules, from the center to the distal respectively (S. Kim and Dynlacht 2013) (Figure. 5B iii). C-tubules extend to the end of basal body only, whilst the other A- and B-tubules elongate further to become axonemal microtubules. The basal body has two important domains: distal appendages (DA) and subdistal appendages (SDA) that contribute respectively to the initiation and growth of the ciliary axoneme and to the binding of microtubule fibers to aid the delivery of ciliary cargos (Sánchez and Dynlacht 2016; Tateishi et al. 2013).

The DA is a protein complex that is generated at the distal end of the mother centriole and plays an important role in the initiation of primary ciliogenesis (Ishikawa and Marshall 2011; Sánchez and Dynlacht 2016) (Figure. 3). Five proteins are identified as main DA components: CEP83, SCLT1, CEP123 (CEP89), CEP164 and FBF1(Bowler et al. 2019; Kurtulmus et al. 2018; Sánchez and Dynlacht 2016; Tanos et al. 2013). Those proteins are strictly organized, hence losing the innermost DA protein CEP83 leads to the loss of all other four factors from the DA. However, losing CEP164 or CEP123 shows no effect to the localization of CEP83 and SCLT1 from the DA (Tanos et al. 2013). A recent study identifies LRRC45 as another DA protein, positioned between SCLT1 and FBF1 (Kurtulmus et al. 2018). Intact DAs are required for docking of the ciliary cargo at the distal end of the basal body in primary cilia generation. Therefore, impaired DA show a severe phenotype of ciliogenesis failure (Kurtulmus et al. 2018; Tanos et al. 2013). Interestingly, the strength of this phenotype does not always reflect the hierarchy of DA. For instance, upon disruption of CEP83 or FBF1 there is an almost 100% loss of primary cilia (Tanos et al. 2013). This implies that the DA is constructed in a stepwise manner following the hierarchy, but all proteins are necessary for its function (Sánchez and Dynlacht 2016; Tanos et al. 2013).

The SDA is another protein complex, located at the side of basal body under the DA (Figure. 3). Different from the role of the DA, the SDA is needed as a microtubule linker. The SDA is also hierarchically built as the DA and the core unit of the SDA is ODF2 (Figure. 3) (Tateishi et al. 2013). ODF2 is localized at the surface of the basal body to coordinate CCDC68, CCDC120, and TCHP recruitment. CCDC120 and TCHP then recruit Ninein (Figure. 3) (Huang et al. 2017). Finally, CCDC68, 120, and Ninein aid assembly of the outermost component, CEP170 (Figure. 3). Different from the DA, SDA disruption does not show a

serious problem in ciliogenesis. However, study of mouse testis epithelial cells shows that ODF2 mutants affect primary ciliogenesis and DA formation due to the requirement of its N/C-terminus structure for recruitment of DA proteins (Tateishi et al. 2013).

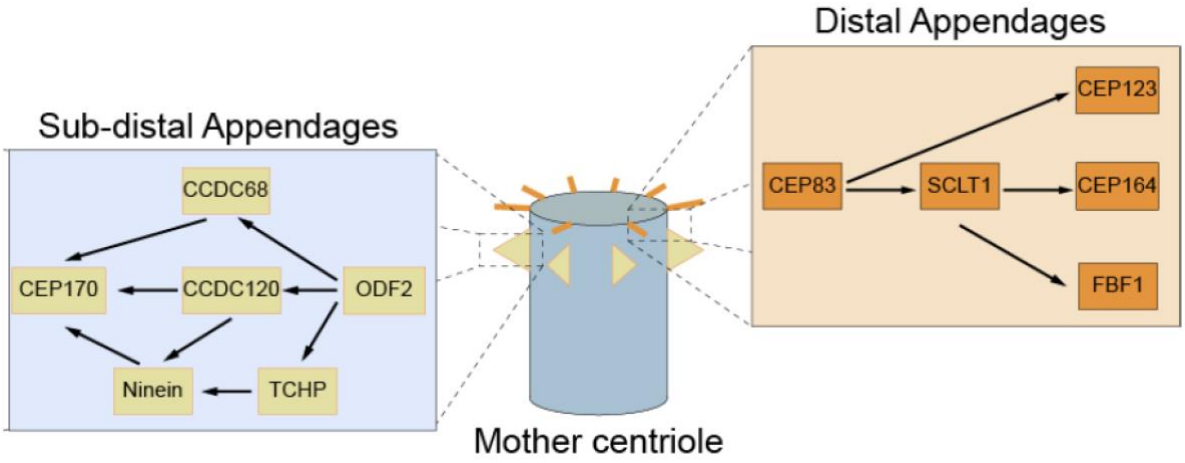

Figure. 3: The hierarchy of distal and subdistal appendages at the mother centriole.

The image shows the organization of the distal and subdistal appendages by hierarchy. This figure is referenced from PhD dissertation, B. Kurtulmus, 2019.

1.2.2 Transition zone

The composition of the ciliary membrane and inner ciliary environment is different from the plasma membrane and cytosol because the commuting of cytosolic components into cilia is restricted by the transition zone (TZ). The TZ complex is constructed from the top of transition fibers (DA) to the proximal part of cilia (Figure. 4). It strictly controls the passing of lipids, tubulin, and proteins, functioning similarly to the nuclear pole complex, which acts as a gate keeper in nuclei (Garcia-Gonzalo et al. 2011; Gonçalves and Pelletier 2017; Reiter, Blacque, and Leroux 2012). A feature of TZ ultra-structure known as the Y-link was identified by electron microscopy. The Y-links works to anchor each ciliary doublet microtubule to the membrane (Gilula and Satir 1972; Hartwell et al. 1974). TZ Y-link structure is divided into three modules: NPHP which binds the microtubule doublet, MKS which interacts with the ciliary membrane, and CEP290 which cross-connects the NPHP and MKS modules (Chih et al. 2012; Mollet et al. 2005; Sang et al. 2011) (Figure. 4). These three modules not only interact each other, but also associate with other ciliary components such as the BBSome and intraflagellar transport (IFT) which delivers ciliary cargos into cilia (Garcia-Gonzalo et al. 2011; Garcia-Gonzalo and Reiter 2012, 2017) (Figure. 4).

There are many studies showing that single or multi-mutation of TZ proteins cause ciliogenesis disorders and abnormal cilia elongation (Baala et al. 2007; Garcia-Gonzalo and Reiter 2017; Ramsbottom et al. 2018; Tammachote et al. 2009). Defective mutation of the CEP290 module in human kidney cells and MKS modules in mouse kidney cells show extremely elongated cilia (Ramsbottom et al. 2018; Smith et al. 2006). On the other hand, mutation of NPHP modules leads to a defect in photoreceptor cilia (Garcia-Gonzalo and Reiter 2017). Interestingly, it is known that a single gene mutation in the TZ can cause varying cilia phenotypes in different types of cells, even from the same organism. One example is that CEP290 deficiency shows over-axonemal elongation without any cilia loss in fibroblast and kidney cells (Ramsbottom et al. 2018; Shimada et al. 2017), but fails to generate connecting cilia and outer segments in photoreceptor cells (Rachel et al. 2012). Another example is that depletion of MKS1 and TMEM67 in mouse kidney cells lead to the formation of more than two cilia per single cell, whereas in the testis the sperm tail becomes extremely shortened and outer photoreceptor morphogenesis is disrupted in the retina (Tammachote et al. 2009). This indicates that the structure of the TZ can be cell type specific and that its hierarchy is changeable.

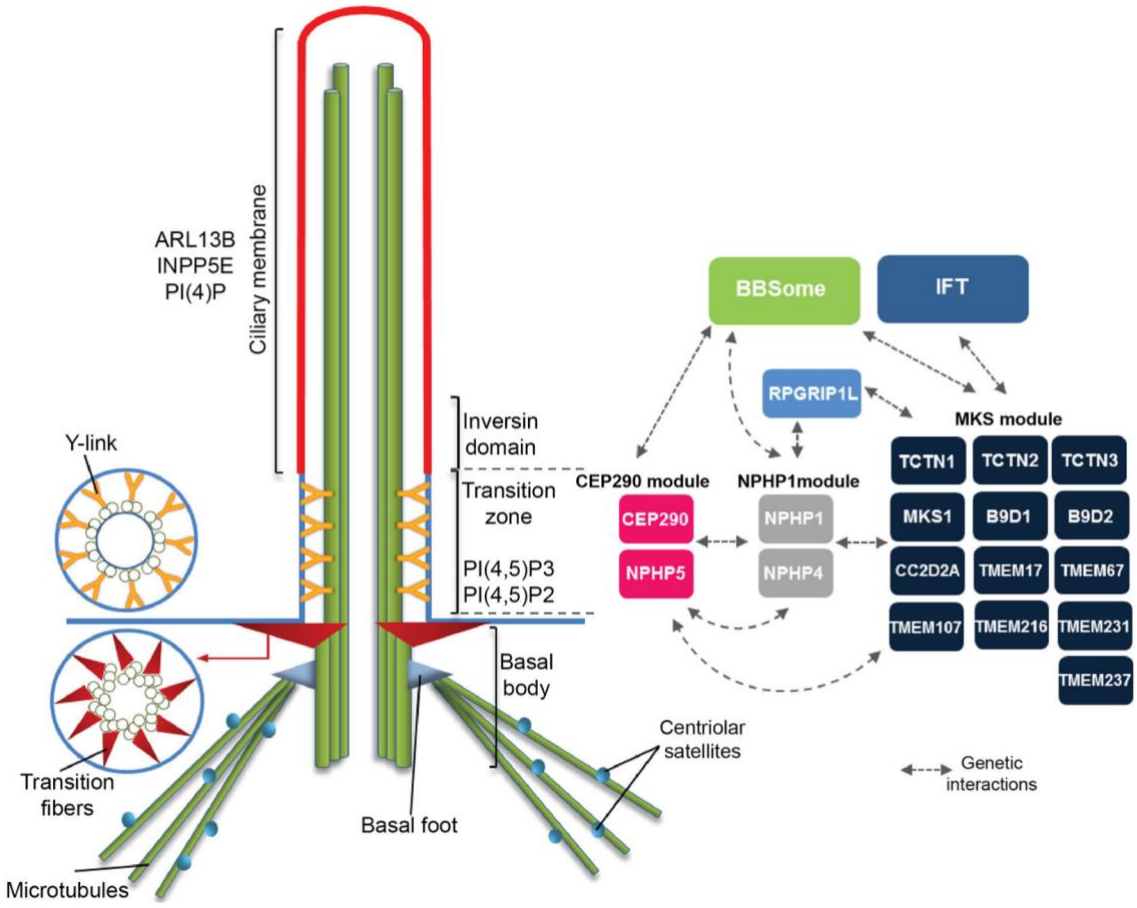

Figure. 4: The overview of the transition zone.

This model of primary cilia represents the structure of the transition zone (TZ). The TZ is briefly sub-grouped into three: CEP290 module, NPHP1 module, and MKS module. Two-tailed dot arrows show

the reported genetic interactions between each component. Transition fibers and basal foot are called distal appendages and subdistal appendages, respectively. The figure is adapted from (Gonçalves and Pelletier 2017).

1.2.3 Axoneme

The axoneme is the microtubule-based structure of cilia (Figure. 5A). It is known that the basal body's microtubules have a triplet 9+0 structure, formed from A-, B-, and C-tubules from inner to outer respectively within the mother centriole (Figure. 5B-iii) (Ishikawa and Marshall 2011; Wheway, Nazlamova, and Hancock 2018). A- and B-doublet microtubules both elongate from the basal body as axonemal microtubules (Figure. 5A and B), however the innermost A-tubules normally grow up to nearly reach the tip of ciliary axoneme. In contrast, B-tubules halt their extension in the middle of axoneme (Figure. 5B-i and ii) (Gluenz et al. 2010; Johnson 1998; Kramer, Moerman, and Inglis 2007). It was widely believed that the model of 9+0 axonemal microtubules remains stable from the basal body to the tip of axoneme, but recent ultra-structure studies reveal that this 9+0 microtubule structure is only maintained until the lower bottom of axoneme and just a limited number of microtubules (6+0 or 4+0) are able to reach the tip of axoneme (Kiesel et al. 2020; Sun et al. 2019).

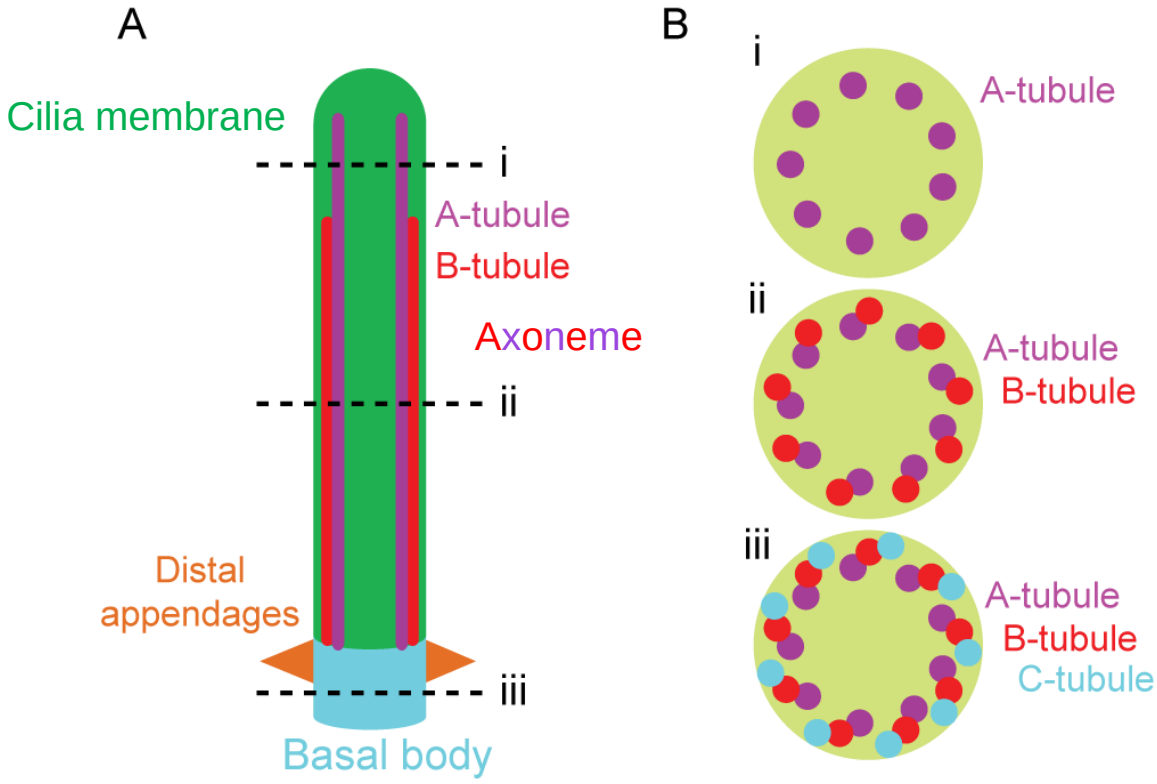

Figure. 5: Axonemal microtubule structure in primary cilia.

A. The simple model image of primary cilia. Doublet A- and B-tubules (the axoneme) are generated from the basal body as axonemal microtubules. B-tubules stop growing before the fibers reach the tip

of axoneme, but A-tubules can elongate to the tip as a singlet. **B.** Cross section images of ciliary microtubules from each dot bar (i-iii) from **A**.

The structure of axonemal microtubules differ from cytosolic microtubules by their tubulin post-translational modifications (Gadadhar et al. 2017; K. He, Ling, and Hu 2020; Wloga et al. 2017). Tubulin acetylation occurs on both A- and B-tubules at a similar level and enhance tubulin flexibility (K. He, Ling, and Hu 2020; Orbach and Howard 2019). An acetyl group is added to the specific locus on lysine 40 (K40) of α-tubulin, catalyzed by tubulin acetyl transferase (αTAT1) (Figure. 6) (K. He, Ling, and Hu 2020; Shida et al. 2010). Removal of acetylation from this residue is conducted by two deacetylases: Histone deacetylase 6 (HDAC6) and Sirtuin 2 (SIRT2) (Figure. 6) (K. He, Ling, and Hu 2020). It is thought that tubulin acetylation stabilizes cilia structure due to evidence from several studies. For example, reduction of acetylation due to αTAT1 depletion has been shown to cause a cilia assembly delay (Shida et al. 2010) and hyper-acetylation by knockdown of HDAC6 or SIRT2 led to observations of over-elongated axonemes and blocked cilia disassembly (Pugacheva et al. 2007; Zhou et al. 2014).

However, almost all other tubulin modifications are added only to B-tubule residues, such as polyglutamylation, glycylation, and detyrosination (Gadadhar et al. 2017; K. He, Ling, and Hu 2020; Lechtreck and Geimer 2000; Wloga et al. 2017). Tubulin polyglutamylation is generated as monoglutamylation and polyglutamylation at glutamate residues in both α- and ß-tubulin C-terminal tails (K. He, Ling, and Hu 2020). The initiation of glutamylation is organized by the tubulin tyrosine ligase-like (TTLL) 4, 5, and 7, and polyglutamylation is catalyzed by TTLL1, 6, 11, and 13, whereas deglutamylation is regulated by the cytosolic carboxypeptidase (CCP) family 1-6 (Figure. 6) (K. He, Ling, and Hu 2020). The process of tubulin glycylation is similar to glutamylation and is catalyzed by the same TTLL family proteins: TTLL3 and 8 for initiation and TTLL10 for elongation (Figure. 6) (K. He, Ling, and Hu 2020; Wloga et al. 2017). Different from tubulin glutamylation, no clear enzyme has been identified as a deglycylase. Both glutamylation and glycylation are vital for the proper structure and function of cilia.

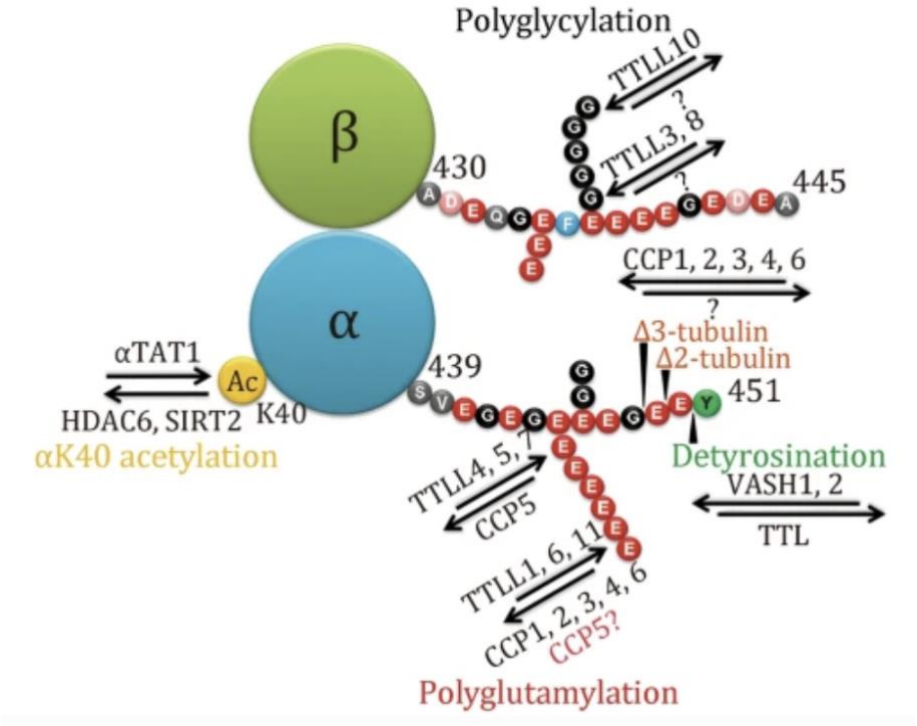

Figure. 6: Tubulin post-translational modifications in the ciliary axoneme. This model figure shows the location of each tubulin's post-modifications and which enzymes control them. The figure is adapted from (K. He, Ling, and Hu 2020).

The connection of axonemal microtubules to the structure of cilia is well-understood in lower eukaryotes for both motile and immotile cilia, such as the flagellar of Chlamydomonas and sensory cilia of *C. elegans* respectively (Kramer, Moerman, and Inglis 2007; Snow, Ou, Gunnarson, Regina, et al. 2004; Wloga et al. 2017). These cilia are segmented into two parts: the middle segment and the distal segment (Kramer, Moerman, and Inglis 2007; Snow, Ou, Gunnarson, Walker, et al. 2004). It is known that the middle segment contains doublet axonemal microtubules domain enriched in several tubulin modifications, such as glutamylation, glycylation, acetylation, and detyrosination, whereas the distal segment is the singlet axonemal microtubule domain (Figure. 5A) (van der Burght et al. 2020; Cornelia I. Bargmann 2006; Kramer, Moerman, and Inglis 2007; Prevo, Scholey, and Peterman 2017). There are two ways to determine the middle/distal segment: (1) using electron-microscope to detect the doublet-singlet microtubule transition in the axoneme and (2) using doublet microtubule specific markers such as glutamylated and glycylated tubulin (Figure. 6) together with whole cilia markers such as ARL13B, SSTR3, IFT88, and acetylated tubulin, then calculating the distal segment part by the total axoneme minus the doublet microtubule segment.

Structurally speaking, the middle segment is physically stable and strong thanks to the enrichment of tubulin modifications, especially glutamylation, glycylation, and acetylation (Gadadhar et al. 2017; K. He, Ling, and Hu 2020). On the contrary, the distal segment is generated from singlet microtubules with only tubulin acetylation and with a lower number of

axonemal microtubule (3+0, 4+0 or 6+0) than the proximal axoneme (9+0), therefore, the structure is fragile and unstable (Flood and Totland 1977; Sun et al. 2019).

In mammalian models, there are a few studies indicating this segmentation is structurally conserved. Mouse olfactory cilia can be separated into the middle and distal segment by fluorescence microscopy using ARL13B (axoneme) and EFHC1 (the middle segment) (Williams et al. 2014). Mouse kidney epithelial primary cilia also show the axonemal doublet/singlet transition by electron microscopy (Flood and Totland 1977) and electron tomography (Sun et al. 2019). On the other hand, in the structural study, the functional importance of this segmentation in mammalian primary cilia is still poorly understood. However, it is strongly indicated that the middle/distal segment in primary cilia plays a vital role in their signaling function because there are several signaling related proteins that only accumulate at the distal tip of cilia (Cherry et al. 2013; Haycraft et al. 2005; Wheway, Nazlamova, and Hancock 2018).

1.2.4 Intraflagellar transport (IFT)

The IFT complex plays an essential function in constructing cilia. It rolls like a biological freight train, running on rails made by microtubule. The IFT complex possesses a bipolar function that is not only able to carry ciliary products from the basal body to the ciliary tip to help cilia growth, but also able to retrieve ciliary components at the tip to support cilia disassembly (Bhogaraju, Engel, and Lorentzen 2013; Fu et al. 2016; Prevo, Scholey, and Peterman 2017; Wingfield et al. 2017).

This train complex is classified simply into three parts: a core IFT-A/B sub-complex, BBSome, and flagellar-specific kinesin and dynein motors (Bhogaraju, Engel, and Lorentzen 2013; Fu et al. 2016; Funabashi et al. 2018; Prevo, Scholey, and Peterman 2017; Snow, Ou, Gunnarson, Walker, et al. 2004). The IFT-A/B sub-complex is a core domain of the IFT complex and is composed of more than ten different proteins (Taschner and Lorentzen 2016) (Figure. 9). It is believed that the IFT-B complex mainly works as an antegrade transporter, which receives ciliary cargos from the base of cilia to carry to the tip. On the contrary, the IFT-A complex has a capacity to be responsible for retrograde transportation (Marshall and Rosenbaum 2001; Taschner and Lorentzen 2016). However, this antegrade/retrograde model remains controversial as results suggest that it is not easy to easy to separate the roles of the IFT-A/B complex clearly (Blacque et al. 2006; Huet et al. 2014; Mukhopadhyay et al. 2010). The BBSome is known as a ciliary membrane recruiter associated with the IFT-A/B complex that stabilizes its function (Lee, Chung, and Doo Chung 2015). BBSome components are

generated by eight core units + one sub-core unit (Figure. 9) and a single deletion of BBSome core-units (BBS1, 2, 4, 7, 8, 9 or 18) in human retinal epithelial cells dramatically decreases the length of cilia (Prasai et al. 2020).

When the IFT-A/B complex and BBSome are the main body, IFT specific motor proteins are the engine and wheels of this biological train. IFT-kinesins are able to move anterogradely from the base to the tip and IFT-dynein run in the opposite direction (Prevo, Scholey, and Peterman 2017; Taschner and Lorentzen 2016) (Figure. 8). It is known that sensory and primary cilia have two different types of kinesin motors such as Heterotrimeric kinesin-2 and Homodimeric kinesin-2 (Prevo, Scholey, and Peterman 2017) (Figure. 8 and 9). Sensory cilia studies in worms show that Heterotrimeric kinesin-2 is formed by two motor legs and one head protein that can only move along the doublet microtubule, but Homodimeric kinesin-2 is allowed to pass along both doublet and singlet microtubule in cilia (Prevo et al. 2015; Prevo, Scholey, and Peterman 2017) (Figure. 8 and 9). In addition, Homodimeric kinesin-2 can walk on microtubules nearly two times faster than Heterotrimeric kinesin-2 (Pan et al. 2006; Snow, Ou, Gunnarson, Walker, et al. 2004), but its microtubule binding ability is weak (Imanishi et al. 2006). In contrast to IFT kinesins, a single IFT dynein-2 DYNC2 works for cilia growth (Prevo, Scholey, and Peterman 2017; Taschner and Lorentzen 2016) (Figure. 9). DYNC2 contributes this retrograde movement from the tip to the bottom of the axoneme, which is vital for cilia disassembly (Vuolo et al. 2020). The structure of DYNC2 is built by two symmetrical interacting hetero-hexameric units (Pfister et al. 2006; Toropova et al. 2019) (Figure. 9).

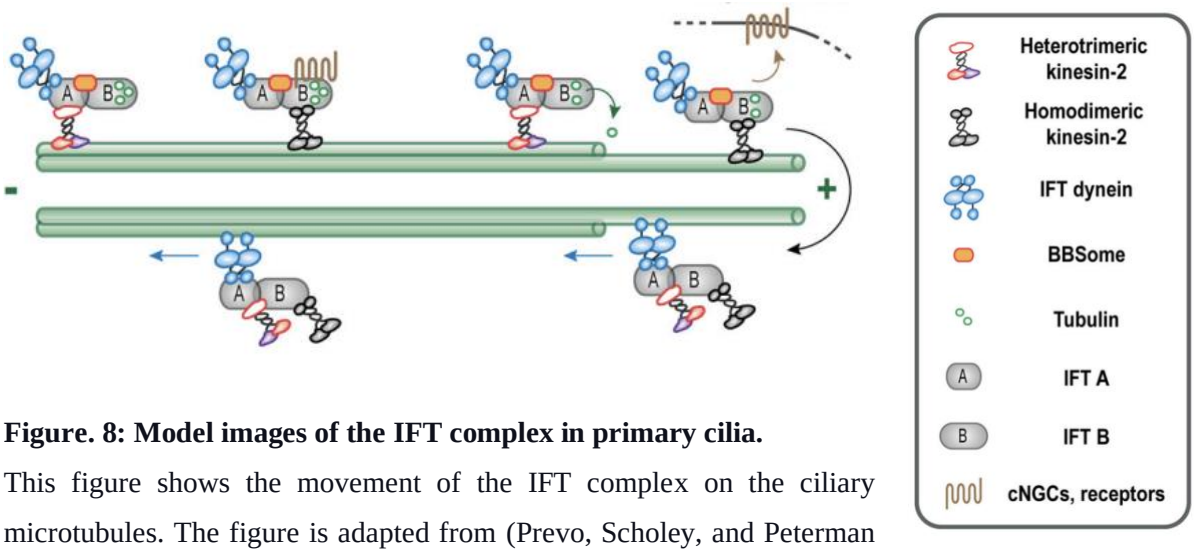

Figure. 8: Model images of the IFT complex in primary cilia.
This figure shows the movement of the IFT complex on the ciliary microtubules. The figure is adapted from (Prevo, Scholey, and Peterman 2017).

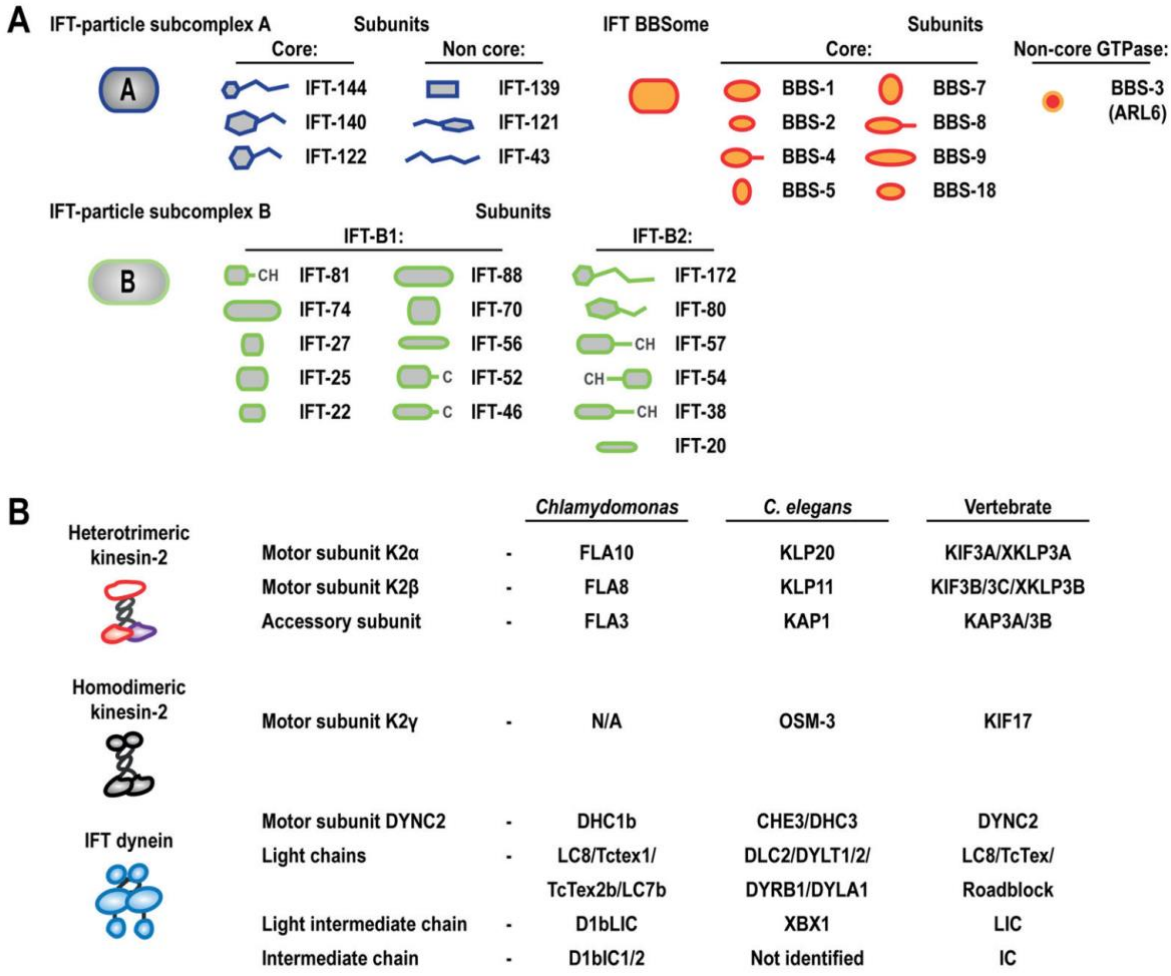

Figure. 9: The proteins of the IFT complex sub domains.

A. Description of IFT-A, IFT-B, and BBSome components. **B.** Information of IFT specific motor proteins from different species. The figure is adapted from (Prevo, Scholey, and Peterman 2017).

1.2.5 Ciliary tip

Quite a few results from electron microscopy show that the ciliary distal tip is exposed to the extracellular environment (Flood and Totland 1977; Gilula and Satir 1972; Rupik 2013; P. Satir, Pedersen, and Christensen 2010). One of the important roles of the ciliary distal tip is as a signaling scaffold, for instance, for calcium ion receptors in worm and sonic hedgehog-related proteins in mammalians only accumulate at the ciliary tip (Haycraft et al. 2005; Kramer, Moerman, and Inglis 2007; Pedersen and Akhmanova 2014).

Another role of the tip is cilia length control. When the antegrade IFT complex releases ciliary cargos containing tubulin, lipids, and membrane proteins at the tip, they fuse to the distal cilia tip as newer cilia (Prevo, Scholey, and Peterman 2017; Peter Satir 2017). At the same time, the retrograde IFT complex collects those components from the tip to carry out of the axoneme. Therefore, antegrade and retrograde transportation machinery balance well to maintain the

length of cilia (Kurtulmus et al. 2018; Marshall and Rosenbaum 2001; Prevo, Scholey, and Peterman 2017).

In contrast to the IFT complex, type-4 kinesin proteins are able to negatively control the cilia growth as a distal cap (M. He et al. 2014; Lewis et al. 2017). In vivo and vitro data have elucidated that human and mouse kinesin-4 KIF7 is clearly accumulated at the tip of axoneme and has a capacity to bind plus-ended microtubules to inhibit further microtubule elongation, thereby restricting cilia elongation (M. He et al. 2014; Schwarz et al. 2017). Surprisingly, it is also reported that KIF7 is lacking an active motor domain and is unable to move on microtubule (M. He et al. 2014). Currently, there is no convincing answer to explain how kinesin-4 localizes on the tip.

Recent studies determined that a small vesicle (ectosome) is released from the ciliary tip in human and mouse cells, in a process called ectocytosis (Nager et al. 2017; Phua et al. 2017; Wang et al. 2019). Ectocytosis mostly occurs after signaling activation and ectosomes are enriched in activated signaling-related membrane proteins (Nager et al. 2017). Though it is strongly indicated that there is a link between ectocytosis and signaling pathways, there is no clear consensus of the fate of the ectosome after secretion as to whether it just removes active receptors at the tip to down-regulate the signal transduction or transfers the active signaling molecules to another cell for cell-to-cell communication. Similar to ectocytosis, small vesicle release at the distal tip is also observed in mammalian photoreceptors (Young 1967). In this case, photoreceptor cells release elder discs from the tip to RPE cells to be recycled by phagocytosis (Young 1967).

1.3 Cilia assembly

Cilia assembly is organized by multi-scheme (Figure. 10). Cell cycle arrest in G_1/G_0 phase, cell confluency, and signaling activation are triggers for cilia formation (Ishikawa and Marshall 2011; Sánchez and Dynlacht 2016). The initial process of cilia assembly begins with recruitment of a guanine nucleotide exchange factor, Rabin8, to the pericentriolar recycling endosome, where it is activated by Rab11 (Westlake et al. 2011). The active Rabin8/Rab11 complex upregulates Rab8a to accumulate endosomal ciliary vesicles (CVs) at the distal appendages (DA) of the mother centriole. Expansion of CVs is controlled by EHD1, which drives cilia membrane assembly and axoneme elongation in collaboration with other regulators (TTBK2, INPP5E and PIPKl) (Čajánek and Nigg 2014; Goetz, Liem, and Anderson 2012; Lu et al. 2015). The kinase TTBK2 also removes the ciliogenesis suppressor CP110 from the DA to promote cilia formation. During cilia elongation, the transition zone is generated at the base

of cilia to transport the cilia building blocks selectively. Finally, CVs containing lipids, microtubules, and ciliary proteins are carried by the IFT complex from the basal body to the cilia, to build up the cilia antenna (Ishikawa and Marshall 2011; Sánchez and Dynlacht 2016).

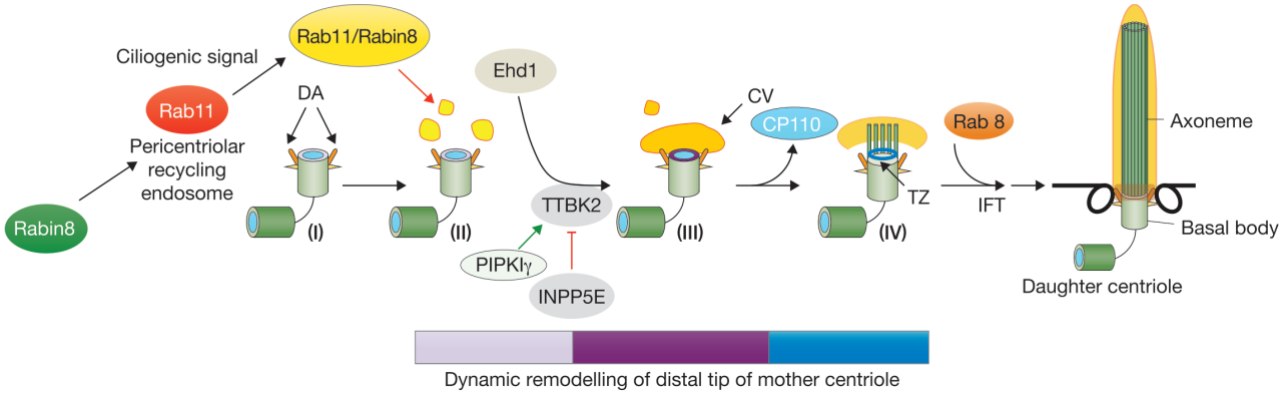

Figure. 10: Hierarchy of the initiation process in primary cilia.

There is a sequential process of cilia formation. (I). Generation of the distal appendages (DA) as a scaffold of ciliary vesicles (CV). (II). Formation of pre-mature CV at the DA that are recruited by the Rab11-Rabin8 complex. (III). EHD1-regulated expansion of CV at the DA and removal of cilia formation repressor CP110 from the basal body. (IV). The construction of the transition zone (TZ) and extension of the ciliary axoneme and membranes, which is regulated by intraflagellar transport (IFT) machinery and BBSome. The figure is adapted from (Sánchez and Dynlacht 2016).

1.4 Cilia disassembly

Compared to cilia assembly, understanding of the cilia disassembly processes is still unclear and fragmented (Sánchez and Dynlacht 2016). Upon triggering of serum re-stimulation and cell cycle re-entry, primary cilia start to disassemble from the proximal end of cilia by several mechanisms (Figure. 11). The Aurora A kinase-HEF1-dependent pathway is one of the major cilia disassembly factors. These proteins phosphorylate and accumulate Histone deacetylase HDAC6 to reduce microtubule stabilization, which induces cilia disassembly (Plotnikova et al. 2012). Moreover, it is reported that Nde1-Trichoplein and Pitchfork play a role in upregulating Aurora A pathway activity (Inaba et al. 2016). Another pathway is de-polymerization kinesins KIF24- and KIF2a-dependent axonemal microtubule disassembly. The S/G2 phase kinase NEK2 and the G2/M phase kinase PLK1 activate KIF24 and KIF2a respectively at the basal body to decrease microtubule fibers from the ciliary base (S. Kim et al. 2015; Miyamoto et al. 2015). Furthermore, recent studies mention that ectocytosis at the tip of cilia is a supporting cilia disassembly pathway when those cilia retrieval pathways are disrupted (Nager et al. 2017; Wang et al. 2019).

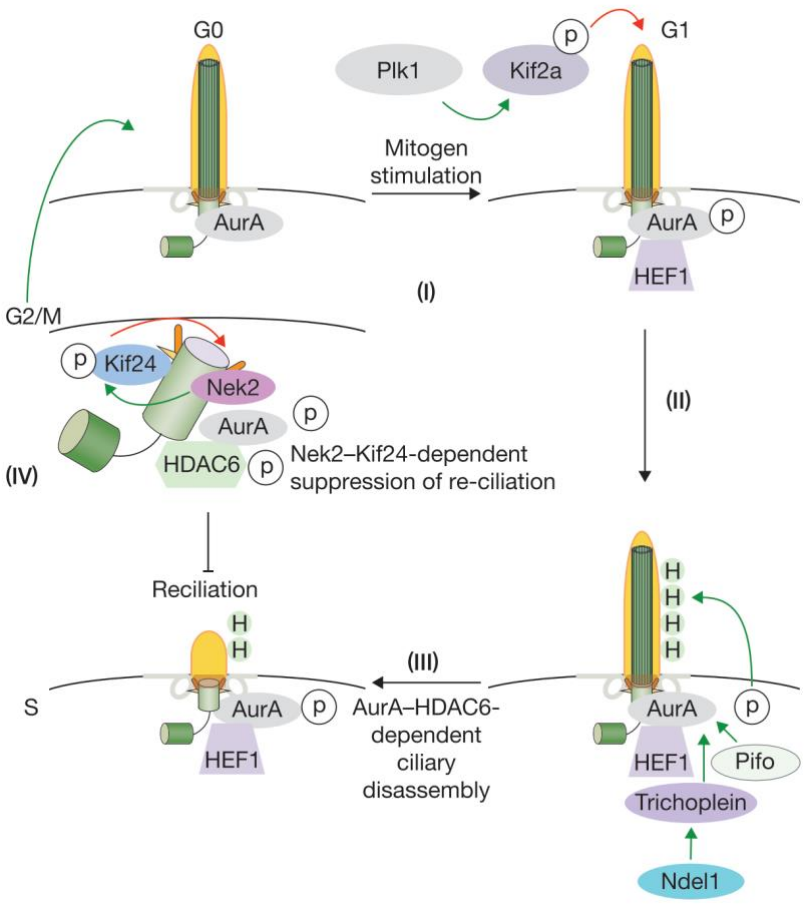

Figure.11: An overview of cilia disassembly pathways. (I). PLK1-dependent KIF2a axonemal microtubule depolymerization is triggered by cell cycle re-entry into G2/M phase. (II). The Aurora A and HEF1 pathway is regulated by serum re-stimulation and Nde1-Trichoplein and Pitchfork (Pifo). (III). Aurora A pathway-based HDAC6 cilia disassembly. (IV). The KIF24-NEK2 pathway promotes microtubule de-polymerization and blocks cilia re-formation. The figure is adapted from (Sánchez and Dynlacht 2016).

1.5 Primary cilia and signal transduction

One of the main functions of primary cilia is as a signaling scaffold. In the past few decades it was reported that an intact cilia structure is required for several signaling pathways such as Hedgehog (Hh), Wingless (Wnt), TGF, mTOR, Notch, and Hippo pathways (Ishikawa and Marshall 2011; Schou et al. 2015; Wheway, Nazlamova, and Hancock 2018). The Hh pathway is the most well studied pathway connected with the function of primary cilia (van der Burght et al. 2020; Goetz and Anderson 2010; Haycraft et al. 2005; Pedersen, Mogensen, and Christensen 2016). Regarding other signaling pathways, it is still not clear whether their activity is directly linked to the function of primary cilia or not, but more and more evidence is reported day by day (M. Kim et al. 2014; Mönnich et al. 2018; Simons et al. 2005; Tö et al. 2015; Wann and Knight 2012; Wheway, Nazlamova, and Hancock 2018; Xu et al. 2019). At the same time, the connection between primary cilia and signaling pathways have contradicting results, for example the canonical Wnt pathway (Simons et al. 2005; N. Sugiyama et al. 2011). Nevertheless, dysfunctional mutation of primary cilia causes signal transductions disorders indicating ciliary signaling function is not isolated from the signaling pathways.

It has been well-characterized that the Hh pathway requires functional primary cilia for its activation in mammalian cells (Nachury 2014; Pathi et al. 2001; Peter Satir and Christensen

2007). Hh was first identified in the 1970s in the fruit fly as being essential for body segmentation (Wood et al. 1980) and later this pathway was also shown to be conserved in vertebrates (Echelard et al. 1993; Krauss, Concordet, and Ingham 1993). It was identified that mammalian cells have three different types of Hh pathways: Sonic (major), Indian (minor), and Desert (minor) and the activation mechanisms of all three Hh pathways are similar and partly overlap (Pathi et al. 2001). Activity of those three Hh signaling pathways are changed between each cell type, hence enabling them to control more complicated gene regulations. Therefore, dysfunction of Hh signal transduction causes variable problems in organ formation (Goetz and Anderson 2010).

Here I show the simple model of Sonic hedgehog (Shh) signal transduction (Figure. 12 left). In the signal OFF state, a negative Shh regulator Patched-1 (PTCH1) is localized at ciliary membrane to inhibit the entry of activator Smoothened (Smo) into cilia (Briscoe and Thérond 2013; Corbit et al. 2005; Rohatgi, Milenkovic, and Scott 2007) (Figure. 12 left). Another negative regulator, Sufu, at the distal cilia tip directly binds Shh-related transcriptional factors Gli1, 2 and 3 (Glis) to hold them at the ciliary tip (Haycraft et al. 2005) (Figure. 12 left). Therefore, no transcriptional factor can bind promotor regions to upregulate Shh-related gene expression. On the other hand, in the signal ON state, the Shh ligand protein binds PTCH1 to change the conformation, meaning it is unable to block Smo entry into cilia (Corbit et al. 2005)(Figure. 12 right). Smo at the cilia inhibits Sufu's holding ability, allowing Glis to transfer to the nuclei through primary cilia (Bai, Stephen, and Joyner 2004; Nachury 2014). Finally, Glis bind promotor regions to upregulate Shh-related gene expression (Figure. 12 right).

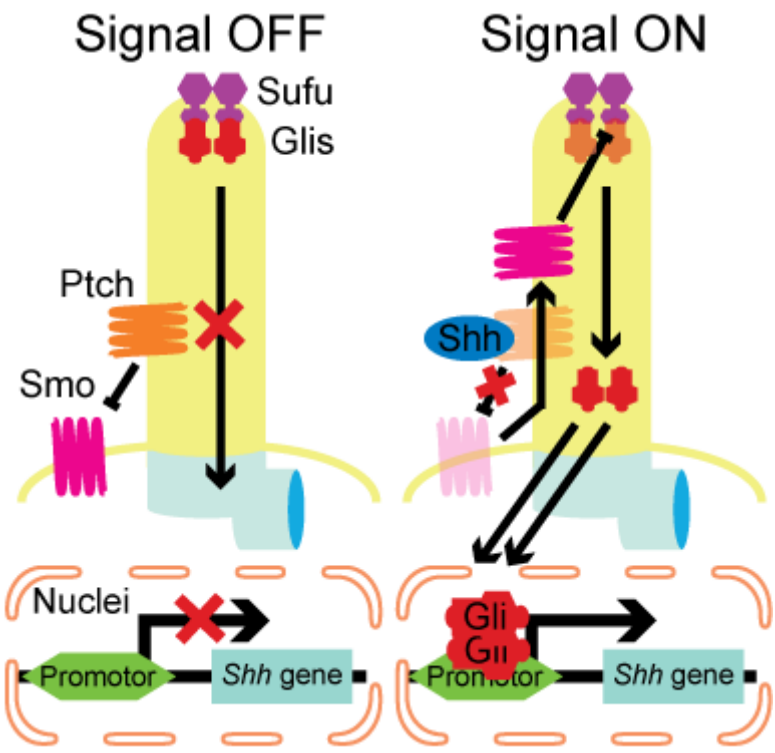

Figure 12: Overview of Sonic hedgehog pathway signal transduction. Signal OFF state: a negative regulator Patched-1 (Ptch) suppresses the entry of the positive regulator Smoothened (Smo) into the cilia. Another repressor Sufu binds the Shh-transcription factors Glis (Gli1, 2, 3) to keep them at the distal tip of the axoneme. Therefore, no Shh-related gene upregulation is processed. Signal ON state: Shh ligand interacts with Ptch and inactivates it, which promotes Smo entry into cilia. Smo inactivates Sufu, which allows transfer of Glis into nuclei. Glis bind the promotor region to enhance Shh-related gene expression.

1.6 Ciliopathy

When primary cilia are impaired by mutations, how are our bodies affected? In the past few decades, scientists and medical doctors have reported that there are strong connections between defective cilia components and body development problems that are categorized nowadays as ciliopathies (Ishikawa and Marshall 2011; Tammachote et al. 2009; Wheway, Nazlamova, and Hancock 2018). A ciliopathy is a kind of genetic disease which causes several body developmental problems, such as birth, kidney, brain, and eyes. Scientists believe signal transducers such as the Wnt and Shh pathways are negatively affected by abnormal cilia formation, which leads to these development problems (Baala et al. 2007; Kilander et al. 2018; Y. Kim et al. 2018; May-Simera et al. 2018; Oh and Katsanis 2013). Genetically speaking, defective mutation in cilia formation reduces the activities of signaling pathways, such as for WDR11 or DYNC2H1 mutants (Y. Kim et al. 2018; Oh and Katsanis 2013). Interestingly, though gene mutations of transition zone components CEP290 and MKS3 cause cilia super-elongation, these mutant cells show a reduction of Shh pathway activity (Aguilar et al. 2012a; Baala et al. 2007; Ramsbottom et al. 2018). Therefore, it is strongly indicated that proper length of cilia is required for signal transduction.

2. Aim of this study

Primary cilia are antenna-like organelles that play an important role in several signaling pathways such as sonic hedgehog and Wnt. Therefore, dysfunction of primary cilia by gene mutations causes multi-organ development problems that are categorized as ciliopathies. Pathological mutations of cilia components often result in no cilia formation and a low signaling response in patient cells. It shows that the existence of primary cilia is key for signal transduction in our body. Moreover, several mutations show shorter and longer lengths of cilia, which also lead to low signaling activity. It is strongly indicated that the proper length of primary cilia is also required for signal transduction.

Here, my PhD study aimed to elucidate the link between cilia length control and their signaling function. For this, I referenced lower eukaryote primary cilia studies. *C elegans* sensory cilia are segmented into two domains: the middle segment that gives structural stability and the distal segment that is a signaling scaffold. Compared with lower eukaryotes, the function of middle/distal segments are not well understood in mammalian models. Therefore, first I characterized this segmentation in human and mouse primary cilia using specific cilia markers. Second, I elucidated the function of Septin, which has been identified as a novel distal segment growth repressor by siRNA-based loss-of-function screening. Third, I generated over-elongated distal segment cilia cells to understand the effect on signal transduction ability in these cells. Finally, I would like to propose an insight into ciliary signaling function and axonemal segmentation.

3. Results

3.1 Characterization of the middle/distal cilia segmentation in human and mouse cells.

To understand the mechanisms of primary cilia length control, I selected two model cell lines: wildtype (WT) retinal pigment epithelial cells (RPE1) and mouse immortalized fibroblast (NIH3T3) cells. RPE1 and NIH3T3 cells are major model cell lines to study ciliogenesis (S. Kim and Dynlacht 2013; Pedersen, Mogensen, and Christensen 2016; Sánchez and Dynlacht 2016; Wu, Chen, and Tang 2018), and I kept both cell lines in a serum-starved (SS) condition to induce cilia formation. I used ARL13B as a cilia membrane marker, PCNT as a centrosome marker, and CEP164 as a distal appendage marker to visualize primary cilia (Figure. 13A, D). Both RPE1 and NIH3T3 cells increased percentage of ciliated cells after SS in a time-dependent manner and the length of cilia was also elongated later in the SS condition (Figure. 13B, C, E, F). The average cilia length maximized around 3 µm after 24-48 h SS (Figure. 13C, F). Ciliogenesis is heterogeneous thus axonemal length had huge variances at all time-points (RPE1: 0.5 to 6.5 µm and NIH3T3: 0.5 to 6 µm).

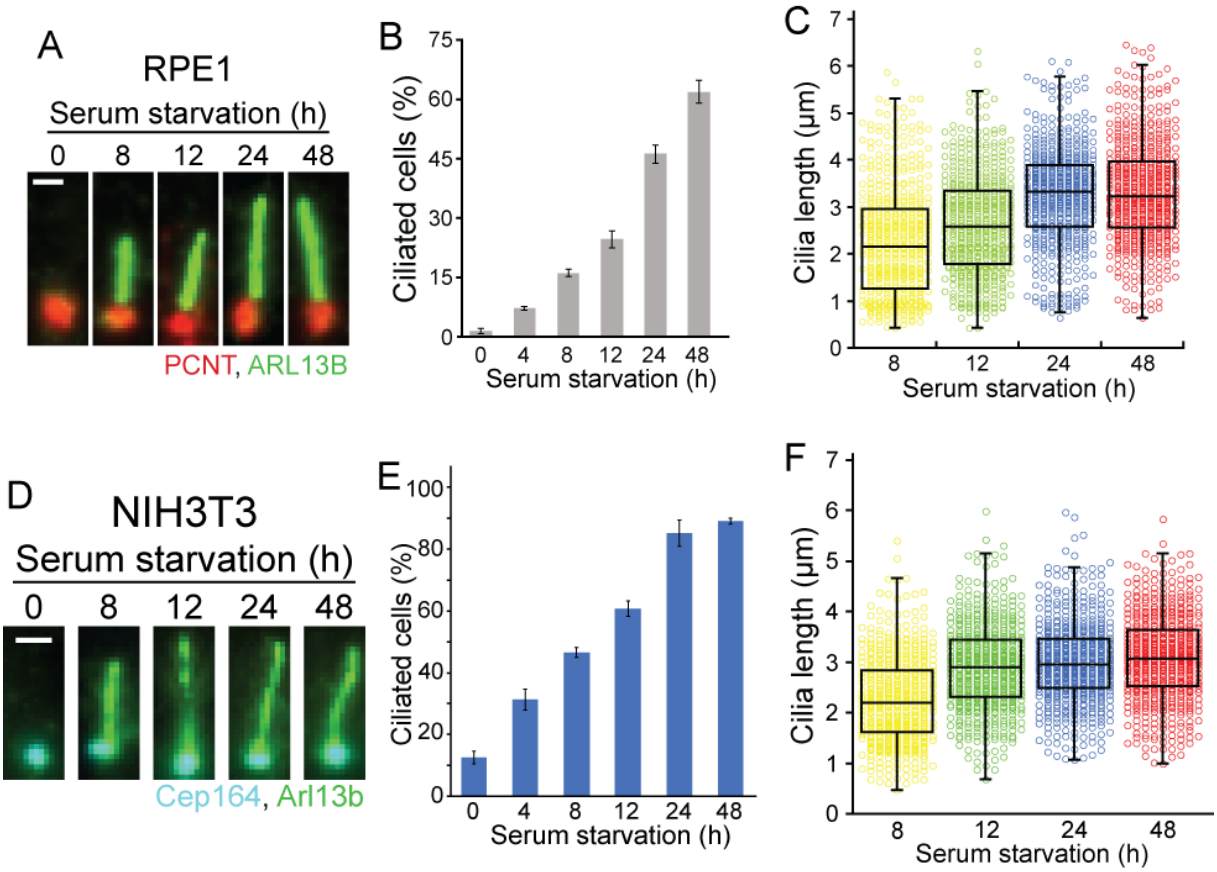

Figure. 13: Primary ciliogenesis and the length of cilia change at different time points after serum starvation (SS) in human retinal pigment and mouse fibroblast cells. A. Primary ciliogenesis after 0, 8, 12, 24, and 48 h SS in RPE1 cells. Scale bar is 1 µm. **B.** The percentage of ciliated RPE1 cells after SS, from **A.** n = 3 biological replicates, > 150 cilia each. **C.** Dot plot shows

the length of cilia in RPE1 cells after SS, from **A.** n = 3 biological replicates, >150 cilia each. **D.** Primary ciliogenesis after 0, 8, 12, 24, and 48 h SS in NIH3T3 cells. Scale bar is 1 μm. **E.** The percentage of ciliated NIH3T3 cells after SS, from **D.** n = 3 biological replicates, >150 cilia each. **F.** Dot plot shows the length of cilia in NIH3T3 after SS, from **D.** n = 3 biological replicates, > 150 cilia each. **B** and **E** data include mean St.dev.

To understand a deeper structure of mammalian primary cilia, I next analyzed whether primary cilia have the middle/distal segmentation as in lower eukaryotes cilia such as *C. elegans*. The structure of a worm's sensory cilia is characterized two parts: the middle segment that has a doublet axonemal microtubule domain to stabilize cilia structure, and the distal segment that has a singlet ciliary microtubule domain contributing to a scaffold for signaling proteins (Kramer, Moerman, and Inglis 2007; Snow, Ou, Gunnarson, Walker, et al. 2004) (for more detail see the introduction part: 1.2.3 Axoneme). On the other hand, whilst axonemal segmentation is not clearly defined in mammalian primary cilia, some ultrastructure studies suggest mouse kidney cells possess a doublet/singlet microtubule transition at cilia (Flood and Totland 1977; Sun et al. 2019). To test whether this cilia segmentation is conserved in mammalian cells, I decided to use GT335 antibody that identifies polyglutamylated microtubule, which is enriched at the doublet ciliary microtubule, as the middle segment marker together with whole cilia markers such as ARL13B or acetylated tubulin (K. He, Ling, and Hu 2020; Lechtreck and Geimer 2000; Wloga et al. 2017). If this axonemal segmentation is preserved in mammalian primary cilia, I would be able to visualize separately the middle segment (GT335 positive length on axoneme) from the distal segment (Whole cilia length – GT335 length) (Figure. 14A).

Tthe middle and distal segments were distinguished in RPE1 cells using the polyglutamylated tubulin and whole cilia markers (Figure. 14B). As previously reported (K. He, Ling, and Hu 2020), tubulin acetylation accessed nearly the tip of the axoneme in different cilia length groups (Figure. 14C). On the other hand, tubulin polyglutamylation occupied almost the full range of axoneme in shorter cilia group (< 2 μm), but this occupation was reduced in proportion to their length (Figure. 14D). This indicates that the ratio of distal segment out of whole cilia increases in longer cilia (Figure. 14D). Moreover, the population with a longer distal segment was dramatically raised in later SS condition cells compared with earlier (Figure. 14E). This cilia segmentation was also observed in NIH3T3 cells (Figure. 15A-C).

These results suggested that the middle/distal segmentation is conserved in higher organisms such as human and mouse and that the distal segment length is dependent on the size of primary cilia.

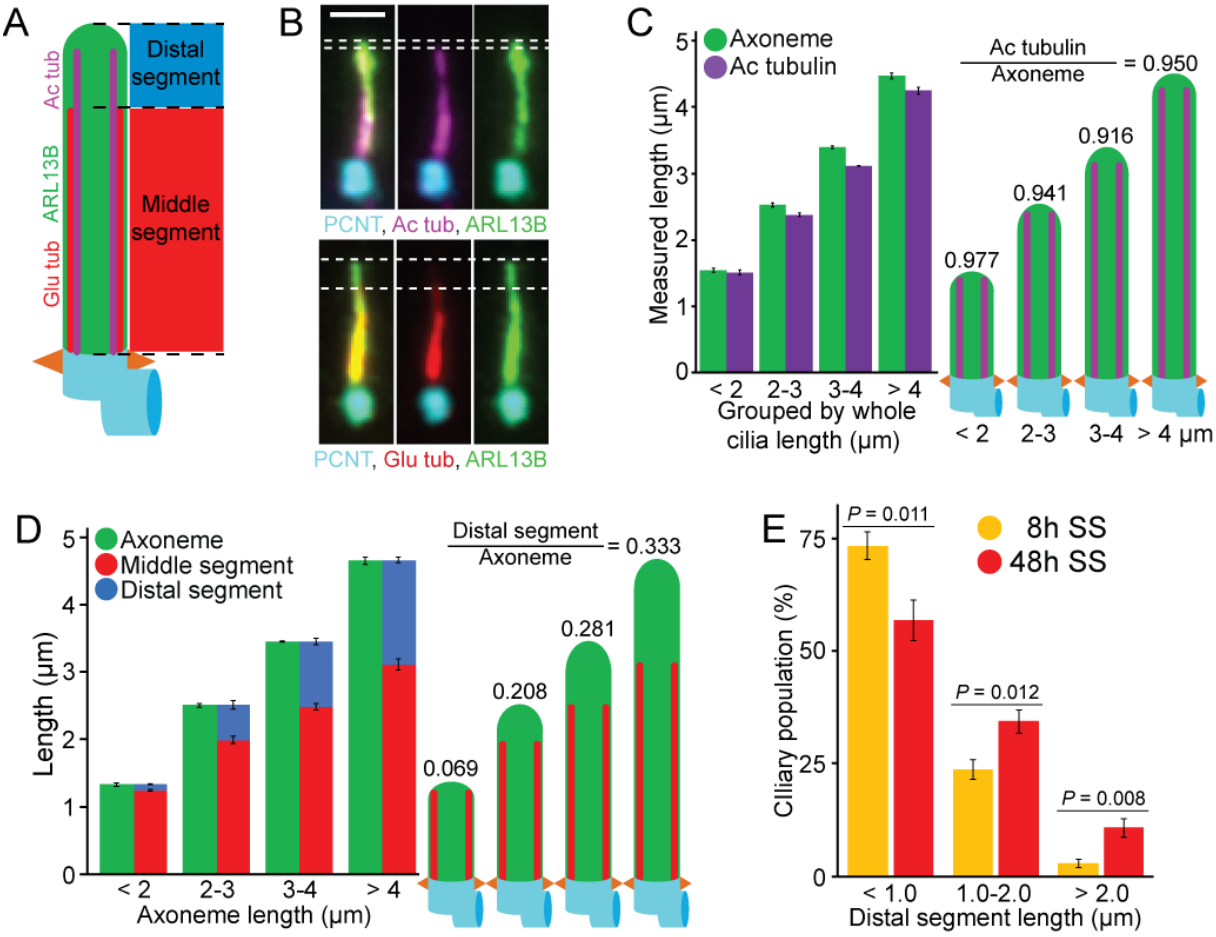

Figure.14: Cilia segmentation in RPE1 cells. A. The model image of the middle and distal segment in primary cilia. The middle segment is a doublet microtubule domain that is identified by tubulin polyglutamylation. The distal segment is a singlet microtubule domain from the end of the middle segment to the tip of cilia. **B.** Staining of the different cilia components. Scale bar = 1.5 μm. White dot bars represent the gap between the end of each singlet/doublet microtubule and/or whole ciliary membrane. **C.** The average length of acetylated tubulin and whole cilia in the different cilia length group (< 2, 2-3, 3-4 and > 4 μm) with the models. n = 3 biological replicates, 400 cilia each. The numbers upon the model images mean the ratio of acetylated tubulin/whole cilia. **D.** Average length of the middle segment and whole cilia in the different cilia length group (< 2, 2-3, 3-4 and > 4 μm) with the models. n = 3 biological replicates, >700 cilia each. The numbers upon the model images mean the ratio of distal segment/whole cilia. **E.** The population analysis of the average length of the distal segment after 8h and 48h SS. n = 3 biological replicates, >150 cilia each. **C** and **D** data include mean St.dev. **E** data includes mean St.dev. and *P* values are calculated by two-tailed unpaired student t-test.

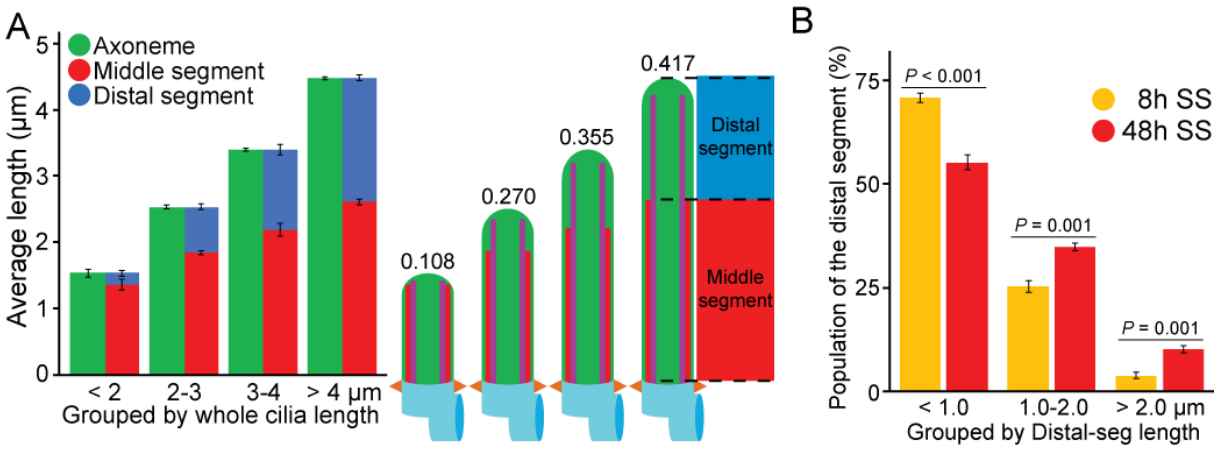

Figure. 15: Cilia segmentation in NIH3T3 cells. A. Average length of the middle segment and whole cilia in the different cilia length group (< 2, 2-3, 3-4 and > 4 μm) with the models. n = 3 biological replicates, > 600 cilia each. The numbers upon the model images mean the ratio of distal segment/whole cilia. **B.** The population analysis of the average length of the distal segment after 8h and 48 h SS. n = 3 biological replicates, > 150 cilia each. **A** data includes mean St.dev. **B** data includes mean St.dev. and *P* values are calculated by two-tailed unpaired student t-test.

3.2 Perturbation of actin and microtubule cytoskeletons elongate the middle/distal segment in different ways.

When cilia grow longer, the ratio of distal segment from whole cilia also increases in mammalian cells (Figure. 14D, 15A). Next, I would like to observe how different treatments induce cilia elongation, to check the middle/distal segment pattern change. For this, I added some chemicals that are known to be cytoskeleton perturbators such as nocodazole and cytochalasin D (CytoD). Previous studies show that lower dosed microtubule polymerization inhibitor nocodazole and actin polymerization inhibitor CytoD promote cilia over-extension (J. Kim et al. 2010; Sharma et al. 2011). Average cilia and acetylated tubulin length were dramatically elongated in RPE1 cells after 3 h of 200 nM CytoD and/or 100 nM nocodazole (Figure. 16A-C). Double treatment of actin and microtubule perturbators additionally affected the cilia growth, which indicates that each cytoskeleton controls cilia length via a different mechanism. Interestingly, CytoD-treated RPE1 cells showed extension of both segments but keeping the same proportions as the control, whilst nocodazole treatment increased only the length of distal segment (Figure. 16C).

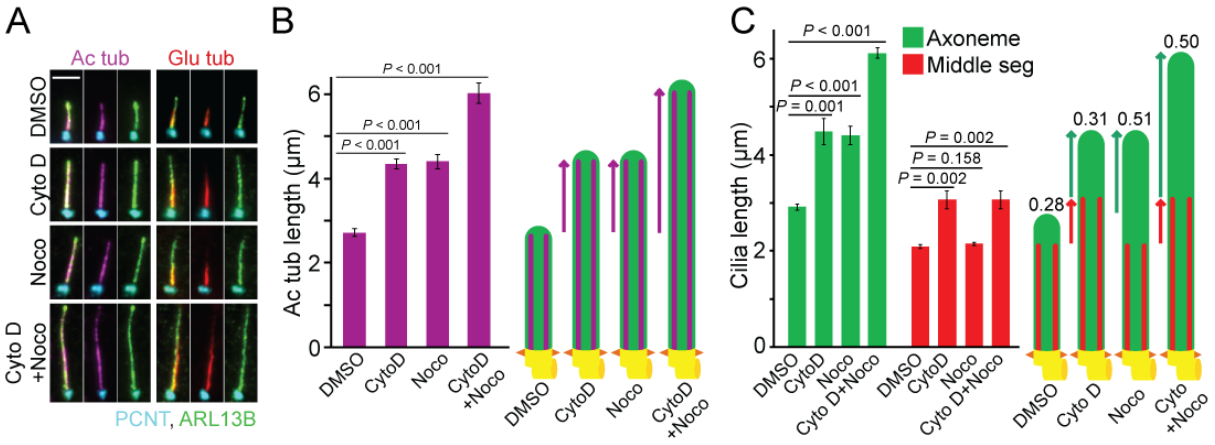

Figure. 16: Actin and microtubule perturbators change cilia segmentations differently in RPE1 cells. A. Primary cilia length changes after 3 h indicated chemical treatment in ciliated RPE1 cells. Scale bar is 3μm. **B**. Average length of acetylated tubulin elongation by indicated treatments, from **A** with the model. **C**. Average length of the middle segment and whole cilia change from **A** with the model. The number on the models show the ratio of the distal segment/whole cilia. **B** and **C** data are from three times independent experiments and 100 cilia are quantified each. **B** and **C** data include meaning St.dev. and *P* values are calculated by two-tailed unpaired student t-test.

3.3 Screening to identify the regulator of distal segment growth affecting the microtubule cytoskeleton.

Why does nocodazole treatment only affect the distal segment length? To understand this deeper, I decided to identify a factor regulating the distal segment growth via the microtubule cytoskeleton using a small-scale siRNA loss-of -function screening and nocodazole treatment in RPE1 cells. I selected genes which have been previously reported to interact with microtubules and also identified as cilia length regulators: IFT dynein 2 light chain DYNC2L1 (Taylor et al. 2015), IFT kinesin subunit KIF3A and KIF17 (Insinna et al. 2008; Prevo, Scholey, and Peterman 2017; Qiu et al. 2012), MTs interacting proteins MAP4 and SEPT2 (Ghossoub et al. 2013; Hu et al. 2010), tubulin glutaminase TTLL5 and de-glutaminase CCP5 (K. He et al. 2018; Wloga et al. 2017). KIF17 and TTLL5 depleted RPE1 cells decreased total cilia length (Figure.17A, B). CCP5 KD cells elongated both segments, keeping the proportion of each segment as in the control (Figure.17A, B). For the other genes, DYNC2L1, KIF3A, MAP4, and SEPT2, depletion extended only the distal segment like in nocodazole treatment (Figure. 17A, B).

Next, I used DYNC2L1, KIF3A, MAP4, and SEPT2 depletion with nocodazole treatment whilst checking further cilia elongation, in order to detect the distal segment growth factor. If this factor and nocodazole treatment affect the same microtubule-dependent distal segment growth pathway, the gene depletion cells would show no or weak additional cilia

elongation with nocodazole. DYNC2L1, KIF3A, MAP4, and control depleted RPE1 cells additionally elongated cilia length with nocodazole treatment, but only SEPT2 KD cells did not show cilia extension (Figure.17C, D).

Therefore, I decided to concentrate on the analysis of SEPT2 to elucidate the biological mechanism of distal segment growth in mammalian primary cilia.

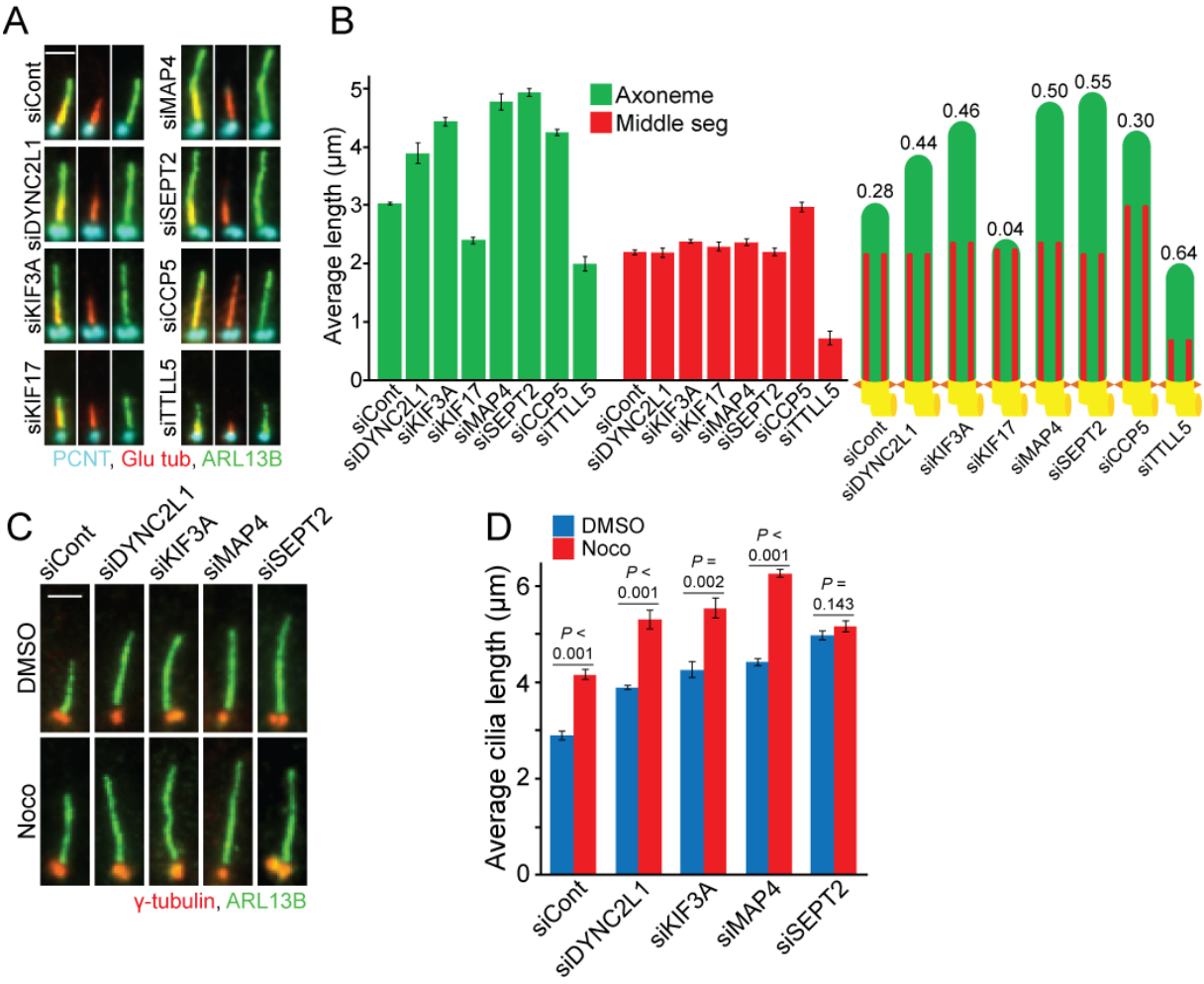

Figure.17: Identification of the distal segment growth factor affecting the microtubule dependent mechanism. A. Images of primary cilia with indicated siRNA in RPE1 cells. Scale bar is 2 μm. **B**. Average length of the middle segment and whole cilia change from **A** with the model. The number on the models show the ratio of the distal segment/whole cilia. **C**. Primary cilia length changes with indicated siRNA after 3 h 100 nM nocodazole treatment in RPE1 cells. Scale bar is 2 μm. **D**. Average length of cilia from **C**. **B** and **D** data are from three times independent experiments and 100 cilia are quantified each. **B** and **D** data include meaning St.dev. and *P* values are calculated by two-tailed unpaired student t-test.

3.4 Septin is a highly conserved protein complex localizing both in the cytosol and to cilia.

SEPT2 is a one of the building blocks of the Septin family and is a highly conserved protein complex which supports cell division, cell migration, and membrane protein stabilization (Neubauer and Zieger 2017; Palander, El-Zeiry, and Trimble 2017; Valadares et al. 2017). Septin family protein structure has three GTP-binding domains, a phosphoinositide-binding polybasic region, a Septin unique domain and null or several coiled-coil domains (Figure.18A) (Neubauer and Zieger 2017; Valadares et al. 2017). It is known that there are 13 Septin family proteins in mammalian cells, categorized into 4 sub-groups: SEPT2 (SEPT1, 2, 4, and 5), SEPT6 (SEPT8, 10, 11, and 14), SEPT7, and SEPT3 (SEPT9 and 12) (Figure.18B). Septin forms repeated hetero-polymer complexes like fiber, ring, and sheet within cells (Figure.18C and D). Each sub-group of Septin can be substituted by the other Septins in vitro and in vivo, for instance SEPT2 can be switched SEPT4 (Figure.18E) (Sandrock et al. 2011). Moreover, only single Septin sub-group mutation or depletion disrupts the whole structure of Septin (Sellin et al. 2011). Interestingly, there are quite a few homologs of Septin in mammalian cells but their expression is tightly regulated. Several human cancer cells are known to highly produce one of each sub-group of Septin: SEPT2, SEPT7, SEPT6, and SEPT9 (Sellin et al. 2011).

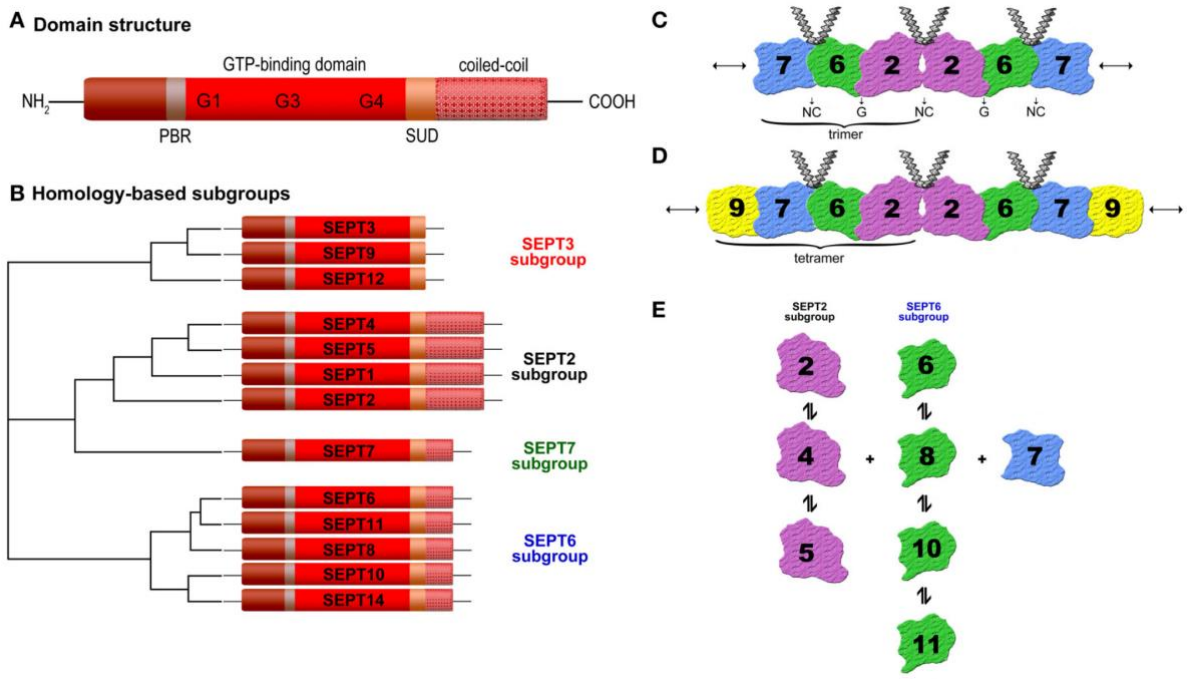

Figure.18: Overview of mammalian Septin family proteins. A. Common structure of Septin proteins. All of Septins have a GTP-binding domain, Phosphoinositide-binding polybasic region (PBR) and Septin unique domain (SUD), and coiled-coil domains except for SEPT3 subgroup. **B.** The Septin family is divided into four sub-groups: SEPT3 (SEPT9), SEPT2, SEPT7, and SEPT6. **C.**

Structure of the Septin complex from repeated trimers (SEPT7-6-2-2-6-7). **D.** Structure of the Septin complex from repeated tetramers (SEPT9-7-6-2-2-6-7-9). **E.** The same sub-group Septin proteins can be substituted from others. The images are adapted from(Neubauer and Zieger 2017).

It is reported that a Septin filament is observed in sperm tails, motile cilia, and primary cilia (Palander, El-Zeiry, and Trimble 2017). Therefore, I first observed endogenous SEPT2 and SEPT7 localization in RPE1 cells. White-field fluorescence microscopy clearly showed that SEPT2 and SEPT7 are enriched at the cytosol as fiber structures and also on the ciliary axoneme in RPE1 cells (Figure. 19A). However, still I did not observe which part Septin localizes to on the axoneme due to the limited resolution. To improve this limitation, I used Stimulated emission depletion microscopy (STED). I generated stably SEPT2 and SEPT7 expressing cell lines to amplify the signals and those Septin proteins behaved the same as endogenous Septins (Figure. 20E). SEPT2 and SEPT7 were located inside of the axonemal membrane ARL13B but nearly overlapped ciliary acetylated tubulin in super-resolution images (Figure. 19B). In addition to, SEPT2 started to accumulate from the upper part of the transition zone to cilia (Figure. 19C, D).

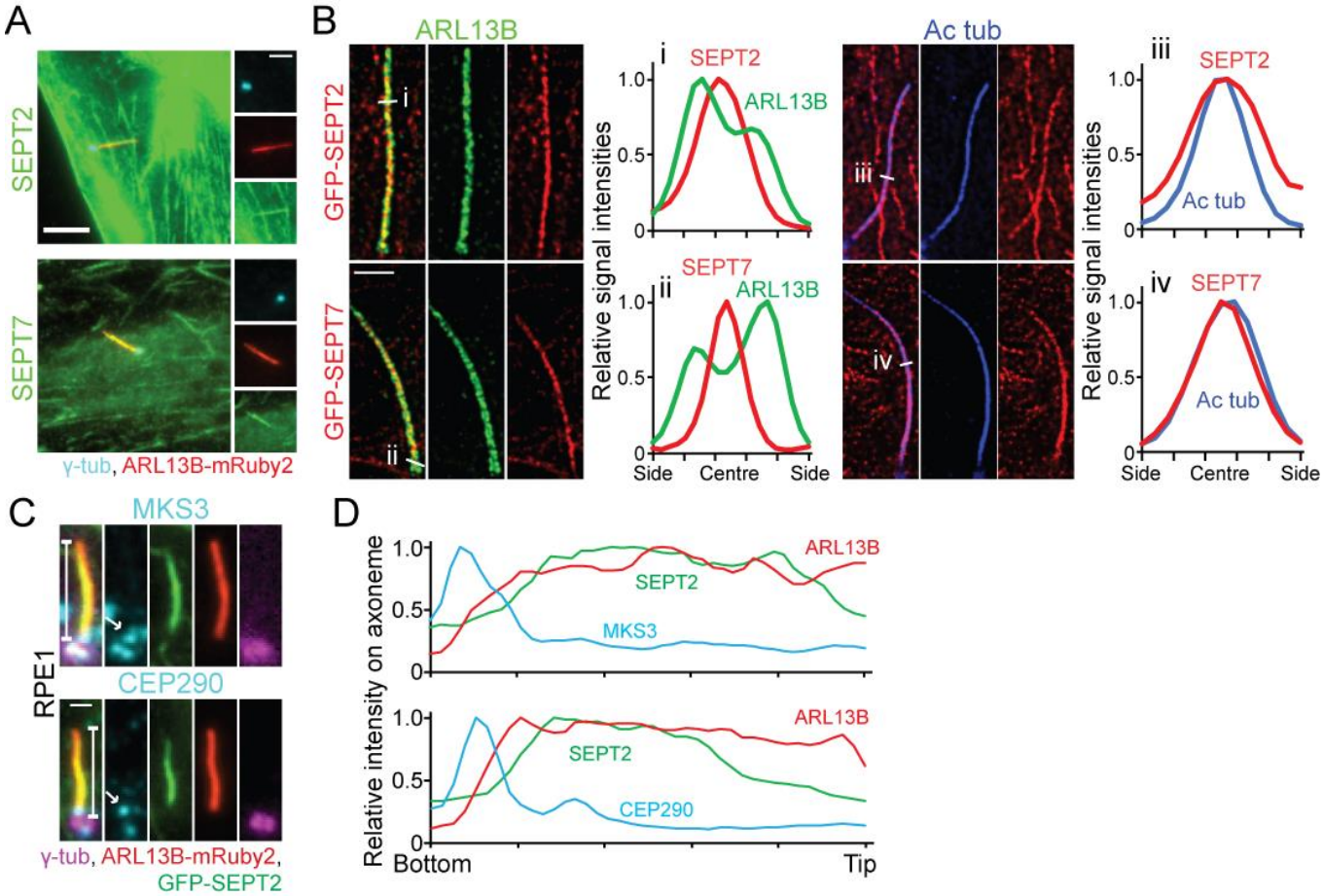

Figure. 19: Observation of mammalian Septin localization in primary cilia. A. Endogenous SEPT2 and SEPT7 are localized on the ciliary axoneme and in the whole cytosol. Scale bar is 4 μm (large) and 2 μm (small). **B**. Super resolution microscopy shows SEPT2 and SEPT7 neatly co-localize with ciliary microtubules. Scale bar = 0.5 μm. **(i)-(iv),** Relative indicated protein signals at white lines from images. **C**. Septin localizes at cilia but not the transition zone. Scale bar is 1 μm. White arrow points the specific signal of MKS3 and CEP290. White bar on the side of axoneme is used for **D**. **D**. Relative signal intensities of indicated proteins from **C**.

3.5 Depletion of each sub-group of Septin elongated cilia length and increased total rate of ciliogenesis in RPE1 cells.

From siRNA-based screening (Figure.17), SEPT2 KD increased only the distal segment length, but it is not yet known whether this phenotype is limited to SEPT2 or not. I depleted one of each sub-group of Septin: SEPT2, SEPT6, SEPT7, or SEPT9 to check cilia phenotypes. All four Septin depleted RPE1 cells increased both total cilia length and the percentage of ciliated cells (Figure. 20A, B, C). Each siRNA efficiency was proven by immunoblot (Figure. 20D). In contrast to my data, previous studies show that SEPT2 and 7 depletion reduced ciliated cells and SEPT2, 7, and 9 KD shortened cilia length in mammalian cells (Ghossoub et al. 2013; Hu et al. 2010). With siRNA gene depletions, we always have to be careful of off-target effects, because for many cases siRNA targets not only a specific region, but also similar sequenced regions (Jackson et al. 2003). To prove my siRNA results did not come from siRNA off-target effect, I generated stably expressing GFP-fused Septin proteins with siRNA resistance silent mutations in RPE1 cells. To control the expression level of these proteins, I used a doxycycline (DOX) induced protein expression system (Gossen and Bujard 1992). GFP-SEPT2, GFP-SEPT6, and SEPT7-GFP expressed fiber structures as endogenous Septins with 10 ng/ml DOX conditions and the proteins were stable with the indicated siRNA (Figure. 20E). Importantly, longer cilia phenotypes seen in SEPT2, 6, or 7 depletion were returned back to normal by the expression of the GFP-fused siRNA resistant Septin (Figure. 20E-F).

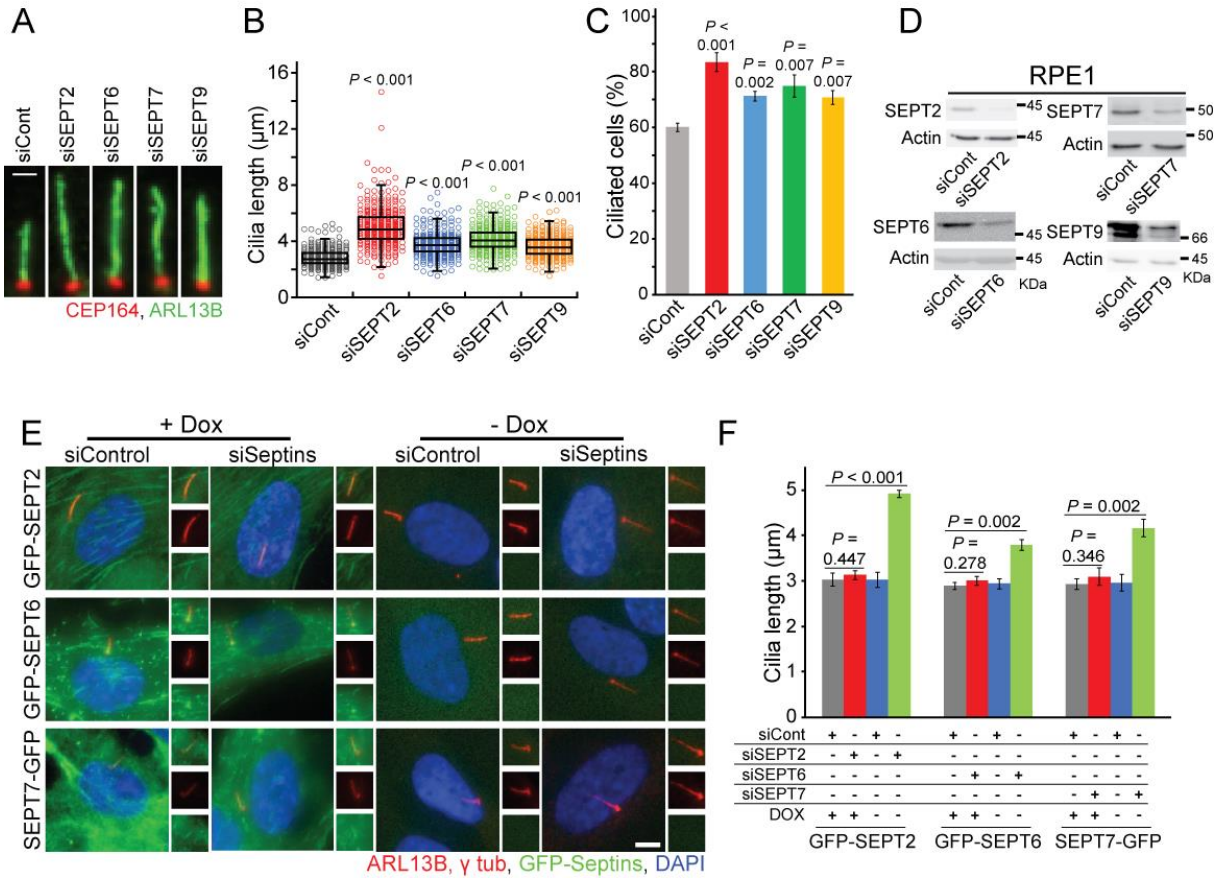

Figure. 20: Other Septin sup-groups specifically control ciliogenesis and cilia growth as SEPT2 in RPE1 cells. A. Cilia length changes with indicated siRNA. Scale bar is 1.5 μm. **B.** Dot plots represent cilia length from **A**. **C.** Percentage of ciliated cells is increased by Septin gene depletion. **D.** Indicated siRNA efficiency is proved by immunoblot. Actin is used as a loading control. **E.** Rescue experiment of Septin cilia phenotype by expression of GFP-fused Septin proteins with silent mutation around siRNA targeted sequences. Scale bar is 5 μm. **F.** Average length of cilia changes with indicated conditions from **E. B, C** and **F** data are from three times independent experiments and > 80 cilia are quantified each. **B, C** and **F** data include meaning St.dev. and *P* values are calculated by unpaired Wilcoxon-Mann-Whitney Rank Sum Test (**B)** or two-tailed unpaired student t-test (**C** and **F**).

3.6 SEPT2 gene knockout in RPE1 cells extended only the distal segment.

Next, I generated a *SEPT2* gene knockout (KO) RPE1 cells using the CRISPR/Cas9 system to analyze deeper the mechanism of distal segment growth control by Septin (Jinek et al. 2012). I designed two different guideRNA to target exon 4 and 6 of the human *SEPT2* gene and finally I achieved four isolated RPE1 SEPT2 KO cells without any endogenous SEPT2 signal (Figure. 21A, B). All the SEPT2 KO RPE1 cells formed longer cilia and showed higher ciliated cells compared to WT cells, as seen in the siRNA-based results (Figure. 21C-E). Moreover, over-elongated cilia were reverted by the expression of GFP-

SEPT2 proteins in all SEPT2 KO clones (Figure. 21F). Moreover, electron microscope images also showed over-elongated cilia in SEPT2 KO cells (Figure. 21G, H). I analyzed the cilia segmentation in clones 10 and 16 of RPE1 SEPT2 KO cells. As in depletion of SEPT2, both SEPT2 KO clones only elongated the distal segment and SEPT2 did not change the localization of ciliary tubulin acetylation (Figure. 22A-C).

A

SEPT2 KO Clone No.	Reference genome seq	Guide RNA	Target exon	Sequence mutations	Translation
7	ENSG00000168385	g21	4	Deletion: 241326055 to 241326064 locus	R64Stop
16	ENSG00000168385	g21	4	Insertion: 228 bp from pX458 to 241326052 locus	V62Stop
10	ENSG00000168385	g22	6	Insertion: 239 bp from pX458 to 241336063 locus	T152Stop
				Deletion: 241336062 to 241336063 locus	D142Stop
13	ENSG00000168385	g22	6	Deletion: 241336062 locus	L171Stop

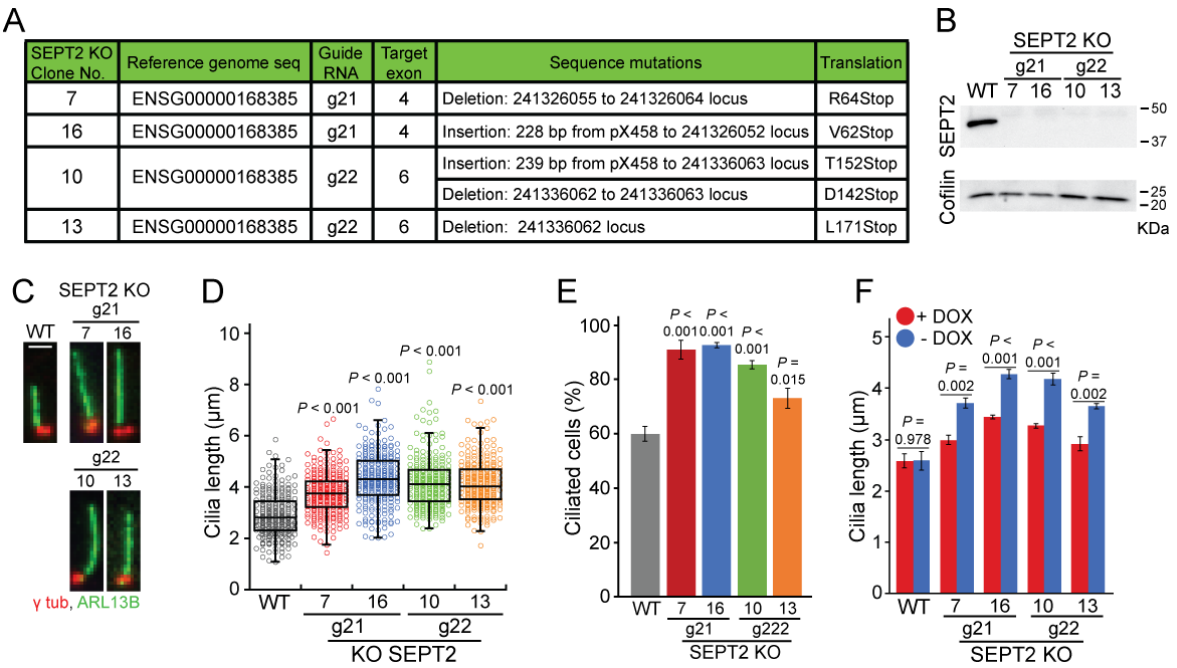

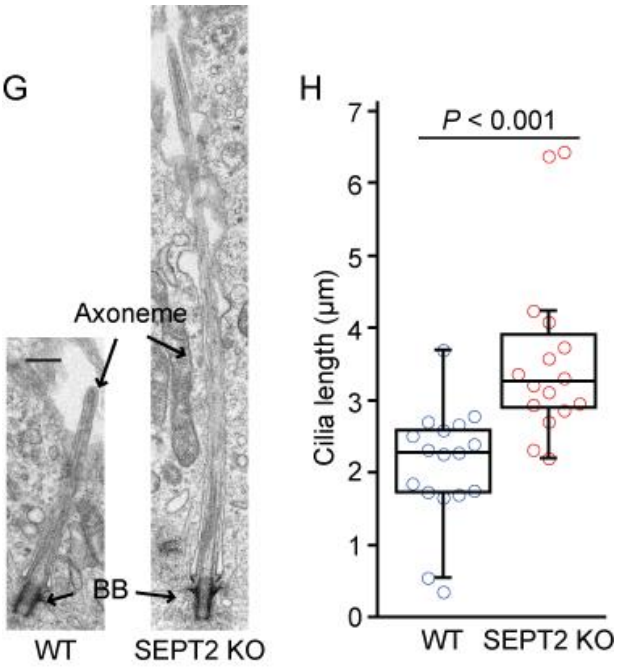

Figure. 21: SEPT2 gene knockout in RPE1 cells show the same cilia phenotypes as the siRNA-based Septin depletion results. A. Profiling of each SEPT2 gene knockout (KO) single isolated RPE1 cells. **B.** Endogenous SEPT2 protein is completely lost in SEPT2 KO RPE1 cells that is performed by immunoblot. Cofilin is a loading control. **C.** Each SEPT2 KO cell generates longer cilia. Scale bar is 2 μm. **D.** Dot plots show the cilia length of WT and SEPT2 KO RPE1 cells from **C**. **E.** Percentage of ciliated cells in RPE1 WT and SEPT2 KO cells. **F.** Cilia length phenotype of SEPT2 KO cells are rescued by the expression of GFP-SEPT2 proteins. **G,** Electron microscopy of WT and KO SEPT2 cilia. Black arrows point axoneme and basal body (BB), scale bar: 400 nm. **H,** Dot plots show the individual cilia length, from **G**. n = 15 cilia from two independent experiments. **D, E** and **F** data are from three times independent experiments and > 80 cilia are quantified each. **D, E, F** and **H** data include mean St.dev. and *P* values are calculated by unpaired Wilcoxon-Mann-Whitney Rank

Sum Test (**D** and **H)** or two-tailed unpaired student t-test (**E** and **F**). **G** figure were obtained from our collaborator Dr Annett Neuner from ZMBH.

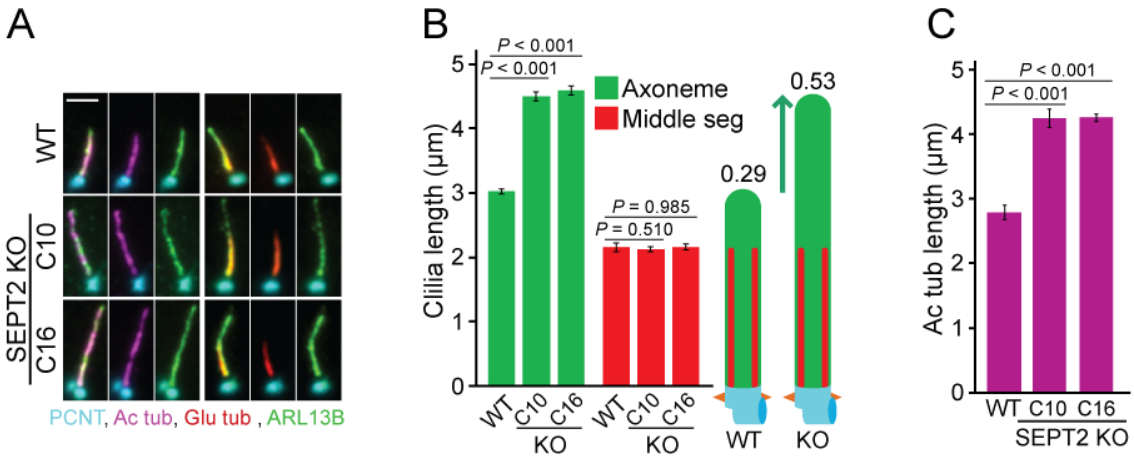

Figure. 22: The middle/distal cilia segmentation changes in SEPT2 KO cells. A. SEPT2 KO RPE1 cilia change only the length of the distal segment. Scale bar is 2 μm. **B.** Average length of the middle segment and whole cilia, from **A** with the model cilia image. Number on the model shows the ratio of the distal segment/whole cilia. **C.** Average length of the ciliary acetylated tubulin, from **A. B** and **C** data are from three times independent experiments and 100 cilia are quantified each. **B** and **C** data include meaning St.dev. and *P* values are calculated by two-tailed unpaired student t-test.

3.7 Low-dosed nocodazole reduced endogenous Septin at cilia to elongate the distal segment.

It is known that Septin is able to work together with actin and microtubules in cells (Kinoshita 2003; Valadares et al. 2017) and cilia length is affected by both cytoskeleton perturbations (J. Kim et al. 2010; Sharma et al. 2011). Does Septin control ciliary length using both cytoskeletons or not? To check this, I applied 3 h DMSO, CytoD, or nocodazole to already ciliated WT and SEPT2 KO RPE1 cells (Figure. 23A). Both the middle and distal segments were additionally increased with CytoD treatment but there was no significant change with nocodazole in SEPT2 KO cells (Figure. 23A, B). Importantly, nocodazole treatment dropped the protein level of SEPT2 and SEPT7 at cilia in RPE1 cells (Figure. 23C, D). This could be a reason why nocodazole treatment elongate the distal segment that reduces ciliary Septin level, mimicking the loss of function of Septin at cilia.

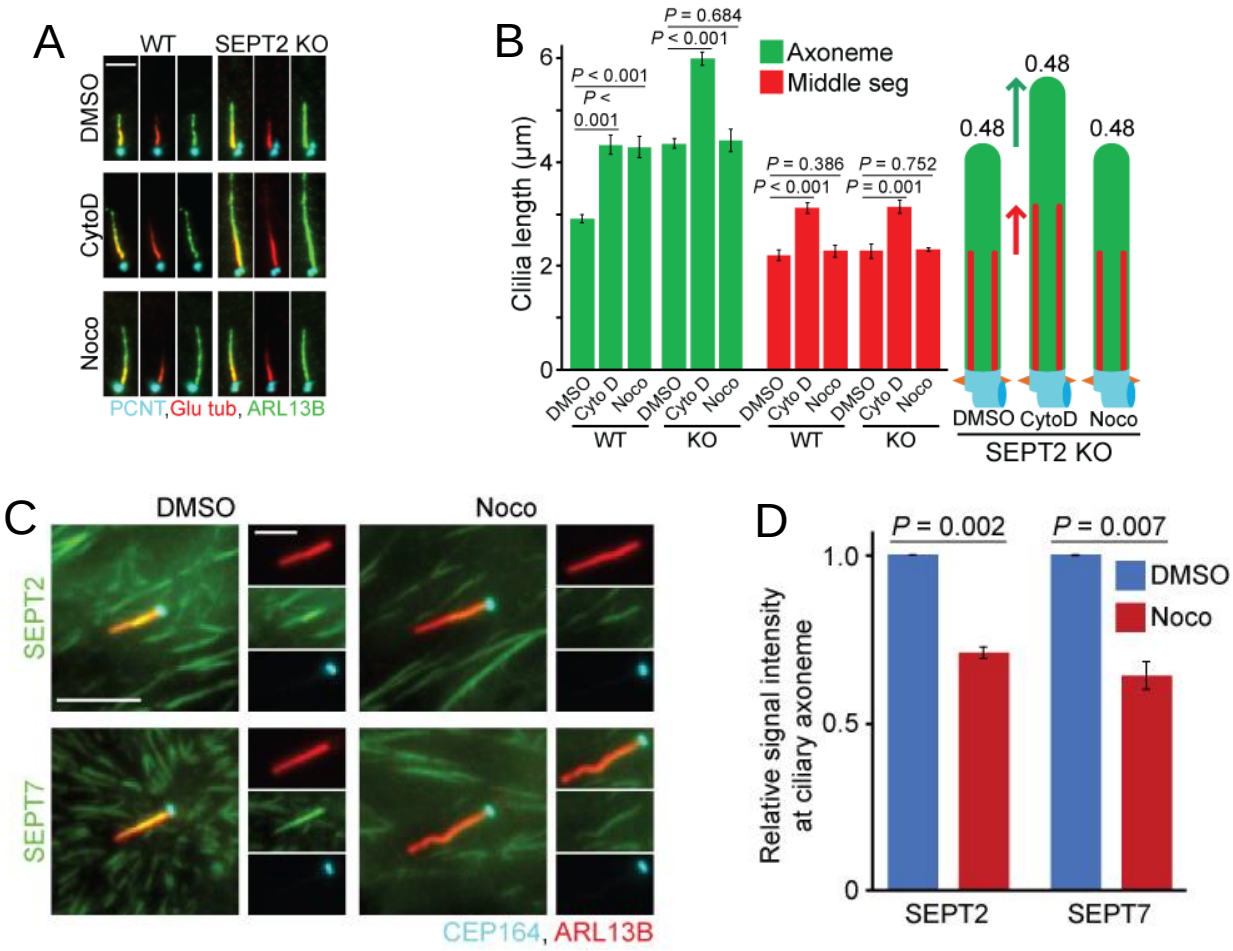

Figure. 23: Nocodazole treatment reduces endogenous SEPT2 and SEPT7 level at cilia in RPE1 cells. A. Actin and microtubule polymerization inhibitors change the cilia segmentation in RPE1 WT and SEPT2 KO cells. Scale bar is 3 μm. **B.** Average length of the middle segment and whole cilia after 3 h indicated chemicals, from **A** with the model. Number on the model shows the ratio of the distal segment/whole cilia. **C.** Endogenous SEPT2 and SEPT7 level at cilia are reduced by 3 h nocodazole treatment in RPE1 WT cells. Scale bar: 5 μm (large) or 2.5 μm (small). **D.** Average relative signal intensity of endogenous SEPT2 or SEPT7 from axoneme from **C**. SEPT2 or SEPT7 signal is quantified from whole cilia then averaged by cilia length. **B** and **D** data is from three times independent experiments quantified 100 cilia each. **B** and **D** data include meaning St.dev. and *P* values are calculated by two-tailed unpaired student t-test.

3.8 Depletion of Sept2 and Sept7 increased the length of the distal segment in NIH3T3 cells.

To open up the story of Septin role in primary cilia, I also tested NIH3T3 cells in the condition of Sept2 or Sept7 gene depletion. Four sets of an siSept2 or siSept7 pool clearly dropped endogenous Sept2 or Sept7 protein levels, respectively (Figure. 24A). Different from RPE1 cells, the percentage of ciliogenesis did not change in NIH3T3 cells with Sept2 or Sept7 depletion, but single Sept2 or 7 depleted cells elongated only the distal segment as in

the results for loss of SEPT2 in human cells (Figure. 21, 22, 24B, 24D). Moreover, application of CytoD extended elongation of both segments in the control and Sept2 KD NIH3T3 cells but had no additional effect with nocodazole (Figure. 24E, F).

Combining this with all Septin data from RPE1 and NIH3T3 cells, I can suggest that Septin is one of the negative regulators of distal segment growth.

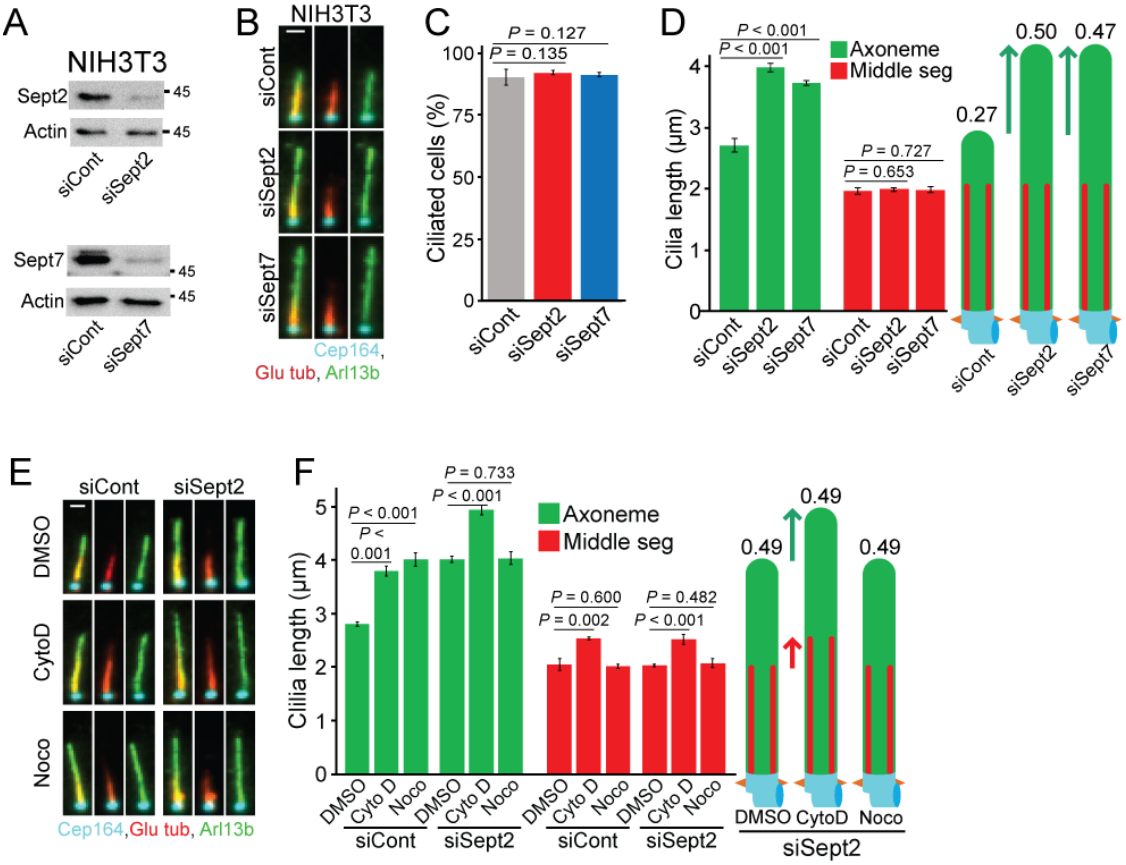

Figure. 24: Sept2 and Sept7 depletion in NIH3T3 cells increase the distal segment length as in RPE1 cells. A. The efficiency of Sept2 or Sept7 depletion is proven by immunoblot. Actin is used as a loading control. **B.** Loss of Sept2 or 7 elongates the length of only the distal segment in NIH3T3 cells. Scale bar is 1 μm. **C.** Percentage of ciliated cells shows no effect from Septin gene depletion in NIH3T3 cells. **D.** Average length of the middle segment and whole cilia, from **B** with the model. Number on the model shows the ratio of the distal segment/whole cilia. **E.** Actin and microtubule polymerization inhibitors affect differently in control or Sept2 KD NIH3T3 cells. Scale bar is 1 μm. **F.** Average length of the middle segment and whole cilia, from **E** with the model. Number on the model shows the ratio of the distal segment/whole cilia. **C, D** and **F** data are from three times independent experiments and ≥ 100 cilia are quantified each. **C, D** and **F** data include meaning St.dev. and *P* values are calculated by two-tailed unpaired student t-test.

3.9 Impaired SEPT2 in RPE1 cells changed KIF7 localization at both the tip and base of cilia.

Here, I would like to next identify the molecular mechanism of distal segment growth by Septin. It is previously noted that the Intraflagellar transport (IFT) complex and MT plus-end binding cap protein are able to control the length of cilia (M. He et al. 2014; Prevo, Scholey, and Peterman 2017). The IFT complex is composed of more than ten different proteins and carries to and takes from the cilia building blocks such as membrane proteins, tubulins, and lipids to bipolarly regulate cilia growth (Bhogaraju, Engel, and Lorentzen 2013; Prevo, Scholey, and Peterman 2017). On the other hand, the ciliary cap protein KIF7 binds at distal cilia microtubules to suppress microtubule polymerization (M. He et al. 2014). I expected that Septin influences both or either of these two functions.

To elucidate this, I checked endogenous localization of IFT components: IFT88 and KIF17 or KIF7 in both RPE1 WT and SEPT2 KO cells (Figure. 25A). IFT88 and KIF17 signals at cilia showed no clear difference in both WT and SEPT2 KO cells, but surprisingly, KIF7 signal at the tip of axoneme greatly dropped in SEPT2 KO cells compared with WT (Figure. 25A, B). In addition to, I observed an accumulated KIF7 level at the ciliary base in SEPT2 KO cells (Figure 25A, B). Importantly, KIF7 signal reduction at the tip of cilia and accumulation at the base were reverted when GFP-SEPT2 protein was expressed in SEPT2 KO cells (Figure. 25C, D).

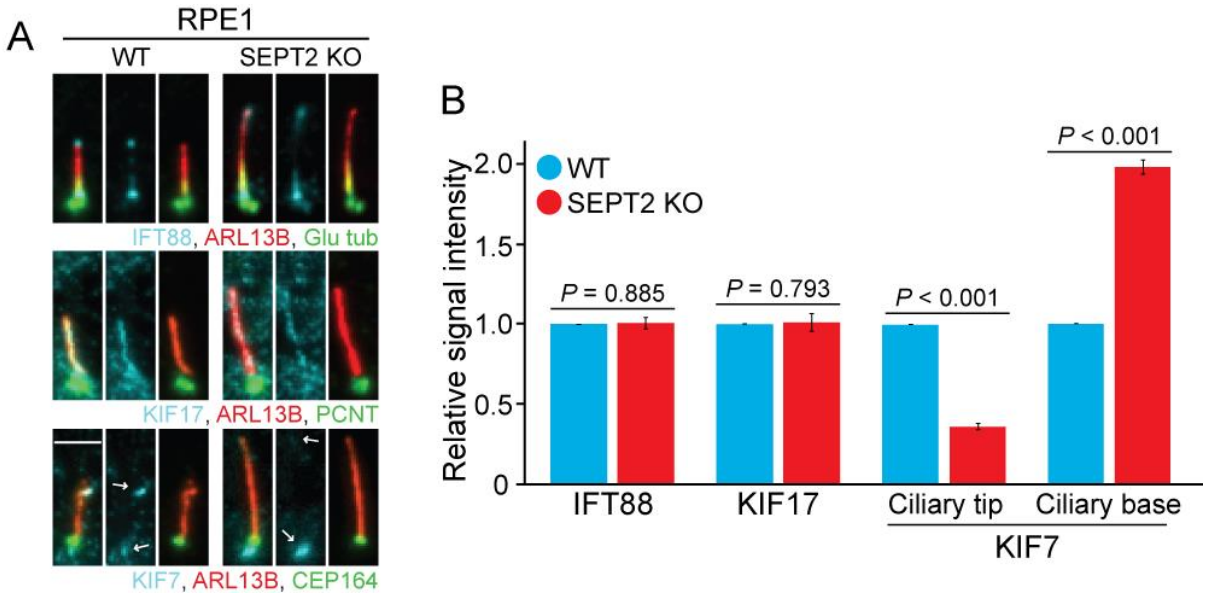

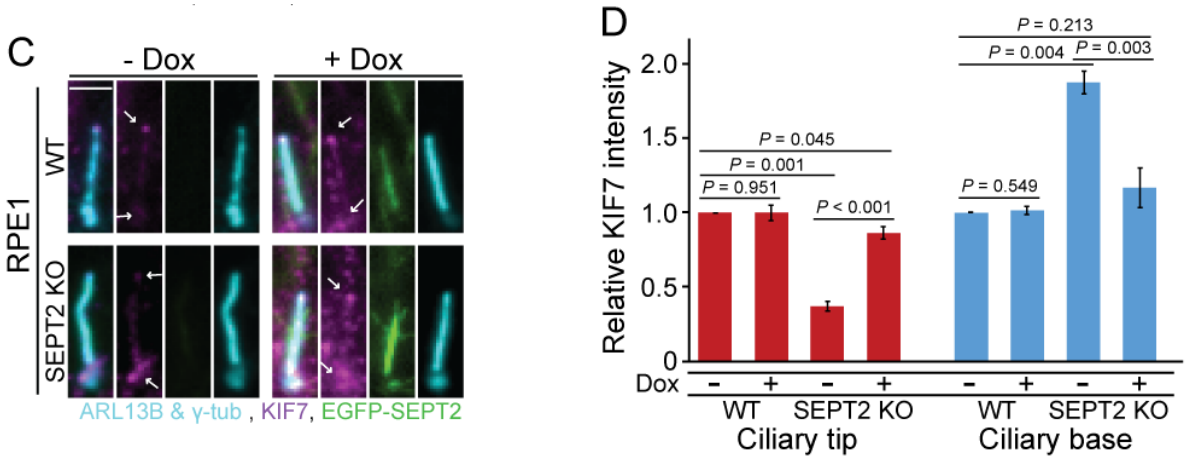

Figure. 25: A ciliary cap protein KIF7 decreases at the tip of cilia in RPE1 SEPT2 KO cells. A. Localizations of IFT complex proteins and a ciliary cap protein in RPE1 WT and SEPT2 KO cells. Scale bar is 3 μm. **B.** Average relative signal intensity of indicated proteins from **A**. Integrated total IFT88 and KIF17 signal are measured at the whole cilia then divided into cilia length. KIF7 signal intensity is quantified at the tip and base of cilia. **C.** KIF7 specific localization at cilia is rescued by the expression of GFP-SEPT2 in SEPT2 KO cells. Scale bar is 2 μm. **D.** Average relative signal intensity of KIF7 from **C**. KIF7 signal intensity is quantified at the tip and base of cilia. **B** and **D** data are from three times independent experiments and > 80 cilia are quantified each. **B** and **D** data include meaning St.dev. and *P* values are calculated by two-tailed unpaired student t-test.

3.10 KIF7 loss induced distal segment over-growth in RPE1 WT cells but not SEPT2 KO.

It is indicated that Septin is a novel factor for KIF7 positioning at cilia and KIF7 is the factor in the regulation of cilia length. I next depleted the KIF7 protein in both RPE1 WT and SEPT2 KO cells to check cilia elongation. If KIF7 works with Septin to regulate the distal segment growth, KIF7 KD in WT cells would phenocopy SEPT2 KO but no additional effects would be seen in SEPT2 KO cells. Importantly, both the tip and base KIF7 signals were dropped by KIF7 siRNA treatment in WT cells and there was no clear difference in the total ciliated cells (Figure. 26A-C). KIF7 single depletion in RPE1 WT cells dramatically elongated only the distal segment as in SEPT2 KO cells, but there was no significant effect in SEPT2 KO cells with KIF7 depletion (Figure. 26D, E).

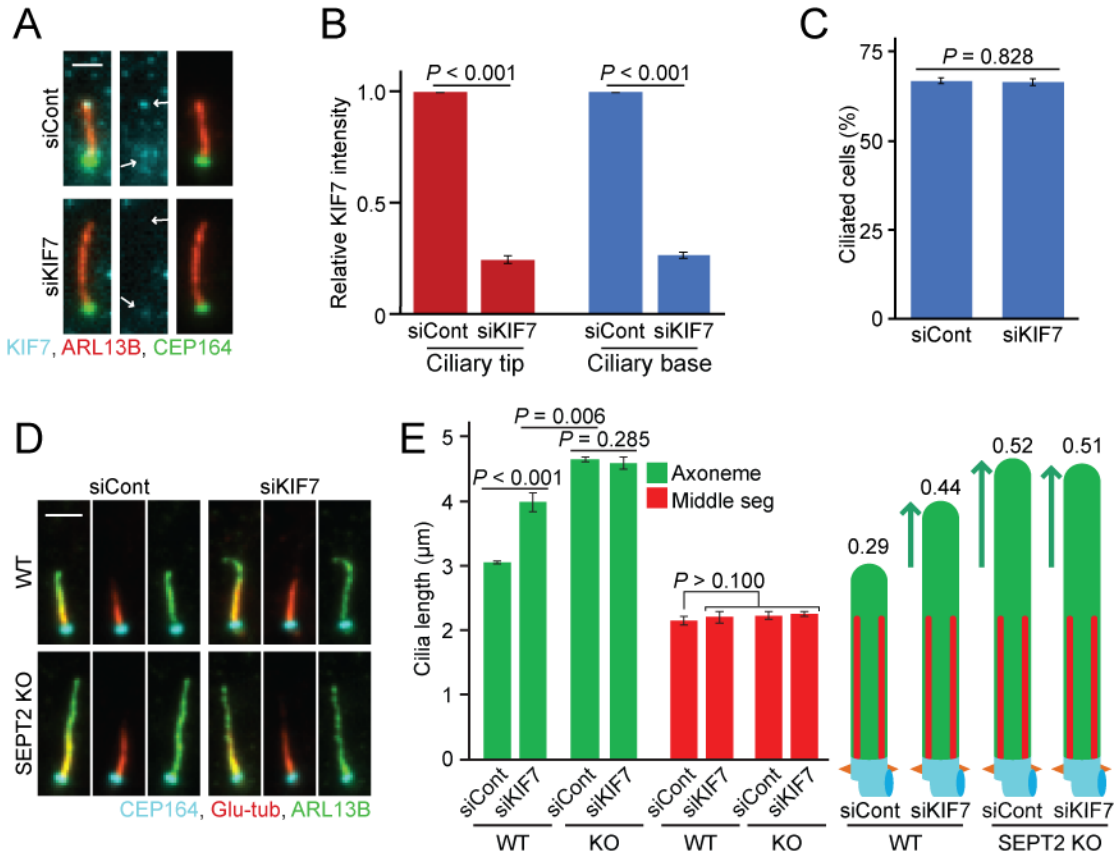

Figure. 26: Depletion of KIF7 elongates only the distal segment in RPE1 WT cells but has no additional cilia effects in SEPT2 KO. A. KIF7 signal intensity is obviously dropped at both the tip and base of cilia in KIF7 depleted RPE1 cells. Scale bar is 1.5 μm. **B**. Average relative signal intensity of KIF7 at cilia from **A**. **C**. KIF7 KD does not affect the average percentage of ciliated cells. **D**. Loss of KIF7 increases the length of the distal segment in WT RPE1 cells but not SEPT2 KO cells. Scale bar is 2 μm. **E**. Average the length of the middle segment and whole cilia from **D** with the model. Number on the model shows the ratio of the distal segment/whole cilia. **B**, **C** and **E** data are from three times independent experiments and > 60 cilia are quantified each. **B**, **C** and **E** data include meaning St.dev. and *P* values are calculated by two-tailed unpaired student t-test.

3.11 Reduction of Kif7 at the distal cilia tip is a key to controlling the distal segment in NIH3T3 cells.

KIF7 data in human ciliated cells strongly suggests that Septin is linked to KIF7 in the regulation of distal segment growth. I investigated Kif7 localization in NIH3T3 cells under the depletion of Sept2, Sept7, and Kif7. As previously described (M. He et al. 2014), Kif7 was only observed at the tip of cilia in NIH3T3 cells (Figure. 27A). Kif7 KD strongly reduced the signal of Kif7 at the tip and Sept2 and Sept7 depletion also dropped Kif7 levels (Figure. 27A, B). Kif7 depletion did not change the total ciliated cells but the distal segment length was stretched (Figure. 27C-E). Furthermore, double depletion of Kif7 and Sept2 or Sept7

presented no significant change in distal segment length compared with each single depletion (Figure. 27C-E).

From all the KIF7 results, I concluded that KIF7 requires Septin for its localization at the distal tip to control the distal segment growth in both human and mouse cells.

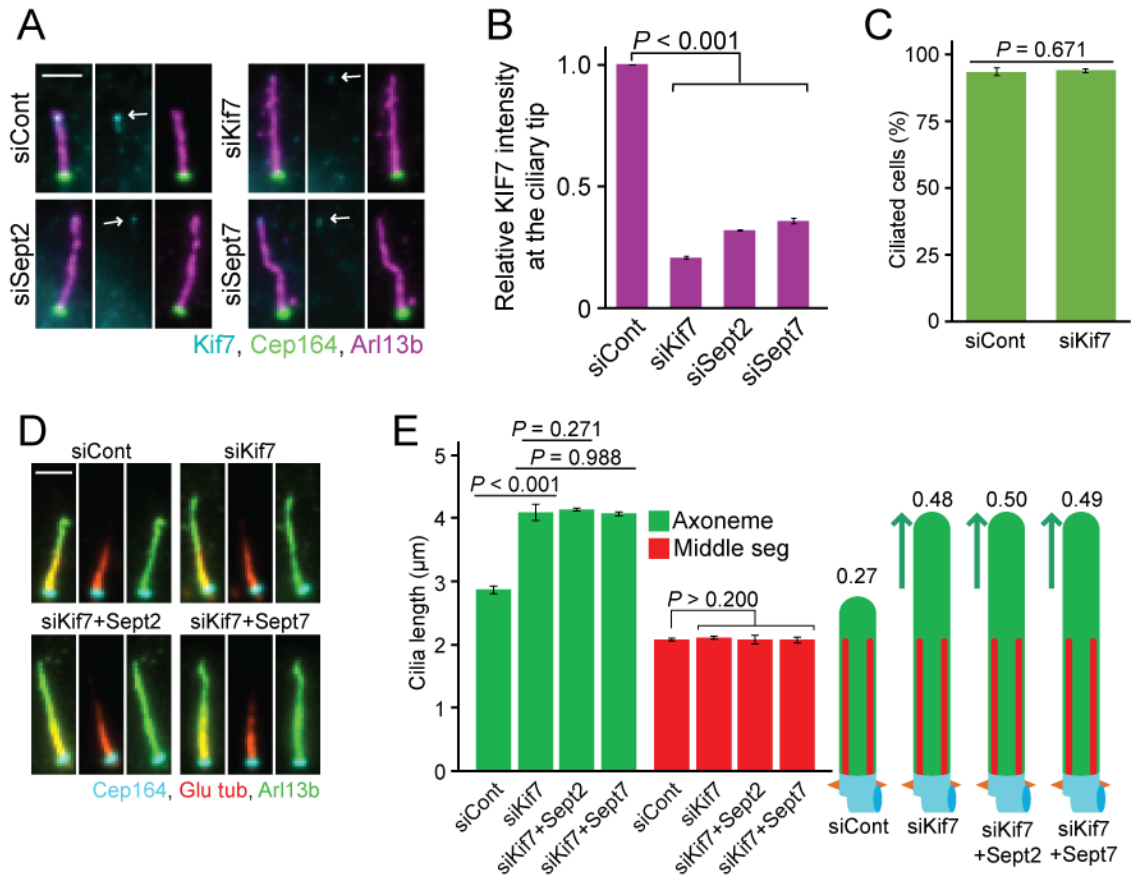

Figure. 27: NIH3T3 cells without Kif7 raise the distal segment elongation. A. Kif7 signal intensity is obviously dropped at the ciliary tip in the condition of Kif7-, Sept2- or Sept7-depletion. Scale bar is 2 μm. **B**. Average relative signal intensity of Kif7 at the tip of axoneme from **A**. **C**. The percentage of ciliated cells shows no difference in either Kif7 depletion or control NIH3T3 cells. **D**. Kif7, Sept2, or Sept7 single KD elongates only the length of distal segment but no additional effect double depletion of Kif7 and Sept2 or Sept7 in NIH3T3 cells. Scale bar is 1.5 μm. **E**. Average length of middle segment and whole cilia from **D** with the model. Number on the model shows the ratio of the distal segment/whole cilia. **B, C** and **E** data are from three times independent experiments and ≥ 100 cilia are quantified each. **B, C** and **E** data include meaning St.dev. and *P* values are calculated by two-tailed unpaired student t-test.

3.12 A functional transition zone is required for positioning KIF7 at the cilia tip to balance distal segment elongation.

Looking carefully at ciliary KIF7 localization in SEPT2 KO RPE1 cells, KIF7 was highly condensed around the ciliary base (Figure. 25A). I hypothesized that KIF7 transportation is

disrupted by dysfunction of the basement structure, especially the transition zone (TZ). It has been well defined that the TZ is a multi-protein complex which localizes at the ciliary base and contributes to cilia growth (Garcia-Gonzalo and Reiter 2017; Takao and Verhey 2016). The TZ works as a gatekeeper in cilia, like the nuclear pole complex for the nucleus, and is able to select only cilia-related products for cilia growth for transport into cilia (More detail found in the introduction). I picked three major TZ components: MKS3, CEP290, and NPHP1 (Gonçalves and Pelletier 2017) to check their localization pattern changes between WT and SEPT2 KO RPE1 cells. MKS3 was localized at the ciliary base nearly overlapping with the distal appendage protein CEP164 in WT cells, but dramatically elongated into the axoneme in SEPT2 KO cells (Figure. 28A, B). MKS3 mis-localization in SEPT2 KO cells was also observed by STED microscopy (Figure. 28C). The CEP290 signal at the base of cilia was expanded to outside of the TZ in SEPT2 KO cells (Figure. 28A, D). On the other hand, the NPHP1 signal at the TZ and the distal and subdistal appendages protein CEP164 and ODF2 respectively did not show any clear difference between WT and SEPT2 KO cells (Figure. 28A, D). It is worth noting that the irregular MKS3 and CEP290 localization patterning in SEPT2 KO cells were recovered by GFP-SEPT2 expression (Figure. 28E-G). Combined these results suggest that Septin has a crucial role to MKS3 and CEP290 positioning.

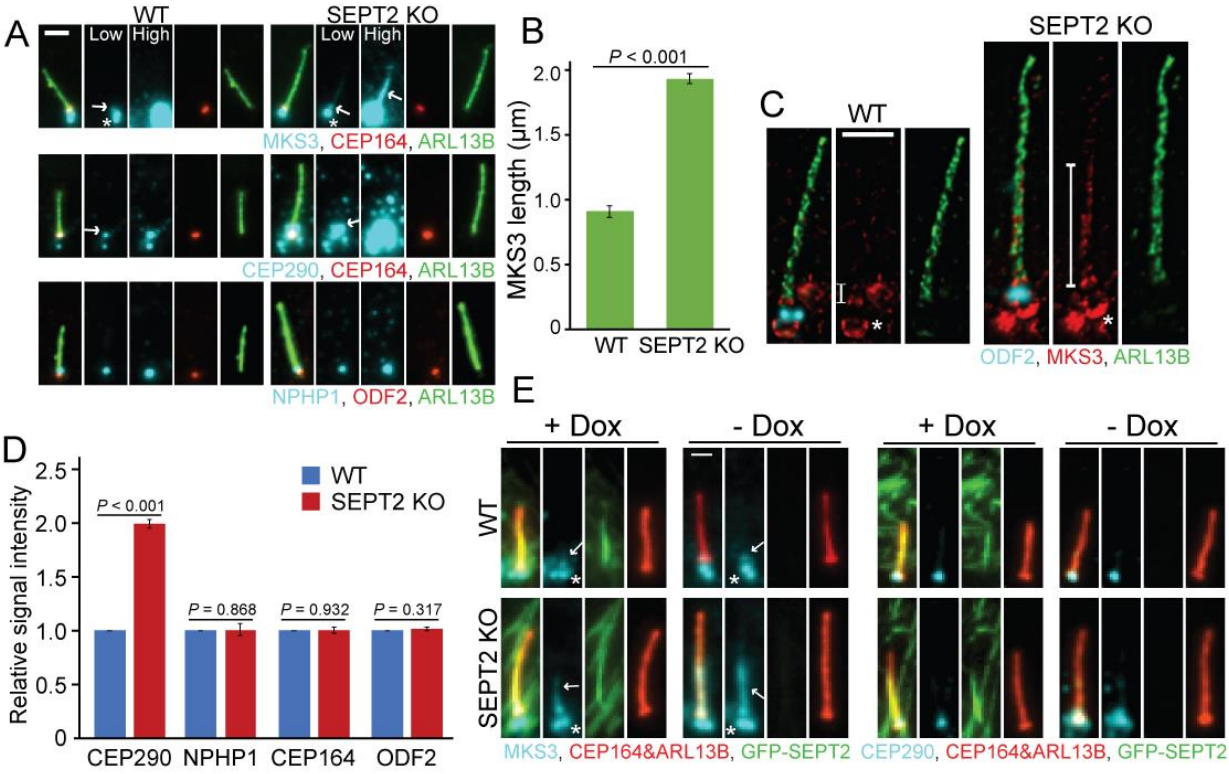

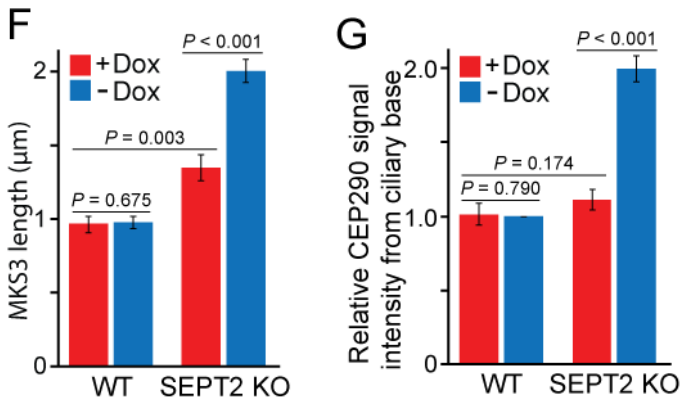

Figure.28: The localization of several transition zone (TZ) proteins is disrupted at the ciliary base in RPE1 SEPT2 KO cells. A. Localization of the TZ, distal appendages (DA) and sub-distal appendages (SDA) proteins in RPE1 WT and SEPT2 KO cells. Scale bar is 1.5 μm. White arrows show specific MKS3 signals and white stars point unspecific signals. Each TZ protein represents both low and high brightness. **B.** Average length of MKS3 at cilia from **A. C.** Stimulated emission depletion (STED) microscopy shows MKS3 mis-localization in SEPT2 KO cells. Scale bar is 1 μm. **D.** Average signal intensity of indicated proteins at the base of cilia from **A. E**. MKS3 and CEP290 mis-localization are rescued by the expression of GFP-SEPT2 in SEPT2 KO cells. Scale bar is 1 μm. **F.** Average length of MKS3 at cilia from **E. G.** Average signal intensity of CEP290 at the base of cilia from **E. B, D, F** and **G** data are from three times independent experiments and 100 cilia are quantified each. **B, D, F** and **G** data include meaning St.dev. and *P* values are calculated by two-tailed unpaired student t-test.

I hypothesized that the over-elongation of MKS3 and the expansion of CEP290 at the base of cilia in SEPT2 KO cells results in a weakened function of the TZ leading to KIF7 reduction at the ciliary tip. To demonstrate this idea, I impaired the TZ structure by depletion of MKS3 or CEP290 in RPE1 WT and SEPT2 KO cells to check cilia segmentation patterning and KIF7 localization. MKS3 or CEP290 protein signal was faded more than 60 % at the TZ under the condition of MKS3 or CEP290 depletion in WT cells (Figure. 29A, B). The total number of ciliated cells had no significant change in WT and SEPT2 KO cells with MKS3 or CEP290 depletion (Figure. 29C). Loss of MKS3 or CEP290 elongated only the distal segment in WT cells, however there was no more elongation in SEPT2 KO cells (Figure. 29D, E). Furthermore, the KIF7 signal at the cilia tip was dramatically diminished but accumulated at the base in WT cells with MKS3 or CEP290 KD (Figure. 29F,-G).

Next, I checked whether TZ structure also influences cilia segmentation and Kif7 localization in mouse cells. I induced impaired TZ condition by Mks3 depletion and siMks3 clearly dropped the specific Mks3 signals at the TZ (co-localized with Cep164) (Figure. 30A, B). The rate of ciliogenesis in Mks3 depleted NIH3T3 cells was the same as control (Figure. 30C). Importantly, Mks3 single depletion elongated only the distal segment but had no additional effects with Sept2 KD in NIH3T3 cells (Figure. 30D, E). Moreover, impaired TZ

structure via Mks3 depletion reduced Kif7 signal at the distal cilia tip compared with the control (Figure. 30F, G).

These results strongly indicate that Septin supports the formation of a proper TZ structure that allows transport of KIF7 to the ciliary tip, where it regulates distal segment growth.

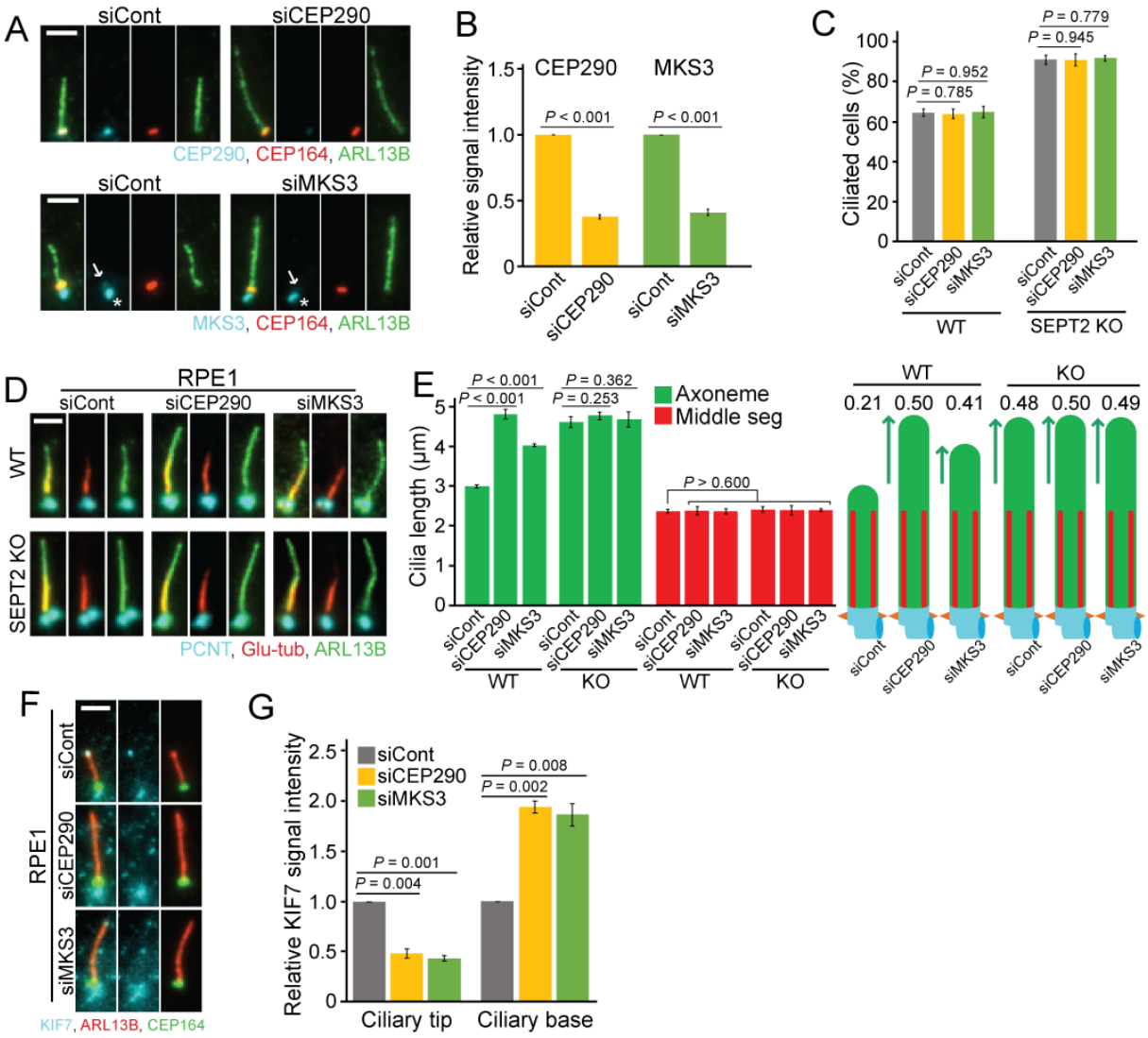

Figure. 29: Depletion of MKS3 or CEP290 only elongates the distal segment and decreases KIF7 transportation to the tip in RPE1 WT but not SEPT2 KO cells. A. siMKS3 or siCEP290 treatment clearly reduces the protein level at the TZ in RPE1 cells. Scale bar is 1.5 μm. White arrow shows specific MKS3 signal and white star points an unspecific signal. **B.** Average signal intensity of indicated proteins at TZ from **A. C.** Percentage of ciliated cells are unchanged in WT and SEPT2 KO cells with MKS3 or CEP290 depletion. **D**. MKS3 or CEP290 KD increases only the distal segment length in WT cells but not SEPT2 KO cells. Scale bar is 2 μm. **E**. Average length of the middle segment and whole cilia from **D** with the model. Number on the model shows the ratio of the distal segment/whole cilia. **F**. KIF7 signal intensity is obviously dropped at the tip but increased at the base

in RPE1 cells with loss of MKS3 or CEP290. Scale bar is 2 μm. **G**. Average relative signal intensity of KIF7 at the base and tip of axoneme change from **F**. **B, C, E** and **G** data are from three times independent experiments and > 60 cilia are quantified each. **B, C, E** and **G** data include meaning St.dev. and *P* values are calculated by two-tailed unpaired student t-test.

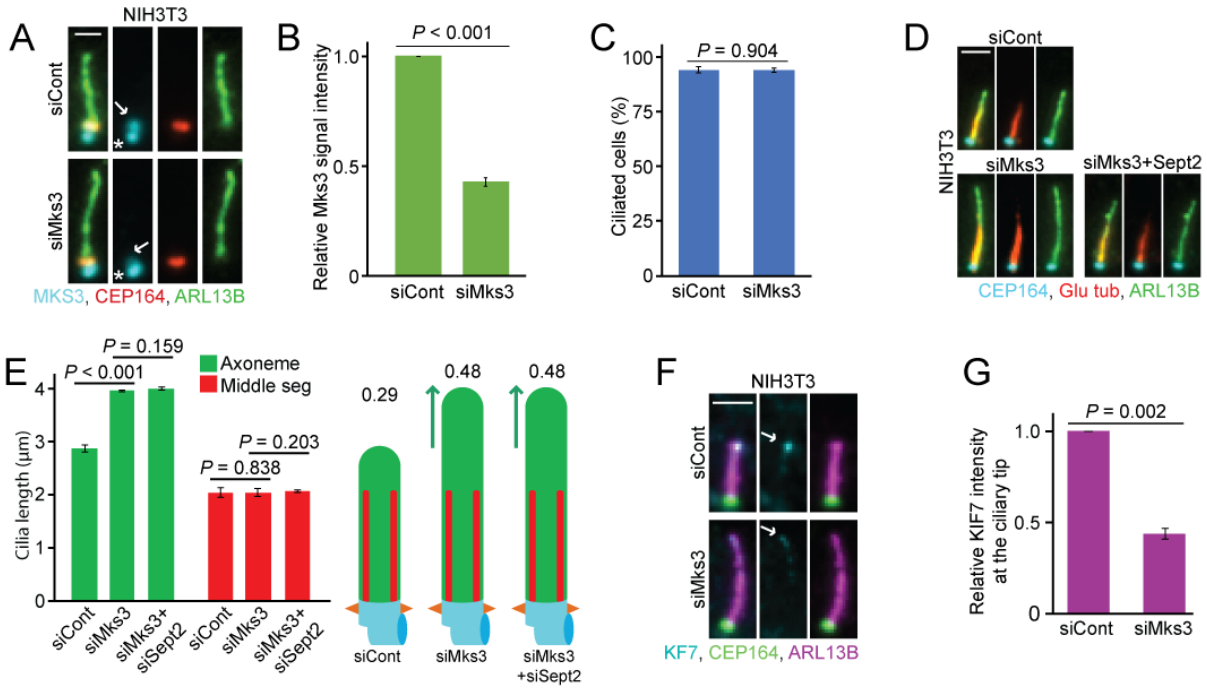

Figure. 30: Impaired TZ by Mks3 depletion in NIH3T3 cells also shows similar cilia phenotypes to those in RPE1 cells. A. siMks3 treatment clearly reduces Mks3 signal at the base of cilia in NIH3T3 cells. Scale bar is 1 μm. White arrow shows specific Mks3 localization and white star points an unspecific signal. **B**. Average specific signal intensity of Mks3 at the TZ from **A. C.** Percentage of ciliated cells are unchanged in NIH3T3 cells with Mks3 depletion. **D**. MKS3 KD increases only the distal segment length in NIH3T3 cells. Scale bar is 2 μm. **E**. Average length of the middle segment and whole cilia from **D** with the model cilia figure. Number on the model shows the ratio of the distal segment/whole cilia. **F**. KIF7 signal intensity at the distal tip is obviously dropped in NIH3T3 cells with Mks3 depletion. Scale bar is 2 μm. **G**. Average relative signal intensity of KIF7 from **F**. **B, C, E** and **G** data are from three times independent experiments and > 70 cilia are quantified each. **B, C, E** and **G** data include meaning St.dev. and *P* values are calculated by two-tailed unpaired student t-test.

3.13 Overgrown-axonemes dynamically change length and lose structural stability.

Septin has an ability to control distal segment growth and organize MKS3, CEP290, and KIF7 localization at cilia in human cells. To gain another insight into the regulation of distal segment control, I generated stable RPE1 WT and SEPT2 KO cells expressing the ciliary axoneme marker ARL13B and the basal body marker gamma tubulin tagged with fluorescent proteins to check cilia dynamics by live-cell cilia imaging. These modulated WT

and SEPT2 KO RPE1 cells can form cilia properly and I first monitored intact cilia dynamics over live-cell imaging in time intervals of 30 mins (total 9.5 h) after 38 h SS (Figure. 31A). In WT cells, cilia constantly maintained their length around 3 µm throughout live-cell imaging and total axonemal growth speeds were nearly balanced, but on the other hand in SEPT2 KO cells, cilia drastically elongated and shortened (Figure. 31B, C). These live-cell imaging results implied that in the absence of Septin, primary cilia lose the ability of constant cilia length maintenance.

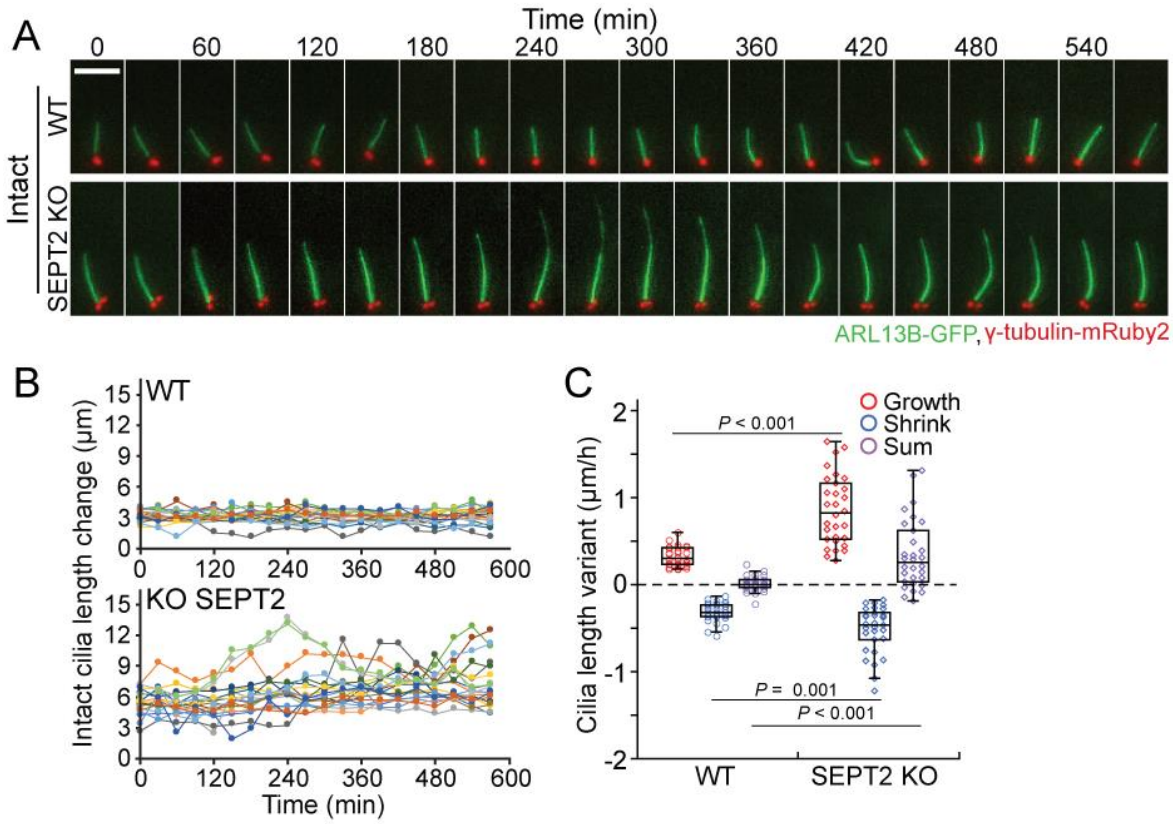

Figure. 31: RPE1 SEPT2 KO cells lose the control of cilia length maintenance in live cells. A. Time-lapse images of intact cilia dynamics changes in RPE1 WT and SEPT2 KO cells after 38 h SS. (30 mins interval, up to 9.5 h). Scale bar: 5 µm. **B.** The length of intact cilia changes during time-lapse imaging from **A**. **C.** The average speed of intact cilia length changes, from **A**. Red, blue and purple dots show growth, shrink and sum (growth + shrink) speed in respectively. **B** and **C** data are n = 30 cilia from 3 independent experiments. **C** data include mean St.dev. and *P* values are calculated by unpaired Wilcoxon-Mann-Whitney Rank Sum Test.

3.14 The balance of the middle/distal segment is essential for maintaining cilia structure to avoid cilia excision events in RPE1 cells.

It is recently reported that live-cell primary cilia sometimes excise their axoneme (cilia excision) or release a small vesicle from the tip of axoneme (ectocytosis) (Nager et al. 2017; Phua et al. 2017; Wang et al. 2019). I next observed cilia excision and ectocytosis during live-cell imaging (Figure. 32A). The rate of ectocytosis was no difference between WT and SEPT2 KO cells, but cilia excision events in SEPT2 KO cells significantly increased compared with WT (Figure. 32B).

To analyze deeper the high incidence of cilia excision events in SEPT2 KO cells, I checked where cilia excision events happened at cilia. I measured the length of cilia at one time-point before the cilia excision event (t = -1) and the remaining cilia length at the time of cilia excision (t = 0) in SEPT2 KO cells (Figure. 32C). Interestingly, most cilia excision occurred at the distal part of cilia (Figure. 32D).

Combining the result of the middle/distal cilia segmentation in SEPT2 KO cells, cilia excision events mainly happen at over-elongated distal segments. Supporting this, previous studies have shown that the distal segment is structurally unstable due to a lower number of axonemal microtubules and fewer tubulin modifications (Bosch Grau et al. 2017; Gadadhar et al. 2017; Sun et al. 2019). Does the risk of cilia excision event change depending on the distal segment length? I observed cilia excision events in RPE1 cells using several cilia segmentation patterns induced by different treatments. First, I depleted KIF7, MKS3, or MAP4, or applied nocodazole in RPE1 cells to induce distal segment over-growth as in SEPT2 KO (Figure. 16, 17, 26. 29). All conditions showed a higher cilia excision rate compared to the control (Figure. 32E, F). Second, I shortened the distal segment length using KIF17 depletion (Figure. 17) and it decreased the rate of cilia excision events (Figure. 32E). Third, I treated cells with siCCP5 or CytoD to elongate both segments but keeping the same segments proportion as the control (Figure. 16). Surprisingly, these conditioned cells showed no significant difference in the incidence of cilia excision compared to control (Figure. 32E, F).

Together these results indicate that maintaining the proper ratio of middle/distal segment is essential for stabilizing the structure of the ciliary axoneme to avoid cilia excision events rather than just distal segment elongation in human cells.

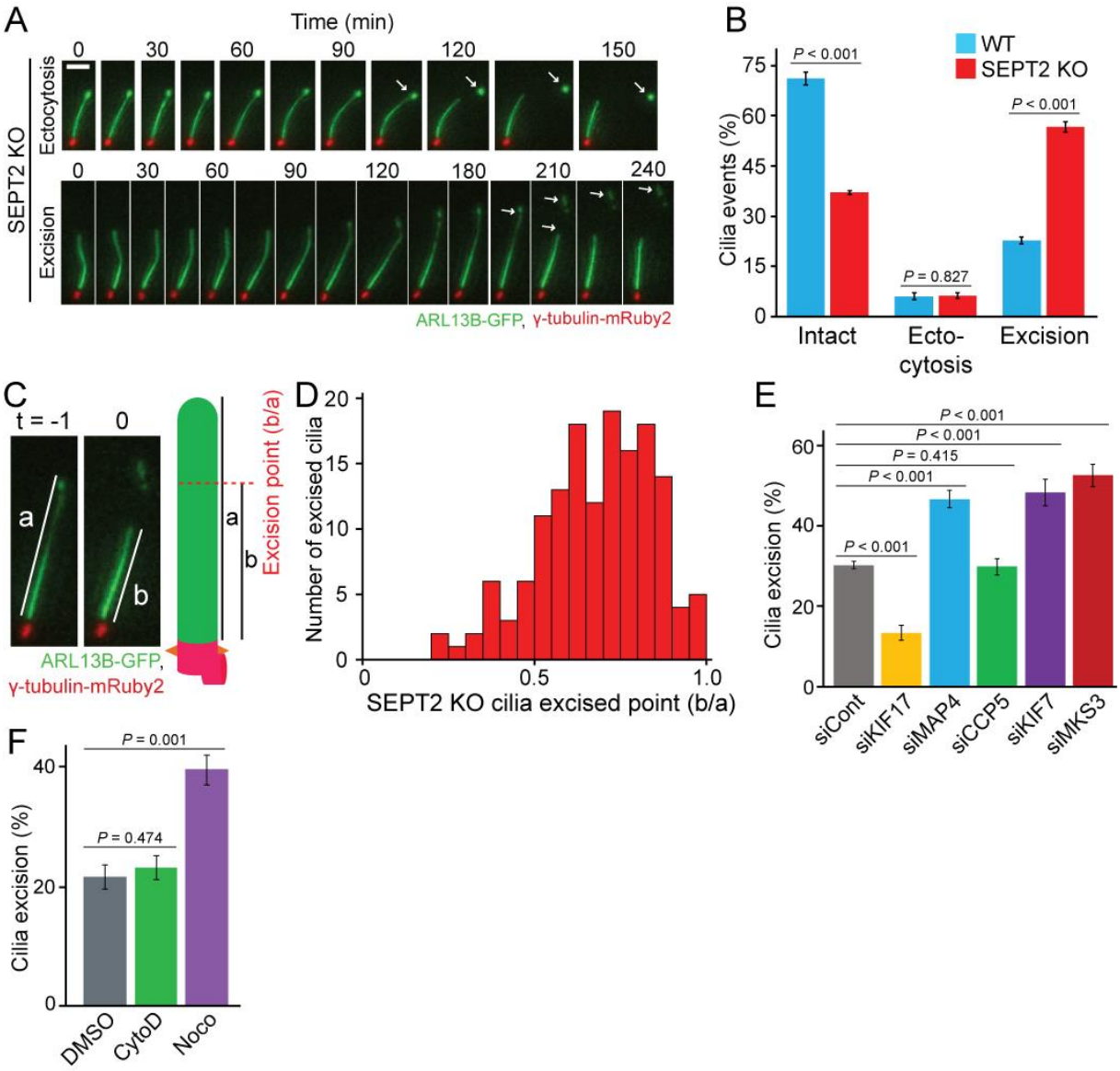

Figure. 32: The incidence of cilia excision events relies on the proportion of the middle/distal segment in RPE1 cells. A. Ectocytosis and cilia excision events of SEPT2 KO RPE1 cells during live-cell imaging. **B**. Percentage of intact cilia, ectocytosis, and cilia excision events during live-cell imaging in WT and SEPT2 KO cells. **C.** Measurement of the place of cilia excision event. The excision point is calculated by b/a ($0 < b/a < 1.0$): one time-point before of cilia excision (t = -1, length = a) and remains axoneme after excision (t = 0, length = b). **D.** Measurement of the cilia excision point in SEPT2 KO cells from **C**. **E.** Percentage of cilia excision changes during live-cell imaging in indicated gene KD in RPE1 cells. **F.** Percentage of cilia excision during live-cell imaging in the condition of indicated chemical treatments in RPE1 cells. **B, E** and **F** data are from three times independent experiments and > 100 cilia are quantified each, and **D** data is from three times independent experiments and 50 cilia are quantified each. **B, E** and **F** data include mean St.dev. and *P* values are calculated by unpaired Wilcoxon-Mann-Whitney Rank Sum Test (**D)** or two-tailed unpaired student t-test (**B**, **E** and **F**).

3.15 Over-elongated distal segment disrupts Shh-related gene upregulation in NIH3T3 cells.

Throughout my PhD study, I have shown that controlling distal segment growth is vital for maintaining cilia structure in mammalian models. The distal segment or distal tip of cilia is known to accumulate signaling-related proteins in a wide range of organisms (Kramer, Moerman, and Inglis 2007; Wheway, Nazlamova, and Hancock 2018). Here, the final question in my project is: what is the importance of the distal segment for the function of primary cilia as a biological signaling receiver?

To answer this, I investigated that Sonic hedgehog pathway (Shh) that requires functional primary cilia for its signal transduction (shown in more detail in the introduction). Functional Shh pathway activity plays an important role in body development and impairment of this pathway causes several ciliopathies (Aguilar et al. 2012b; Kilander et al. 2018; Srivastava et al. 2017). Smoothened (Smo) translocation is a good marker to check the initiation process of the Shh pathway (Nachury 2014; Pedersen, Mogensen, and Christensen 2016). In the stationary state, Smo normally stays at the base of axoneme or cytosolic membrane, under the control of a negative Shh regulator, Pacthed-1 (Ptch) (Figure. 33A left) (Briscoe and Thérond 2013). After the Shh ligand binds Ptch to inhibit its ability, Smo moves to the ciliary membrane to transduce the Shh signal to downstream factors (Figure. 33A right).

From now on, I selected NIH3T3 cells for Shh pathway experiments because this cell line is able to respond to Shh pathway activation nicely (Guo et al. 2018; X. Shi, Zhan, and Wu 2015). I depleted Sept2 or Sept7 to induce the distal segment over-growth, in order to analyze Smo translocation at cilia in NIH3T3 cells after Shh-pathway activation. Sept2 and Sept7 KD cells increased Smo positive cilia faster than the control at each time point (Figure. 33B, C). Moreover, Mks3 depleted cells showed fast Smo accumulation at cilia, but Kif7 depletion had no clear difference compared with the control (Figure. 33D, E). It is expected that the initial step of Shh pathway activation works in NIH3T3 cells generating longer distal segments.

Over-grown distal segment cells are functional whether the final step of the Shh pathway is activated or not. The Shh pathway positively controls Shh related gene expression such as the transcription factors Gli1, 2, 3 and the oncogene Hck, and it is known that Gli1 amplifies its gene expression by a positive feedback loop after activation of the Shh pathway (Fuccillo, Joyner, and Fishell 2006; X. Shi, Zhan, and Wu 2015). Therefore, quantifying the mRNA level of Gli1 by Quantitative PCR (qPCR) is a reasonable way to analyze the level of

the final step of Shh upregulation. The amount of Gli1 mRNA was increased after 4 h and 6 h Shh ligand treatment in both Sept2 KD and control cells, but the cells lacking Sept2 dropped more than half the ability to amplify Gli1 level compared with the control (Figure. 33F). Furthermore, other depletions forming longer distal segments such as Sept7, Kif7, and Mks3 also showed weaker Gli1 mRNA upregulation than the control after 6 h Shh pathway activation (Figure. 33G).

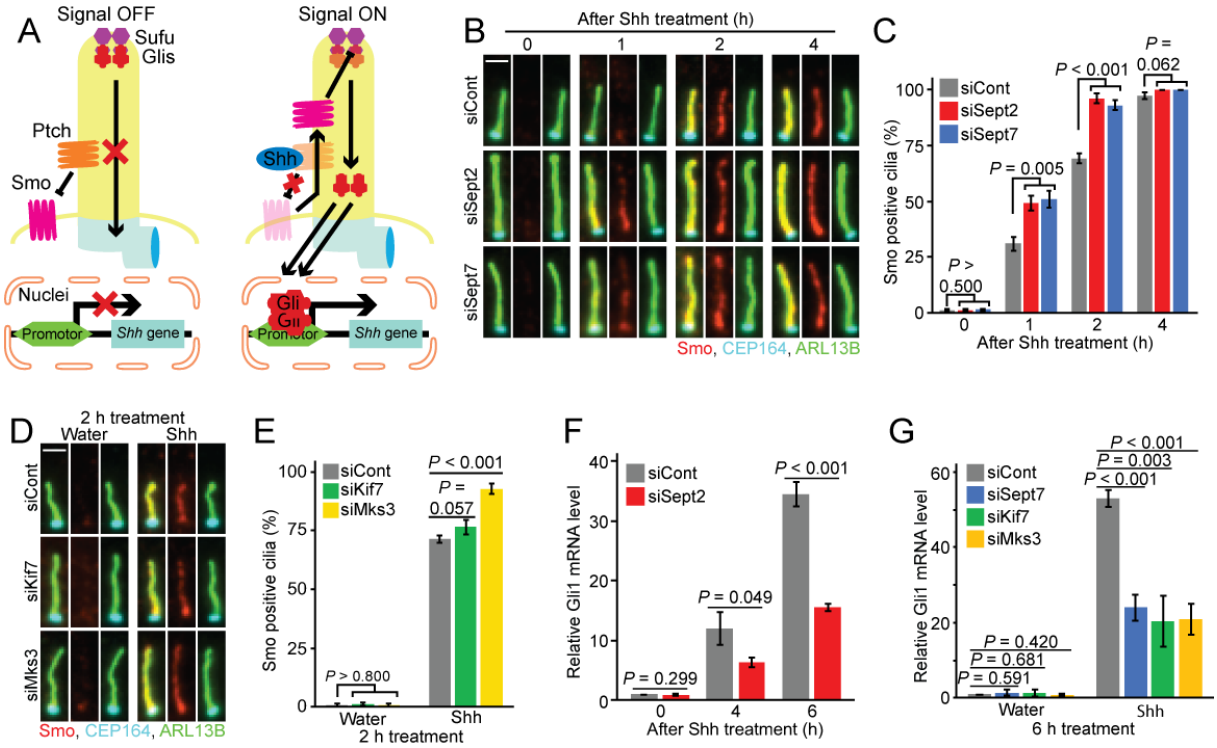

Figure. 33: Longer distal segment cells accelerate Smo translocation but decelerate the gene expression of the Shh pathway in NIH3T3 cells. A. Summary of the ON or OFF state of Shh signaling pathway. See more details in introduction. **B.** Sept2 or Sept7 depleted cells show fast Smo accumulation at cilia after 1, 2, and 4 h Shh treatment. Scale bar is 1.5 µm. **C.** Percentage of Smo positive cilia after 0, 1, 2, and 4 h Shh treatment with indicated siRNA from **B**. **D.** Kif7 or Mks3 depleted cell changes in Smo accumulation at cilia after 2 h Shh or water treatment. Scale bar is 1.5 µm. **E.** Percentage of Smo positive cilia from **D**. **F.** qPCR results represent Gli1 mRNA level upregulation after 0, 4 and 6 h Shh treatment in NIH3T3cells with indicated siRNA treatment. Gapdh is an internal control. **G.** qPCR results represent Gli1 mRNA level upregulation after 6 h Shh treatment in NIH3T3 cells with indicated siRNA treatment. Gapdh is an internal control. **C** and **E** data are from three times independent experiments and > 100 cilia are quantified each. **F** and **G** RNA samples are taken from three independent experiments in the similar condition. **C, E, F** and **G** data include meaning St.dev. and *P* values are calculated by two-tailed unpaired student t-test.

3.16 Intermediate Shh components are reduced at the distal tip in abnormal distal segment cilia.

I hypothesized that a high incidence of cilia excision in unstable distal segment cells causes Shh-related gene upregulation failure. For this, I analyzed intermediate Shh-related proteins that are especially concentrated at the ciliary tip, such as Glis (Gli1, 2, 3) and the suppressor of fused (Sufu) in NIH3T3 cells (Figure. 33A) (Cherry et al. 2013; Haycraft et al. 2005; Li et al. 2012). I observed the ciliary tip Gli3 and Sufu localization changes under the condition of over-grown distal segments in contrast to control cells (Figure. 34A). The amount of Gli3 and Sufu at the tip significantly decreased in cells lacking Sept2, Sept7, Kif7, and Mks3 in comparison to the control (Figure. 34B).

Combined signaling results, I concluded that the reduction of intermediate Shh-components at the distal tip leads to impaired gene upregulation in elongated distal segment cells.

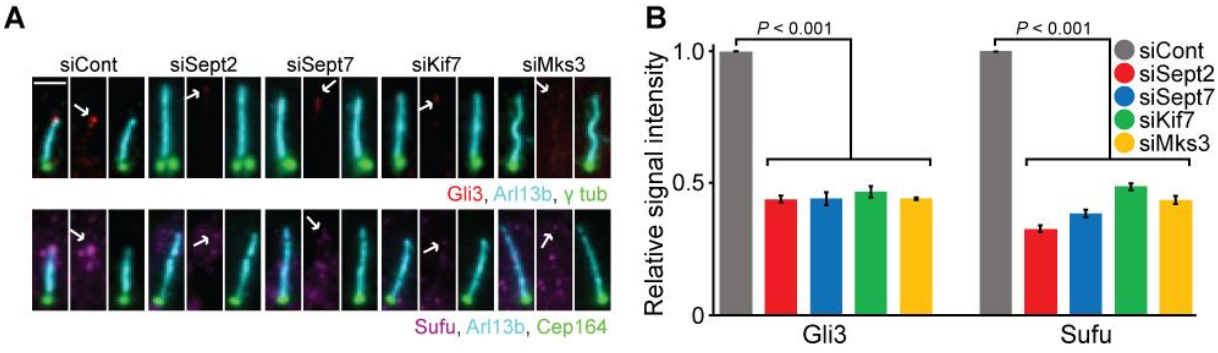

Figure.34: Localization of Shh pathway-related protein Gli3 and Sufu are influenced by the distal segment length. A. The amount of Gli3 and Sufu at the ciliary tip change in NIH3T3 cells with indicated siRNA. Scale bar is 2 μm. White arrows point the specific signals of Gli3 and Sufu at the tip. **B**. Average relative signal intensity of indicated proteins from **A. B** data are from three times independent experiments and 100 cilia are quantified each. **B** data include meaning St.dev. and *P* values are calculated by two-tailed unpaired student t-test.

4. Discussion

Here, I discuss how ciliary segmentation plays an important role in primary cilia structure and function in mammalian cells. The distal segment, which is the signaling domain, is controlled in its growth by Septin. Septin disrupted cells generate over-elongated distal segments and destabilize the ciliary structure leading to higher risk of a cilia excision event and impaired Shh signal transduction.

4.1 The middle/distal cilia segmentation in human and mouse cells

The structure of both motile and immotile cilia in lower eukaryotes such as *C. elegans*, *Chlamydomonas* and *Tetrahymena* are deeper observed than mammalians. These ciliary axonemes are segmented into two domains: the middle segment that gives physical stability and the distal segment that accumulates chemosensory and biological receptors (Cornelia I. Bargmann 2006; Hao et al. 2011; Kramer, Moerman, and Inglis 2007; Snow, Ou, Gunnarson, Regina, et al. 2004; Wloga et al. 2017). Each segment can be distinguished by the different number of side microtubules (doublet: the middle segment, and singlet: the distal segment) and the different tubulin modifications (enriched glutamylation, glycylation, and detyrosination at the middle segment) (Snow, Ou, Gunnarson, Regina, et al. 2004; Wloga et al. 2017). Importantly, some studies using electron microscopy and tomography suggest that this cilia segmentation is also structurally conserved in mouse kidney primary cilia (Flood and Totland 1977; Sun et al. 2019). However, how each segment affects ciliary signaling function is still unclear in mammalian models.

To observe this segmentation in human and mouse cells, I applied an immunofluorescence strategy using different cilia markers such as ARL13B (cilia membrane: whole cilia), acetylated tubulin (doublet/singlet: microtubule whole ciliary microtubule) and glutamylated tubulin (doublet microtubule: the middle segment) (K. He, Ling, and Hu 2020;

Wloga et al. 2017). Measuring the length of glutamylated tubulin and/or whole cilia, I succeeded in distinguishing the middle/distal segment in human RPE1 and mouse NIH3T3 cells (Figure. 14 and 15). Interestingly, the ratio of the distal segment increased in the longer cilia group and later serum starved condition in both cell types (Figure. 14 and 15). My immunofluorescence data supports that cilia segmentation is also conserved in mammalian cells as previously observed by electron microscopy (Flood and Totland 1977; Sun et al. 2019).

4.2 Septin controls distal segment growth to support the transition zone components MKS3 and CEP290 and ciliary cap kinesin KIF7 localization

As long as mammalian primary cilia have this axonemal segmentation, some biological processes must control each segment. To seek this, I next identified the factor regulating the length of distal segment. Through combination of nocodazole treatment with siRNA-based small loss-of-function screening, I found SEPT2 is a repressor for distal segment growth in RPE1 cells (Figure. 17).

Contrary to my results, SEPT2 depletion in mouse or SEPT7 depletion in human cells showed a reduction of ciliogenesis and cilia length (Ghossoub et al. 2013; Hu et al. 2010). I supported my results by multi-Septin depletions and SEPT2 deletion with rescue experiments, electron microscopy, and live-cell imaging (Figure. 20, 21, 22, 31). Still, I would like to discuss the reason why these contradictory data were produced. I thought the cilia length changed easily depending on the experimental set up used to observe longer distal segment growing cells without SEPT2. This is because Septin impaired cells easily broke the cilia structure at the middle (Figure. 31). All previous studies only show indirect immunofluorescence data that are sometimes affected by handling such as washing of coverslips and mounting (Ghossoub et al. 2013; Hu et al. 2010). If cilia are ripped out easily by this physical damage, microscope images will show a reduction in cilia length and even a

lower number of ciliated cells. To support this, when I tried taking electron microscopy images with a collaborator, Dr Annett Neuner, she often got broken cilia images in SEPT2 KO cells when using a high-pressure freezing substitution method. Then we switched to a glutaraldehyde fixation method to cause less stress to the cells and could image the full length of cilia in SEPT2 KO cells (Figure. 21G, H). Therefore, I can probably say that the unstable distal segment elongation in SEPT2 KO cells caused these contradicting results. Furthermore, it indicates that the immunofluorescence results could change easily depending on technically handling.

Interestingly, SEPT2 KO cells lost KIF7 signals at the tip but raised signals at the base of cilia (Figure. 26). Additionally, localization analysis of transition zone (TZ) components showed that SEPT2 KO cells disrupted MKS3 and CEP290 at the base of cilia and led to an impaired TZ due to depletion of each protein (Figure. 28, 29). MKS3 and CEP290 depletion resulted in the distal segment elongation and reduction of KIF7 at the ciliary tip, the same as in SEPT2 KO (Figure. 27, 29). Previous study showed that KIF7 is key to negatively controlling the cilia growth via binding of plus-end ciliary microtubules to halt their elongation (M. He et al. 2014). Combined with my data and previous studies, I would like to propose the model as to how Septin controls distal segment growth (The model. 1).

In WT cells, Septin localizes at cilia, except for the TZ, to support MKS3 and CEP290 proper positioning at the base of cilia. A functional TZ allows KIF7 to pass from the base to the tip, where it binds plus-end ciliary microtubules, thus restricting further distal-end microtubule polymerization to negatively control distal segment growth. In SEPT2 disrupted cells, MKS3 and CEP290 become mis-localized leading to impaired TZ formation. The abnormal TZ cannot transfer KIF7 into the distal cilia tip. At the end, higher free ciliary microtubules can extend without KIF7 suppression, causing excessive distal segment growth.

Why is Septin able to regulate TZ protein localization at cilia? One explanation is that Septin can behave as a membrane diffusion barrier to block MKS3 and CEP290 entry into

cilia. Several studies show that Septin localizes at the plasma membrane to prevent membrane protein translocation to other places (Palander, El-Zeiry, and Trimble 2017; Sandrock et al. 2011; S. Sugiyama and Tanaka 2019). Importantly, MKS3 and CEP290 have membrane binding domains (Drivas et al. 2013; Smith et al. 2006). Therefore, Septin would fill up from the upper TZ to the tip of cilia restricting the entry of the membrane binding TZ components MKS3 and CEP290 to cilia like oil (Septin) and water (MKS3 and CEP290) (The model. 1 left). To support this idea, NPHP1 does not have membrane binding domain (Mollet et al. 2005) neither a significant localization change at the TZ between WT and SEPT2 KO cells (Figure. 28A, B).

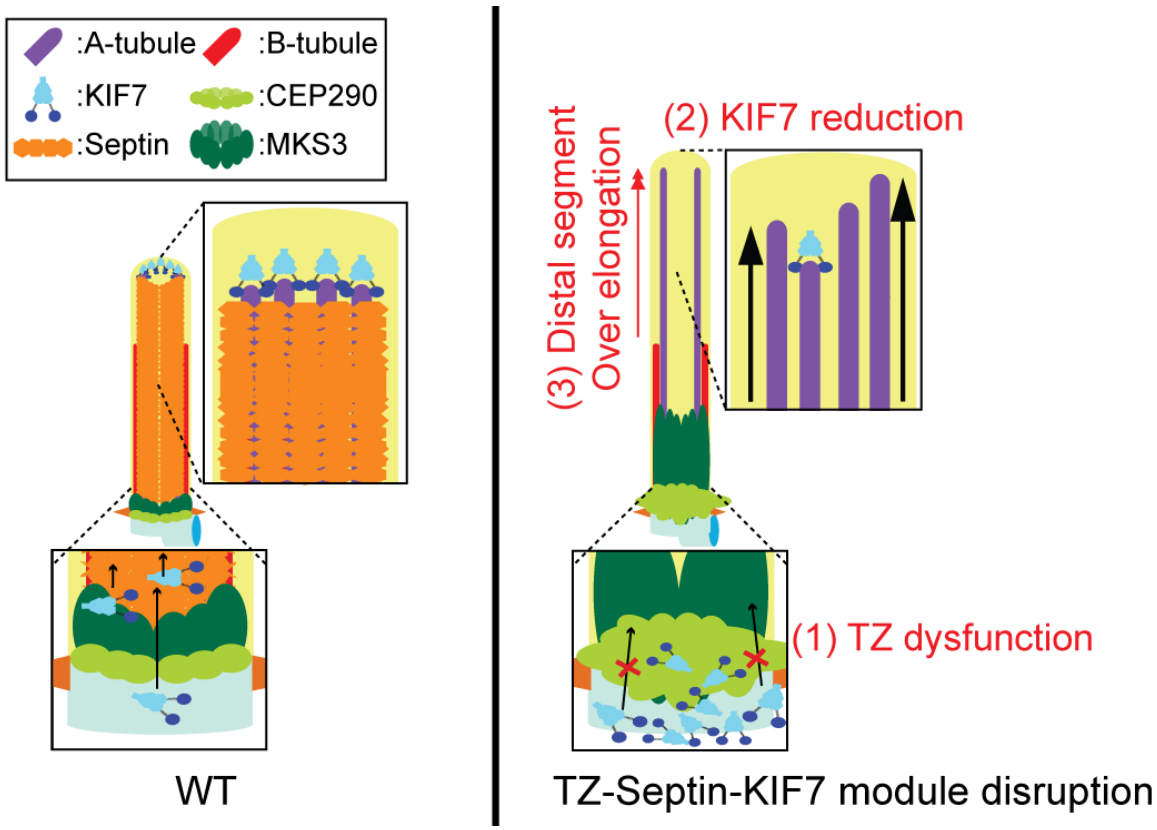

Model 1: The molecular mechanism of distal segment growth is controlled by Septin.

In WT cells, Septin is filled up in the whole cilia untill upper part of the transition zone (TZ) supporting MKS3 and CEP290 localization at the base of cilia. Functional TZ allows passing KIF7 to the distal cilia tip. KIF7 binds the plus-end axonemal microtubule to control the distal segment growth. In SEPT2 KO cells, MKS3 and CEP290 mis-localize at the base of cilia to be impaired the TZ

structure (1). KIF7 is blocked at the base of cilia leading to the reduction of KIF7 level at the distal cilia tip (2). The distal segment continuously elongates without the suppression of microtubule growth by KIF7.

4.3 The proportion of the middle/distal segment involves the incidence of cilia excision events.

Septin works as a negative regulator of distal segment growth. Live-cell imaging results showed that SEPT2 KO cells lost the ability to constantly maintain cilia length compared to WT cells (Figure. 31). High variation of cilia length changes also induced cilia excision events at the distal segment in SEPT2 KO cells (Figure. 32A-D). Moreover, the rate of cilia excision correlated with the ratio of the middle/distal segment, which is not only limited by SEPT2 KO. In WT cells, the ratio of distal segment from whole cilia are around 30 % in RPE1 cells (Figure. 16, 17, 22). This ratio increased up to 40-50 % in the distal segment over-elongated conditions such as SEPT2 KO, MAP4, KIF7, and MKS3 KD, and nocodazole treatment, which caused a high incidence of cilia excision events (Figure. 32B, E, F). On the other hand, the short distal segment condition induced by KIF17 KD reduced cilia excision and even longer cilia, but maintenance of the same proportions of each segment by CCP5 KD or CytoD treatment kept the same cilia excision rate as in the control (Figure. 32E, F). Moreover, previous studies indicate that the distal segment is structurally instable and fragile because it has a lower number of ciliary microtubules and fewer tubulin modifications which increase microtubule stability (Flood and Totland 1977; Gluenz et al. 2010; K. He, Ling, and Hu 2020; Sun et al. 2019). Therefore, I conclude that the risk of cilia excision event is dependent on the occupation of the distal segment from the whole cilia. When the distal segment is abnormally elongated to reach nearly the half size of the total cilia, cilia structure starts to excise due to its physical instability.

4.4 Balancing distal segment elongation plays an important role in keeping the signaling function of primary cilia.

What I would like to discuss next about my project is how control of cilia segmentation affects the signaling function of primary cilia. There are several signaling pathways that require functional primary cilia such as sonic hedgehog (Shh) and Wnt (Oh and Katsanis 2013; Satir and Christensen 2007; Wheway, Nazlamova, and Hancock 2018 and see the detail in introduction).

Interestingly, the over-grown distal segment cells induced by several gene depletions showed different results in the initial step of Shh signal transduction. Sept2, Sept7, or Mks3 KD NIH3T3 cells accumulated Smo at cilia faster than the control but Kif7 KD cells had no significant change (Figure. 33B-E). This reason is probably whether these depletions affect TZ structure or not. Smo translocates from the plasma membrane to the cilia by passing through the TZ after Shh-pathway activation (Pal et al. 2016; Pedersen, Mogensen, and Christensen 2016; Wheway, Nazlamova, and Hancock 2018). My result strongly indicates that dysfunctional Septin lead to disruption of TZ formation, especially CEP290 and MKS3 in human cells (Figure. 28). A dysfunctional TZ led to an over-grown distal segment due to a KIF7 transportation defect in both human and mouse cells (Figure. 29, 30). Not only KIF7 mis-transportation, but an uncompleted TZ lacking MKS3 or CEP290 by a gene depletion, or loss of Septin would cause Smo aberrant accumulation in Shh active state.

Nevertheless, cells generating longer distal segment cilia commonly responded to the initial step of Shh signal transduction as control cells. On the other hand, the final step of Shh-related gene upregulation was severely disrupted in these cells (Figure. 33F, G). Here, I would like to propose two possibilities for the Shh signal transduction defect in over-elongated distal segment cells using the model figure (The model. 2). The first idea is that a cilia excision event leads to loss of Shh-intermediate components at the distal tip, thereby interrupting signal transduction to downstream factors. Depletion of Sept2, Sept7, Kif7, and Mks3 in

NIH3T3 cells reduced Gli3 and Sufu at the distal cilia tip in NIH3T3 cells (Figure. 34). Once the distal segment is over-extended, these cells often break the cilia structure at the distal tip (Figure. 31, 32). Combining these two results, Glis and Sufu at the distal tip are ripped out by a cilia excision event and fail to transduce the signals, thus the final gene upregulation is reduced in longer distal segment cells (The model. 2 middle). The second idea is that reduction of KIF7 destabilizes the distal tip structure such as Glis and Sufu. It is known that vertebrate KIF7 binds Glis-Sufu complex to support its translocation (Briscoe and Thérond 2013). In mouse fibroblasts, loss of KIF7 impaired the localization of Gli2 and Sufu at the distal tip in both stationary and Shh-active phase (M. He et al. 2014). Importantly, there is evidence that Kif7 both positively and negatively influences Shh signaling components such as Gli2, 3, and Sufu (Cheung et al. 2009; Li et al. 2012; Liem et al. 2009), but KIF7 deletion and defective mutation dramatically drop Shh-related gene upregulation (Asadollahi et al. 2018; Ho et al. 2014; Li et al. 2012). Therefore, I can conclude that over-elongation of the distal segment due to loss of KIF7 at the tip negatively influences Shh-related proteins function to disrupt proper signal transduction (The model. 2 right).

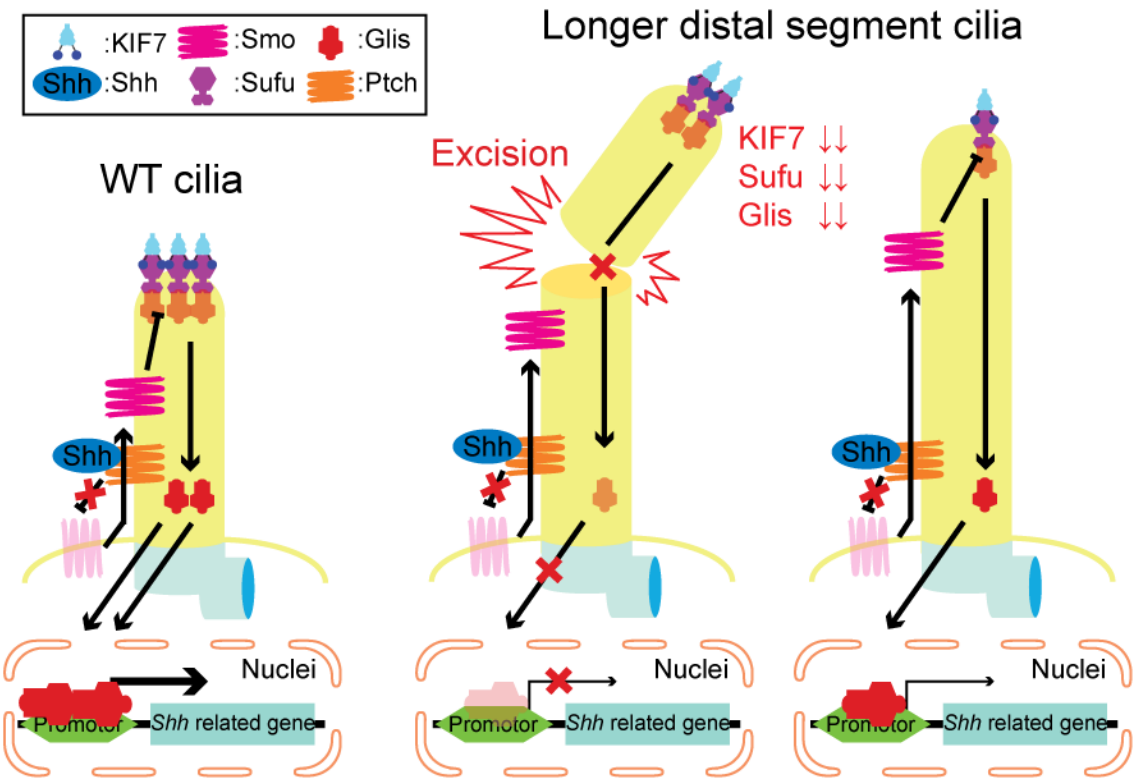

Model 2: The mechanism of Shh signal transduction failure in cells forming longer distal segment primary cilia.

In the active state of Shh pathway in WT cells, Smo translocates into cilia to inhibit Sufu activity. Glis are released at the distal cilia tip and then transfer into the nuclei. Gils finally bind the promotor region to upregulate Shh-related gene expressions. In longer distal segment cilia cells, Smo can be transferred to cilia as the same as WT cells. These cells increase the incidence of cilia excision and decrease the amount of KIF7 at the distal cilia tip. Both results in the reduction of the intermediate Shh-proteins such as Glis and Sufu at the cilia tip. Therefore, Smo often fails to transduce the signal to the downstream factors causing weaker Shh-related gene upregulation.

4.5 Relationship between over-extended distal segment cilia and ciliopathy patient studies

Finally, I would like to link the findings in my PhD project to clinical studies. It is known that several ciliopathy patient cells generate extremely long primary cilia such as in Meckel syndrome, Joubert syndrome, and STAR syndrome (Guen et al. 2016; Ramsbottom et al. 2018; Tammachote et al. 2009). Especially defective mutants of TZ components often

cause Meckel and Joubert syndromes (Ramsbottom et al. 2018; Sang et al. 2011; Sayer et al. 2006; Shimada et al. 2017; Slaats et al. 2016; Tammachote et al. 2009). Interestingly, these patient cells with mutation of MKS3 or CEP290 show dramatically lower Shh-signaling activity and also form longer cilia (Aguilar et al. 2012b; Ramsbottom et al. 2018; Tammachote et al. 2009). However, we are still missing the biological mechanisms as to why longer cilia mutants lose the ability of Shh signal transduction. Appling the ideas of this link between cilia signaling function, cilia segmentation, and excision events to these patients would aid the understanding of the reasons behind these ciliopathy signaling failures. It could perhaps help to improve a clinical treatment to relieve and/or heal these severe genetic diseases at some point in the future.

4.6 Conclusion and Future perspective

Balancing the middle/distal segment is an indispensable ability for keeping the function of primary cilia. With too long a distal segment, it is hard for cilia to maintain themselves leading to breakdown of their structure and loss of vital signaling components at the distal tip of cilia. I strongly believe that the primary cilia field can be slightly opened up by my finding.

For the future approach, It would be interesting to check cilia segmentation in all reported abnormal cilia length phenotypes to see their variations. Moreover, an interesting question would be analyzing how global cilia segmentation patterning is conserved in different tissues such as Neuronal cilia (8-10 μm) and Chondrocyte cilia (2 μm) (Miyoshi et al. 2014; Wann and Knight 2012). Or it would be nice to observe cilia dynamics by live-cell imaging in several ciliopathy patient cells.

Appling the analysis of cilia segmentation and cilia excision events, we will not only gain new insights, but also find attractive biological questions about the primary cilia field.

5. Materials and methods

5.1 The list of siRNAs

Name	**Origin**	**Sequence (5'-3')**	**References**
sihCCP5	Dharmacon	AACAAGCAGAGCAAGCUGUAUUU	(K. He et al. 2018)
Human siCEP290 smart pool	Dharmacon	GGAUUCGGAUGAAAUGAAA GGAAUUGACUUACCUGAUG GAAAGUUAAUGAGCAAUUG GAAGUAGAGUCCCUCAGAA	This study
Mouse siCep290 smart pool	Dharmacon	GCCAAUAAUCAGAUGGAUA AGACUUACCCGAUGGGAUA CGUCCAAACUCCAGAAGAU ACUUAGAGCUGGUGAACGA	This study
Human siDYNC2LI1 smart pool	Dharmacon	GGAAUAAUAUGCCGAAGGA CCAUGUAGACAAAGUGAUA CCUAAUGAUCUCUGGCCCA GGGAAUUAAUGGAAGUGAA	This study
Human siKIF7 smart pool	Dharmacon	GGAUGAUUGAUGUCCGGAA UGCAGGAGCUCGAGCGGAA GCCUGGAGAUCGACGGCAA GCAGAUUGCCUUCUCGGAA	(Schwarz et al. 2017)
Mouse siKIF7 smart pool	Dharmacon	GAGAUUUCCUGGCGGCUUU GGAACUAGGUCGACACAUG GAACUGCGGCUACGCCUAG CCAAGGAGCUGCUGCAUGG	This study
Human siKIF17 smart pool	Dharmacon	GCAACUACUUCCGAUCUAA CGAGAUGUCUGCCGUGGAU CCACAUCCCGUCAUCACAA CGACAUCCCUUUCACCAAG	(Schwarz et al. 2017)

Mouse siKIF17 smart pool	Dharmacon	GGUACGCAGAUGAGCGCAA GAGCAAGAGUCUCGGGUCC AGUAUGAGAUCGCGGUGAA CCGAGCAGAUCUACAACGA	This study
Human siKIF3A smart pool	Dharmacon	CAACUAAUAUGAACGAACA UAUCGUAACUCUAAACUGA GGACCUUUCUCACGUGUAU GGCCAGCAGAUUACAAUUA	This study
sihMAP4_1	Ambion	AACTGGCCAGAAGATACCAAC	(Ghossoub et al. 2013)
sihMAP4_2	Ambion	AAGATAGTCCCAGCCAAGGAT	(Ghossoub et al. 2013)
Human siMKS3 smart pool	Dharmacon	CAUGAAUUCUUACGACUUU GCAGUAAGUGGACGAGAAA CCUUAAAAGAGAAGCGGAA UGACUUAACUGCCGAAGGA	This study
Mouse siMks3 smart pool	Dharmacon	CAAGAGAUUUUCCGAUUUA GCAUAUGGAGAACGUAUUU GCAGUAAGUGGGCGAGAAA GGGCAGACGUUUCAGAUUG	This study
Non-Targeting Control siRNA	Dharmacon	UGUUUACAUGUCGACUAA	This study
sihSEPT2	Dharmacon	AAGGTGAATATTGTGCCTGTC,	(Kremer, Haystead, and Macara 2005)
ON-TARGETplus Mouse siSEPT2 smart pool	Dharmacon	CAAGAAGGUUAGAGGCCGU AGAUAGAGGCUUCGACUGU AGGCAGGGAUUUACGUUUA CAAGAAUGCAAGCGCAGAU	This study
sihSEPT6	Dharmacon	CAGTTTACAGGAGACATATGAGG	(Wei et al. 2014)

sihSEPT7	Dharmacon	GTCGACATTAATCAACTCA	(Ghossoub et al. 2013)
ON-TARGETplus Mouse siSEPT7 smart pool	Dharmacon	GGGAAGCUCAACAGCGUAU GUACAGAAAAUCCGUGAAA AGAAGAUAAAGGACCGUUU CGACAUUAAUCAACUCAUU	This study
ON-TARGETplus HUMAN siSEPT9 smart pool	Dharmacon	CAGAGCGGCUUGGGUAAAU CGCACGAUAUUGAGGAGAA GAGAUGAUCCCAUUUGCUG GCAUCCACUUCGAGGCGUA	This study
sihTTLL5	Dharmacon	AAGUGGAGGAUUAUGGAAACAU U	(K. He et al. 2018)

5.2 The list of primary antibodies

Name	**Host**	**Dilution**	**Company**
Actin	Mouse	WB 1:1000	Chemicon
ARL13B	Rabbit	IF 1:500	Proteintech 17711-1-AP
ARL13B	Mouse	IF 1:50	NeuroMabs
C3B9 (acrtylated tubulin)	Mouse	IF 1:100	Self made
CEP164	Guinea pig	IF 1:500	Self made
CEP290	Rabbit	IF 1:1000	Bethyl via Biomol
Cofilin	Rabbit	WB 1:1000	Abcam ab42824
Gamma tubulin	Rabbit	IF 1:500	Sigma T5192
Gli3	Goat	IF 1:200	P10071 R&D systems
GT335 (polyglutamylated tubulin)	Mouse	IF 1:500	Adipogen
IFT88	Guinea pig	IF 1:200	Self made
KIF17	Rabbit	WB 1:300, IF 1:100	Abcam ab11261

KIF7	Rabbit	IF 1:200	Gift from Kathryn Anderson lab
MKS3	Rabbit	IF 1:1000	Proteintech 13975-1-AP
NPHP1	Mouse	IF 1:20	Gift of Hanswalter Zentgraf lab
ODF2	Guinea pig	IF 1:500	Self made
PCNT	Guinea pig	IF 1:500	Gift from Elmar Sciebel lab
Septin2	Rabbit	WB 1:300, IF 1:250	Proteintech 11397-1-AP
Septin6	Rabbit	WB 1:300	Sigma
Septin7	Rabbit	WB 1:300, IF 1:100	Proteintech 13818-1-AP
Septin9	Rabbit	WB 1:300	Proteintech 10769-1-AP
Smo	Mouse	IF 1:200	Sant Cruz Sc-166685
Sufu	Rabbit	IF 1:100	Proteintech 26759-1-AP

5.3 The list of secondary antibodies

Name	**Host**	**Dilution**	**Company**
Mouse Alexa 350	Goat	IF 1:50	Thermo Fisher Scientific
Mouse Alexa 488	Goat	IF 1:500	Thermo Fisher Scientific
Mouse Alexa 594	Goat	IF 1:500	Thermo Fisher Scientific
Mouse Alexa 647	Goat	IF 1:500	Thermo Fisher Scientific
Rabbit Alexa 488	Goat	IF 1:500	Thermo Fisher Scientific
Rabbit Alexa 594	Goat	IF 1:500	Thermo Fisher Scientific
Rabbit Alexa 647	Goat	IF 1:500	Thermo Fisher Scientific
Guinea pig Alexa 488	Goat	IF 1:500	Thermo Fisher Scientific
Guinea pig Alexa 594	Goat	IF 1:500	Thermo Fisher Scientific
Guinea pig Alexa 647	Goat	IF 1:500	Thermo Fisher Scientific
Goat Alexa 488	Donkey	IF 1:500	Thermo Fisher Scientific
Mouse Alexa 594	Donkey	IF 1:500	Thermo Fisher Scientific

Rabbit Alexa 647	Donkey	IF 1:500	Thermo Fisher Scientific
Mouse Atto594	Goat	STED 1:100	Sigma
Rabbit Star635p	Goat	STED 1:100	Abberior
Mouse HRP conjugated	Goat	WB 1:1000	Jackson ImmunoResearch
Rabbit HRP conjugated	Goat	WB 1:1000	Jackson ImmunoResearch

5.4 The list of Plasmids

Name	**Description**
L13-Arl13bGFP	pFCGW-N1-Arl13b-GFP (Addgene: #40879) for live-cell imaging
pCMV-SPORT Sept7	Full cDNA of hSEPT7 (BC093642.1) is inserted into pENTR221, from Dharmacon
pENTR221 Sept2	Full cDNA of hSEPT2 (BC014455) is inserted into pENTR221, from DKFZ
pENTR223 Sept6	Full cDNA of hSEPT6 (BC009291) is inserted into pENTR223, from DKFZ
pMD2 vsv G	VSV-G envelope expressing plasmid
psPAX2	Lentivirus packaging plasmid
pSH91	pQCXIZ-TUBG1-mRuby2 for live-cell imaging
pTK58	pX458-gSept2-1 (TTCGGTGAACTTGATTGGGG) for Crispr/Cas9 genome knockout
pTK60	pX458-gSept2-22 (CTGACAGTGGTAGATACCCC) for Crispr/Cas9 genome knockout
pTK76	pRetroX Tre3G-PM-Sept7-GFP for siRNA rescue experiment
pTK77	pRetroX Tre3G-PM-GFP-Sept6 for siRNA rescue experiment
pTK82	pRetroX Tre3G-PM-GFP-Sept2 for siRNA and knockout cell lines rescue experiment
pTK99	pMSCV-Blast-mARL13B-N1-mRuby2 for live-cell imaging
pX458	SpCas9-2A-GFP (Addgene accession no. 48138)

5.5 Primer information

Using primers in this study is detailed in AG Pereira's primer collection.

5.6 Bacteria strains

DH5α	F- 80dlacZ M15 (lacZYA-argF) U169 recA1 endA1hsdR17(rk-, mk+) phoAsupE44 -thi-1 gyrA96 relA1	Clontech Palo Alto

5.7 The list of cell lines

RPE1	Human immortalized retinal pigment epithelial cells
RPE1 Tet3G	Tet-ON 3G inducible Expressin System integrated RPE1 cells
NIH3T3	Mouse immortalized fibroblast
HEK293T	Human embryonic kidney cell 293
GP2-293	Manipulated HEK293 cells for retroviral packaging cells that expresses gag and pol genes

5.8 Basic techniques of molecular biology for DNA cloning

In this study, I used manufactured protocols of basic molecular biological techniques.

Name	Description	Company	Protocol
Q5 DNA polymerase	Amplification for DNA flagment	NEB	https://international.neb.com/protocols/2013/12/13/pcr-using-q5-high-fidelity-dna-polymerase-m0491
T4 DNA ligase	Ligating DNA fragments	NEB	https://international.neb.com/protocols/0001/01/01/dna-ligation-with-t4-dna-ligase-m0202
Restriction enzymes	Digests DNA fragment and plasmid	NEB	https://international.neb.com/tools-and-resources/selection-charts/type-iis-restriction-enzymes

Plasmid Mini Kit	Isolation of plasmid DNA from bacteria	Qiagen	http://mpheijden.tripod.com/files/Miniprep.pdf
PCR Purification Kit	Cleaning up DNA fragment after PCR and gel extraction	Qiagen	http://2012.igem.org/wiki/images/a/a3/QIAquick_PCR-purification.pdf

5.9 Culturing mammalian cells

RPE1 cells were grown in DMEM/F12 (Sigma) supplemented with 10 % fetal bovine serum (FBS, Biochrom), 2 mM L-glutamine (Thermo Fischer Scientific) and 0.348 % sodium bicarbonate (Sigma). NIH3T3 cells were cultured in DMEM high glucose (Sigma) supplemented with 10 % new-born calf serum (PAN-Biotech). HEK293T and GP2-293 were cultured in DMEM high glucose supplemented with 10 % FBS. All cell lines were kept in 37 °C and 5 % CO_2.

5.10 Cilogenesis experiment

24000 cells/ml of RPE1 and NIH3T3 cells were maintained in 24-well plate with normal culture condition. After cells were attached on the plate, washed three times by serum-free condition culture medium then start cilia-induction for 8-48 h. For chemical treatment, 48 h serum-starved cells were added 3 h of 100 nM Nocodazole (Sigma), 200 nM Cytochalacin D (Sigma) and/or DMSO (Sigma) as a control.

5.11 siRNA-based gene knockdown

48000 cells/ml of RPE1 and NIH3T3 cells were seeded on 24-well plate with application for Lipofectamine RNAiMAX transfection reagent (Thermo Fischer Scientific) and 20 nM the final concentration of siRNA. siRNA transfection is followed manufactured protocol.

5.12 Generating stable gene-expression cell line by retro and lentivirus integration

RPE1 cells with stably expressing of Arl13b-GFP, Arl13b-mRuby2, Gamma tubulin-mRuby2, doxycycline-inducible EGFP-SEPT2, EGFP-SEPT6, and/or SEPT7-EGFP were generated by using retrovirus- and lentivirus-mediated gene integration. For retrovirus production, GP2-293 cells were transfected packaging plasmid of pMD2.G and stably expressing gene contained plasmid by polyethyleneimine (PEI 25000, Polysciences) method. For lentivirus production, HEK293T cells was transfected packaging plasmid of pMD2.G and psPAX2, and stably expressing gene contained plasmid by PEI method. 2 days after transfection, 4 ml virus contained medium is mixed with 2 ml FBS and 1 ml host cells culture medium. 2 ml of mixed virus medium is applied for 20,000 cells of RPE1 in 6-well plate for 24-48 h. Stable gene integrated cells were sorted by mild level of indicated fluorescent signal using FACS. Expressing doxycycline-induced construct was added 10 ng/ml doxycycline (Sigma) to the cells for 24 h.

5.13 Generation of knockout cell lines by Crispr/Cas9 system

Crispr/Cas9-mediated chromosomal deletion was used for generating knockout SEPT2 cells in RPE1 Tet3G cells. guideRNA targeting human SEPT2 exon 4 (ggggttcgagttcactctgatgg) and 6 (ccggctacggggatgccatcaac) were sub-cloned into pX458. RPE1 Tet3G cells were transfected guideRNA integrated pX458 by Electroporation (Neon® Transfection System) according to the manufacture's protocol. Green-fluorescent positive cells were sorted as a single cell to 96-well plate by using FACS after 24 h transfection. Single cells keep growing in 2 weeks after sorting. First, single SEPT2 knockout candidate cells were selected by immunoblot to check the SEPT2 protein signal gone. Second, whole DNA of immunoblot selection passed cells were isolated and amplified the gene modified locus using PCR to prove the mutated sequences caused early translation-end (see the details of gene modification: Figure. 21A).

5.14 Sonic hedgehog pathway experiment

To activate Shh signalling pathway, 50 pM recombinant Human Shh Protein (in water, R&D systems: 8908-SH-005) was applied for NIH3T3 cells in 0-6 h.

5.15 Live-cell imaging

40,000 cells/ml of RPE1cells stably expressing Arl13b-GFP, and/or Gamma tubulin and/or SEPT2 were cultured in HEPES-buffered DMEM/F12 without phenol red (Thermo Fischer Scientifics) supplemented with 10 % FBS, 1 % L-glutamine and 1 % penicillin–streptomycin (Sigma) in 4-divided round dish. 24 h After cells seeded, culture medium was exchanged to serum-free condition for ciliogenesis induction. Doxycycline-inducible GFP-SEPT2 expressed cells for rescue experiment, 5 ng/ml doxycycline was added cells after seeded till live-cell imaging end. For chemical treatment, 100 nM nocodazole, 200 nM CytoD or DMSO were applied for cells 30min before imaging. Images were acquired as Z-stacks by Nikon Ti-TuCam microscope with a Nikon Plan Apo VC 60x NA 1.4 oil immersion objective and Andor Neo sCMOS camera in every 15 mins for approximately 10 h. Z-stacked maximum intensity projections were created using Nikon NIS-Elements softwwere. The cilia length change and quantification of cilia break were manually analysed using Fiji. Figures were assembled in Adobe Photoshop and Illustrator CS3 (Adobe).

5.16 Immunofluorescence (IF)

Cultured cells on coverslips (No.1.5, Thermo Fischer Scientific) were washed once with PBS then added 3 % paraformaldehyde at room temperature 3 min and/or cold methanol at −20 °C, 5 min for fixation. Fixed cells on the coverslips were mounted 30 min with blocking solution: 3 % BSA (Jackson Immunoresearch), 0.1 % Triton X-100 (Sigma Aldrich) in wet-chamber. Primary antibodies in blocking solution were applied for blocked samples in room temperature ,1 h, wet-chamber. Washing away primary antibodies solution from the samples by PBS, cells were added secondary antibodies in and/or DAPI in blocking solution 30 min at room temperature. Three times washing by PBS for removing exceeded secondary antibodies solution, then coverslips were mounted 4 µl Mowiol solution (EMD Millipore).

5.17 Whitefield microscopy

Whitefield microscope images were acquired as Z-stacks on Nikon NIS-Elements platform using Nikon Ti2 Microscope with Plan Apo λ 100x, 60x or 40x Oil Ph3 DM objectives and Iris 9 A18M631012 camera. Image processing quantification were processed in NIS-Elements and Fiji. For the cilia length, the ciliation rate and Smo translocation into axoneme

were manually analyzed using Z-stacked max-signal intensity projected images. Fluorescence intensities of targeted proteins were manually measured or using Fiji macro program.

5.18 Electron microscopy (collaborated with Dr Annett Neuner)

RPE1 WT and SEPT2 KO cells were seeded on coverslips and cultured at 37 °C and 5 % CO_2 till they reached a density of approximately 80 - 90 %. Both cells were kept 48 h serum starved condition inducing ciliogenesis. Ciliated RPE1 cells were givin to Dr Annett Neuner and she did the following processes. Cells were rinsed with 100 mM PBS 3 times and then fixed with a mixture of 2.5 % GA/1.0 % PFA/ 2 % sucrose in 50 mM cacodylate buffer for 30 min at room temperature. The fixative was washed out with 50 mM cacodylate buffer. After post-fixation with 2 % OsO_4 for approximal 1 h 4 °C and in darkness, cells were rinsed 4 times with dH_2O and incubated overnight at 4 °C in 0.5 % uranyl acetate (in H_20). On the following day coverslips were washed again 4 times with dH_2O and via a dehydration row (40, 50, 70, 80, 90, 95, 100 % ethanol) water was removed by ethanol within the cells. Coverslips were immediately placed on capsules filled with Spurr-resin (Sigma-Aldrich) and polymerized at 60 °C for 24 to 48 h. Embedded cells were sectioned using a Reichert Ultracut S Microtome (Leica Instruments, Vienna, Austria) to a thickness of 80 nm. Post-staining with 3 % uranyl acetate and lead citrate was performed. Serial-sections were imaged at a Jeol JE-1400 (Jeol Ltd., Tokyo, Japan), operating at 80 kV, equipped with a 4k x 4k digital camera (F416, TVIPS, Gauting, Germany). Micrographs were adjusted in brightness and contrast using ImageJ.

5.19 Stimulated emission depletion microscopy (STED)

STED images were acquired as Z-stacks on Leica TCS SP8 STED 3X super-resolution microscope platform mounted on Leica DMi8, inverted microscope with HC PL APO 100x/1.40 STED White Oil objective. The imaging software was controlled by Leica Application Suite 3 (LAS). Image processing and analysis were performed by Huygens deconvolution pro and Fiji.

5.20 Immunoblotting

For immunoblot analysis, cells were added 8 M Urea with benzonase (Sigma, 1:1000 dilution) on room temperature for 1 h to extract the whole cell lysate. The cell lysate was

measured protein concentration by Bradford reagent (Sigma) and the same amount of lysate were loaded to SDS–PAGE. Separated proteins on the gel were transferred onto PVDF membranes, then blocked with 5 % milk in PBST 30 min. The membrane was incubated with primary antibodies in over-night 4 °C. HRP-conjugated secondary antibodies were applied for the membrane 1 h, then the membrane was activated by ECL and processed image.

5.21 RT-PCR

After 48h serum starved NIH3T3 cells with indicated siRNAs were applied for recombinant Shh (50 pM) in 0-6h for the activation of Shh pathway. mRNA was isolated using NucleoSpin® RNA Plus (Machery-Nagel) followed manufactured protocol. 1 µg of Total mRNA was reverse-transcribed into cDNA using SensiFAST^{TM} cDNA Synthesis Kit (Bioline) according to the manufacture's protocol. 100 ng cDNA was analyzed by quantitatively PCR using SensiFAST^{TM} SYBR Lo-ROX Kit (Bioline) and 7500 Fast Real-Time PCR System (Applied Biosystems) followed manufactured protocol.

5.22 Statistics and reproducibility

Statistical analyses for the cilia length measurement, fluorescence-signal intensity measurements, the percentage of ciliated cells quantification, RT-PCR were tested by Wilcoxon test and/or two-tailed Student's t-tests as described in each figure reagent. Significance probability values were $P < 0.05$. Statistical tests were performed in Excel (Microsoft) and KaleidaGraph (Synergy Softwwere). Live-cell imaging experiments were repeated two or three times independently. Electron microscopy and immunoblot were two times biological replicated. STED microscopy results were performed twice at least. All the cilia length measurement, ciliation assay, RT-PCR and signal intensities experiments were performed three times biological replicates independently. Sample sizes were noted in the figure legends.

6. References

Aguilar, Andrea et al. 2012a. "Analysis of Human Samples Reveals Impaired SHH-Dependent Cerebellar Development in Joubert Syndrome/Meckel Syndrome." *Proceedings of the National Academy of Sciences of the United States of America* 109(42): 16951–56.

Asadollahi, Reza et al. 2018. "Clinical and Experimental Evidence Suggest a Link between KIF7 and C5orf42-Related Ciliopathies through Sonic Hedgehog Signaling /631/208/1516 /692/699 Article." *European Journal of Human Genetics* 26(2): 197–209. https://doi.org/10.1038/s41431-017-0019-9 (April 8, 2021).

Baala, Lekbir et al. 2007. "The Meckel-Gruber Syndrome Gene, MKS3, Is Mutated in Joubert Syndrome." *The American Journal of Human Genetics* 80(1): 186–94. https://www.sciencedirect.com/science/article/pii/S0002929707609331?via%3Dihub (July 11, 2019).

Bai, C. Brian, Daniel Stephen, and Alexandra L. Joyner. 2004. "All Mouse Ventral Spinal Cord Patterning by Hedgehog Is Gli Dependent and Involves an Activator Function of Gli3." *Developmental Cell* 6(1): 103–15. https://pubmed.ncbi.nlm.nih.gov/14723851/ (April 22, 2021).

Besschetnova, Tatiana Y. et al. 2010. "Identification of Signaling Pathways Regulating Primary Cilium Length and Flow-Mediated Adaptation." *Current Biology* 20(2): 182–87.

Bhogaraju, Sagar, Benjamin D Engel, and Esben Lorentzen. 2013. "Intraflagellar Transport Complex Structure and Cargo Interactions." *Cilia* 2(1): 10. http://www.ncbi.nlm.nih.gov/pubmed/23945166 (June 7, 2018).

Blacque, Oliver E. et al. 2006. "The WD Repeat-Containing Protein IFTA-1 Is Required for Retrograde Intraflagellar Transport." *Molecular Biology of the Cell* 17(12): 5053–62. https://pubmed.ncbi.nlm.nih.gov/17021254/ (January 18, 2021).

Bosch Grau, Montserrat et al. 2017. "Alterations in the Balance of Tubulin Glycylation and Glutamylation in Photoreceptors Leads to Retinal Degeneration." *Journal of cell science* 130(5): 938–49. http://jcs.biologists.org/lookup/doi/10.1242/jcs.199091%5Cnhttp://www.ncbi.nlm.nih.gov/pubmed/28104815.

Bowler, Mathew et al. 2019. "High-Resolution Characterization of Centriole Distal Appendage Morphology and Dynamics by Correlative STORM and Electron

Microscopy." *Nature Communications* 10(1): 993. http://www.nature.com/articles/s41467-018-08216-4 (May 7, 2019).

Briscoe, James, and Pascal P. Thérond. 2013. "The Mechanisms of Hedgehog Signalling and Its Roles in Development and Disease." *Nature Reviews Molecular Cell Biology* 14(7): 418–31. https://pubmed.ncbi.nlm.nih.gov/23719536/ (April 8, 2021).

van der Burght, Servaas N. et al. 2020. "Ciliary Tip Signaling Compartment Is Formed and Maintained by Intraflagellar Transport." *Current Biology* 30(21): 4299-4306.e5. https://doi.org/10.1016/j.cub.2020.08.032.

Čajánek, Lukáš, and Erich A. Nigg. 2014. "Cep164 Triggers Ciliogenesis by Recruiting Tau Tubulin Kinase 2 to the Mother Centriole." *Proceedings of the National Academy of Sciences of the United States of America* 111(28). https://pubmed.ncbi.nlm.nih.gov/24982133/ (April 22, 2021).

Cherry, Amy L. et al. 2013. "Structural Basis of SUFU-GLI Interaction in Human Hedgehog Signalling Regulation." *Acta Crystallographica Section D: Biological Crystallography* 69(12): 2563–79.

Cheung, Helen Oi Lam et al. 2009. "The Kinesin Protein Kif7 Is a Critical Regulator of Gli Transcription Factors in Mammalian Hedgehog Signaling." *Science Signaling* 2(76): ra29–ra29. https://stke.sciencemag.org/content/2/76/ra29 (July 31, 2020).

Chih, Ben et al. 2012. "A Ciliopathy Complex at the Transition Zone Protects the Cilia as a Privileged Membrane Domain." *Nature Cell Biology* 14(1): 61–72. https://pubmed.ncbi.nlm.nih.gov/22179047/ (January 15, 2021).

Corbit, Kevin C. et al. 2005. "Vertebrate Smoothened Functions at the Primary Cilium." *Nature* 437(7061): 1018–21. https://pubmed.ncbi.nlm.nih.gov/16136078/ (April 22, 2021).

Cornelia I. Bargmann. 2006. "Chemosensation in C. Elegans."

Drivas, Theodore G et al. 2013. "Binding Domains Causes Retinal Degeneration Find the Latest Version : Disruption of CEP290 Microtubule / Membrane-Binding Domains Causes Retinal Degeneration." *The Journal of Clinical Investigation* 123(10): 4525–39.

Echelard, Yann et al. 1993. "Sonic Hedgehog, a Member of a Family of Putative Signaling Molecules, Is Implicated in the Regulation of CNS Polarity." *Cell* 75(7): 1417–30.

Flood, Per R., and Geir K. Totland. 1977. "Substructure of Solitary Cilia in Mouse Kidney." *Cell and Tissue Research* 183(2): 281–90.

Fu, Wenxiang et al. 2016. "Role for the IFT-A Complex in Selective Transport to the Primary Cilium." *Cell Reports* 17(6): 1505–17.

https://www.sciencedirect.com/science/article/pii/S2211124716314048?via%3Dihub (January 16, 2019).

Fuccillo, Marc, Alexandra L. Joyner, and Gord Fishell. 2006. "Morphogen to Mitogen: The Multiple Roles of Hedgehog Signalling in Vertebrate Neural Development." *Nature Reviews Neuroscience* 7(10): 772–83. www.nature.com/reviews/neuro (January 11, 2021).

Funabashi, Teruki et al. 2018. "Interaction of Heterotrimeric Kinesin-II with IFT-B-Connecting Tetramer Is Crucial for Ciliogenesis." https://doi.org/10.1083/jcb.201801039 (July 9, 2018).

Gadadhar, Sudarshan et al. 2017. "Tubulin Glycylation Controls Primary Cilia Length." *Journal of Cell Biology* 216(9): 2701–13.

Garcia-Gonzalo, Francesc R., and Jeremy F. Reiter. 2012. "Scoring a Backstage Pass: Mechanisms of Ciliogenesis and Ciliary Access." *Journal of Cell Biology* 197(6): 697–709.

Garcia-Gonzalo, Francesc R et al. 2011. "A Transition Zone Complex Regulates Mammalian Ciliogenesis and Ciliary Membrane Composition." *Nature Genetics* 43(8): 776–84. http://www.nature.com/articles/ng.891 (April 9, 2019).

Garcia-Gonzalo, Francesc R, and Jeremy F Reiter. 2017. "Open Sesame: How Transition Fibers and the Transition Zone Control Ciliary Composition." *Cold Spring Harbor perspectives in biology* 9(2): a028134. http://www.ncbi.nlm.nih.gov/pubmed/27770015 (April 11, 2019).

Ghossoub, R. et al. 2013. "Septins 2, 7 and 9 and MAP4 Colocalize along the Axoneme in the Primary Cilium and Control Ciliary Length." *Journal of Cell Science* 126(12): 2583–94. http://jcs.biologists.org/cgi/doi/10.1242/jcs.111377.

Gilula, Norton B., and Peter Satir. 1972. "The Ciliary Necklace a Ciliary Membrane Specialization." *Journal of Cell Biology* 53(2): 494–509. http://rupress.org/jcb/article-pdf/53/2/494/1266296/494.pdf (January 15, 2021).

Gluenz, Eva et al. 2010. "Beyond 9+0: Noncanonical Axoneme Structures Characterize Sensory Cilia from Protists to Humans." *The FASEB Journal* 24(9): 3117–21. https://faseb.onlinelibrary.wiley.com/doi/epdf/10.1096/fj.09-151381 (August 6, 2020).

Goetz, Sarah C., Karel F. Liem, and Kathryn V. Anderson. 2012. "The Spinocerebellar Ataxia-Associated Gene Tau Tubulin Kinase 2 Controls the Initiation of Ciliogenesis." *Cell* 151(4): 847–58. http://dx.doi.org/10.1016/j.cell.2012.10.010 (April 22, 2021).

Goetz, Sarah C, and Kathryn V Anderson. 2010. "The Primary Cilium: A Signaling Center

During Vertebrate Development." https://www.ncbi.nlm.nih.gov/pmc/articles/PMC3121168/pdf/nihms-302889.pdf (February 11, 2019).

Gonçalves, João, and Laurence Pelletier. 2017. "The Ciliary Transition Zone: Finding the Pieces and Assembling the Gate." *Molecules and Cells* 40(4): 243–53. http://dx.doi.org/10.14348/molcells.2017.0054www.molcells.org (April 11, 2019).

Gossen, Manfred, and Hermann Bujard. 1992. "Tight Control of Gene Expression in Mammalian Cells by Tetracycline-Responsive Promoters." *Proceedings of the National Academy of Sciences of the United States of America* 89(12): 5547–51. /pmc/articles/PMC49329/?report=abstract (December 29, 2020).

Guen, Vincent J et al. 2016. "STAR Syndrome-Associated CDK10/Cyclin M Regulates Actin Network Architecture and Ciliogenesis." *Cell cycle (Georgetown, Tex.)* 15(5): 678–88. http://www.ncbi.nlm.nih.gov/pubmed/27104747 (January 3, 2018).

Guo, Shuang et al. 2018. "Resveratrol Activated Sonic Hedgehog Signaling to Enhance Viability of NIH3T3 Cells <B><I>in Vitro</I></B> via Regulation of Sirt1." *Cellular Physiology and Biochemistry* 50(4): 1346–60. https://www.karger.com/Article/FullText/494593 (June 25, 2020).

Hao, Limin et al. 2011. "Intraflagellar Transport Delivers Tubulin Isotypes to Sensory Cilium Middle and Distal Segments." *Nature cell biology* 13(7): 790–98. http://www.ncbi.nlm.nih.gov/pubmed/21642982 (February 13, 2019).

Hartwell, L H, J Culotti, J R Pringle, and B J Reid. 1974. "Genetic Control of the Cell Division Cycle in Yeast." *Science (New York, N.Y.)* 183(4120): 46–51. http://www.ncbi.nlm.nih.gov/pubmed/4587263 (January 4, 2018).

Haycraft, Courtney J et al. 2005. "Gli2 and Gli3 Localize to Cilia and Require the Intraflagellar Transport Protein Polaris for Processing and Function." www.plosgenetics.org (January 28, 2019).

He, Kai et al. 2018. "Axoneme Polyglutamylation Regulated by Joubert Syndrome Protein ARL13B Controls Ciliary Targeting of Signaling Molecules." *Nature Communications* 9(1): 3310. http://www.nature.com/articles/s41467-018-05867-1 (September 26, 2018).

He, Kai, Kun Ling, and Jinghua Hu. 2020. "The Emerging Role of Tubulin Posttranslational Modifications in Cilia and Ciliopathies." *Biophysics Reports* 6(4): 89–104. https://doi.org/10.1007/s41048-020-00111-0 (October 5, 2020).

He, Mu et al. 2014. "The Kinesin-4 Protein Kif7 Regulates Mammalian Hedgehog Signalling by Organizing the Cilium Tip Compartment." *Nature Cell Biology* 16(7): 663–72.

Ho, Joanna et al. 2014. “Downregulation of the Gli Transcription Factors Regulator Kif7 Facilitates Cell Survival and Migration of Choriocarcinoma Cells” ed. Kelvin Yuen Kwong Chan. *PLoS ONE* 9(9): e108248. https://dx.plos.org/10.1371/journal.pone.0108248 (April 8, 2021).

Hu, Qicong et al. 2010. “A Septin Diffusion Barrier at the Base Membrane Protein Distribution.” *Science* 329(2010): 436–39.

Huang, Ning et al. 2017. “Hierarchical Assembly of Centriole Subdistal Appendages via Centrosome Binding Proteins CCDC120 and CCDC68.” *Nature Communications* 8(1): 1–14. www.nature.com/naturecommunications (September 17, 2020).

Huet, Diego, Thierry Blisnick, Sylvie Perrot, and Philippe Bastin. 2014. “The GTPase IFT27 Is Involved in Both Anterograde and Retrograde Intraflagellar Transport.” *eLife* 2014(3). /pmc/articles/PMC4003483/?report=abstract (January 18, 2021).

Imanishi, Miki, Nicholas F. Endres, Arne Gennerich, and Ronald D. Vale. 2006. “Autoinhibition Regulates the Motility of the C. Elegans Intraflagellar Transport Motor OSM-3.” *Journal of Cell Biology* 174(7): 931–37. /pmc/articles/PMC2064385/?report=abstract (January 18, 2021).

Inaba, Hironori et al. 2016. “Ndel1 Suppresses Ciliogenesis in Proliferating Cells by Regulating the Trichoplein-Aurora A Pathway.” *Journal of Cell Biology* 212(4): 409–23. https://pubmed.ncbi.nlm.nih.gov/26880200/ (March 30, 2021).

Insinna, Christine et al. 2008. “The Homodimeric Kinesin, Kif17, Is Essential for Vertebrate Photoreceptor Sensory Outer Segment Development.” *Developmental Biology* 316(1): 160–70. https://pubmed.ncbi.nlm.nih.gov/18304522/ (July 27, 2020).

Ishikawa, Hiroaki, and Wallace F. Marshall. 2011. “Ciliogenesis: Building the Cell’s Antenna.” *Nature Reviews Molecular Cell Biology* 12(4): 222–34. http://www.nature.com/articles/nrm3085 (November 12, 2018).

Jackson, Aimee L. et al. 2003. “Expression Profiling Reveals Off-Target Gene Regulation by RNAi.” *Nature Biotechnology* 21(6): 635–37. http://www.nature.com/naturebiotechnology (December 29, 2020).

Jinek, Martin et al. 2012. “A Programmable Dual-RNA-Guided DNA Endonuclease in Adaptive Bacterial Immunity.” *Science* 337(6096): 816–21. http://science.sciencemag.org/ (December 29, 2020).

Johnson, K A. 1998. “The Axonemal Microtubules of the Chlamydomonas Flagellum Differ in Tubulin Isoform Content.” *Journal of cell science*.

Kiesel, Petra et al. 2020. “The Molecular Structure of Mammalian Primary Cilia Revealed by

Cryo-Electron Tomography." *Nature Structural and Molecular Biology* 27(12): 1115–24.

Kilander, Michaela B.C. et al. 2018. "A Rare Human CEP290 Variant Disrupts the Molecular Integrity of the Primary Cilium and Impairs Sonic Hedgehog Machinery." *Scientific Reports* 8(1): 17335. www.nature.com/scientificreports (March 8, 2021).

Kim, Joon et al. 2010. "Functional Genomic Screen for Modulators of Ciliogenesis and Cilium Length." *Nature* 464(7291): 1048–51. http://www.nature.com/doifinder/10.1038/nature08895 (January 8, 2018).

Kim, Miju et al. 2014. "The MST1/2-SAV1 Complex of the Hippo Pathway Promotes Ciliogenesis." *Nature Communications* 5(1): 5370. http://www.nature.com/articles/ncomms6370 (September 17, 2018).

Kim, Sehyun et al. 2015. "Nek2 Activation of Kif24 Ensures Cilium Disassembly during the Cell Cycle." *Nature Communications* 6(1): 1–13. www.nature.com/naturecommunications (March 30, 2021).

Kim, Sehyun, and Brian David Dynlacht. 2013. "Assembling a Primary Cilium." *Current Opinion in Cell Biology* 25(4): 506–11.

Kim, Yeon-Joo et al. 2018. "WDR11-mediated Hedgehog Signalling Defects Underlie a New Ciliopathy Related to Kallmann Syndrome." *EMBO reports* 19(2): 269–89.

Kinoshita, M. 2003. "Assembly of Mammalian Septins." *Journal of Biochemistry* 134(4): 491–96. https://academic.oup.com/jb/article-lookup/doi/10.1093/jb/mvg182 (January 4, 2018).

Kramer, James M, Donald G Moerman, and P N Inglis. 2007. "The Sensory Cilia of Caenorhabditis Elegans." http://www.wormbook.org. (November 15, 2018).

Krauss, S., J. P. Concordet, and P. W. Ingham. 1993. "A Functionally Conserved Homolog of the Drosophila Segment Polarity Gene Hh Is Expressed in Tissues with Polarizing Activity in Zebrafish Embryos." *Cell* 75(7): 1431–44.

Kremer, Brandon E., Timothy Haystead, and Ian G. Macara. 2005. "Mammalian Septins Regulate Microtubule Stability through Interaction with the Microtubule-Binding Protein MAP4." *Molecular Biology of the Cell* 16(10): 4648–59. /pmc/articles/PMC1237071/ (April 20, 2021).

Kurtulmus, Bahtiyar et al. 2018. "LRRC45 Contributes to Early Steps of Axoneme Extension." *Journal of Cell Science* 131(18). https://jcs.biologists.org/content/131/18/jcs223594 (September 16, 2020).

Lechtreck, Karl Ferdinand, and Stefan Geimer. 2000. "Distribution of Polyglutamylated

Tubulin in the Flagellar Apparatus of Green Flagellates." *Cell Motility and the Cytoskeleton* 47(3): 219–35. https://onlinelibrary.wiley.com/doi/epdf/10.1002/1097-0169%28200011%2947%3A3%3C219%3A%3AAID-CM5%3E3.0.CO%3B2-Q (July 7, 2020).

Lee, Jeongmi, Yun Doo Chung, and Yun Doo Chung. 2015. "Ciliary Subcompartments: How Are They Established and What Are Their Functions?" *BMB Rep* 48(7): 380–87. www.bmbreports.orghttp://dx.doi.org/10.5483/BMBRep.2015.48.7.084 (January 31, 2019).

Lewis, Tylor R. et al. 2017. "Cos2/Kif7 and Osm-3/Kif17 Regulate Onset of Outer Segment Development in Zebrafish Photoreceptors through Distinct Mechanisms." *Developmental Biology* 425(2): 176–90.

Li, Zhu Juan et al. 2012. "Kif7 Regulates Gli2 through Sufu-Dependent and -Independent Functions during Skin Development and Tumorigenesis." *Development (Cambridge)* 139(22): 4152–61. https://dev.biologists.org/content/139/22/4152 (July 31, 2020).

Liem, Karel F, Mu He, Jymmiel R Ocbina, and Kathryn V Anderson. 2009. *Mouse Kif7/Costal2 Is a Cilia-Associated Protein That Regulates Sonic Hedgehog Signaling*. www.pnas.org/cgi/content/full/ (June 29, 2020).

Lu, Quanlong et al. 2015. "Early Steps in Primary Cilium Assembly Require EHD1/EHD3-Dependent Ciliary Vesicle Formation." *Nature Cell Biology* 17(3): 228–40. https://www.nature.com/articles/ncb3109 (March 30, 2021).

Marshall, W F, and J L Rosenbaum. 2001. "Intraflagellar Transport Balances Continuous Turnover of Outer Doublet Microtubules: Implications for Flagellar Length Control." *The Journal of cell biology* 155(3): 405–14. http://www.ncbi.nlm.nih.gov/pubmed/11684707 (November 14, 2018).

May-Simera, Helen Louise et al. 2018. "Primary Cilium-Mediated Retinal Pigment Epithelium Maturation Is Disrupted in Ciliopathy Patient Cells." *Cell Reports* 22(1): 189–205. https://doi.org/10.1016/j.celrep.2017.12.038 (March 30, 2021).

Miyamoto, Tatsuo et al. 2015. "The Microtubule-Depolymerizing Activity of a Mitotic Kinesin Protein KIF2A Drives Primary Cilia Disassembly Coupled with Cell Proliferation." *Cell Reports* 10(5): 664–73. https://pubmed.ncbi.nlm.nih.gov/25660017/ (March 30, 2021).

Miyoshi, Ko et al. 2014. "Lack of Dopaminergic Inputs Elongates the Primary Cilia of Striatal Neurons" ed. David I. Finkelstein. *PLoS ONE* 9(5): e97918. https://dx.plos.org/10.1371/journal.pone.0097918 (January 6, 2020).

Mollet, Géraldine et al. 2005. “Characterization of the Nephrocystin/Nephrocystin-4 Complex and Subcellular Localization of Nephrocystin-4 to Primary Cilia and Centrosomes.” *Human Molecular Genetics* 14(5): 645–56. https://pubmed.ncbi.nlm.nih.gov/15661758/ (January 15, 2021).

Mönnich, Maren et al. 2018. “CEP128 Localizes to the Subdistal Appendages of the Mother Centriole and Regulates TGF-β/BMP Signaling at the Primary Cilium.” *Cell reports* 22(10): 2584–92. http://www.ncbi.nlm.nih.gov/pubmed/29514088 (March 28, 2018).

Mukhopadhyay, Saikat et al. 2010. “TULP3 Bridges the IFT-A Complex and Membrane Phosphoinositides to Promote Trafficking of G Protein-Coupled Receptors into Primary Cilia.” *Genes and Development* 24(19): 2180–93. https://pubmed.ncbi.nlm.nih.gov/20889716/ (January 18, 2021).

Mukhopadhyay, Saikat, Yun Lu, Shai Shaham, and Piali Sengupta. 2008. “Sensory Signaling-Dependent Remodeling of Olfactory Cilia Architecture in C. Elegans.” *Developmental Cell* 14(5): 762–74. https://pubmed.ncbi.nlm.nih.gov/18477458/ (February 25, 2021).

Nachury, Maxence V. 2014. “How Do Cilia Organize Signalling Cascades?” *Philosophical Transactions of the Royal Society B: Biological Sciences* 369(1650): 20130465–20130465. http://rstb.royalsocietypublishing.org/cgi/doi/10.1098/rstb.2013.0465 (November 15, 2018).

Nager, Andrew R. et al. 2017. “An Actin Network Dispatches Ciliary GPCRs into Extracellular Vesicles to Modulate Signaling.” *Cell* 168(1–2): 252-263.e14.

Neubauer, Katharina, and Barbara Zieger. 2017. “The Mammalian Septin Interactome.” *Frontiers in Cell and Developmental Biology* 5(February): 1–9. http://journal.frontiersin.org/article/10.3389/fcell.2017.00003/full.

Oh, Edwin C., and Nicholas Katsanis. 2013. “Context-Dependent Regulation of Wnt Signaling through the Primary Cilium.” *Journal of the American Society of Nephrology* 24(1): 10–18. www.jasn.org (March 30, 2021).

Orbach, Ron, and Jonathon Howard. 2019. “The Dynamic and Structural Properties of Axonemal Tubulins Support the High Length Stability of Cilia.” *Nature Communications* 10(1). /pmc/articles/PMC6479064/?report=abstract (October 5, 2020).

Overgaard, Christian E et al. 2009. “Deciliation Is Associated with Dramatic Remodeling of Epithelial Cell Junctions and Surface Domains.” *Molecular biology of the cell* 20(1): 102–13. http://www.ncbi.nlm.nih.gov/pubmed/19005211 (March 16, 2018).

Pal, Kasturi et al. 2016. “Smoothened Determines β-Arrestin–Mediated Removal of the G Protein–Coupled Receptor Gpr161 from the Primary Cilium.” *The Journal of Cell*

Biology 212(7): 861–75. http://www.ncbi.nlm.nih.gov/pubmed/27002170 (January 15, 2018).

Palander, Oliva, Maha El-Zeiry, and William S. Trimble. 2017. "Uncovering the Roles of Septins in Cilia." *Frontiers in Cell and Developmental Biology* 5(April): 1–7. http://journal.frontiersin.org/article/10.3389/fcell.2017.00036/full.

Pan, Xiaoyu et al. 2006. "Mechanism of Transport of IFT Particles in C. Elegans Cilia by the Concerted Action of Kinesin-II and OSM-3 Motors." *Journal of Cell Biology* 174(7): 1035–45. /pmc/articles/PMC2064394/?report=abstract (January 18, 2021).

Pathi, Suji et al. 2001. "Comparative Biological Responses to Human Sonic, Indian, and Desert Hedgehog." *Mechanisms of Development* 106(1–2): 107–17.

Pedersen, Lotte B., and Anna Akhmanova. 2014. "Kif7 Keeps Cilia Tips in Shape." *Nature Cell Biology* 16(7): 623–25.

Pedersen, Lotte B., Johanne B. Mogensen, and Søren T. Christensen. 2016. "Endocytic Control of Cellular Signaling at the Primary Cilium." *Trends in Biochemical Sciences* 41(9): 784–97.

Pfister, K. Kevin et al. 2006. "Genetic Analysis of the Cytoplasmic Dynein Subunit Families." *PLoS Genetics* 2(1): e1. https://dx.plos.org/10.1371/journal.pgen.0020001 (January 18, 2021).

Phua, Siew Cheng et al. 2017. "Dynamic Remodeling of Membrane Composition Drives Cell Cycle through Primary Cilia Excision." *Cell* 168(1–2): 264-279.e15. http://dx.doi.org/10.1016/j.cell.2016.12.032 (September 14, 2018).

Plotnikova, Olga V. et al. 2012. "Calmodulin Activation of Aurora-A Kinase (AURKA) Is Required during Ciliary Disassembly and in Mitosis." *Molecular Biology of the Cell* 23(14): 2658–70. https://pubmed.ncbi.nlm.nih.gov/22621899/ (March 30, 2021).

Prasai, Avishek et al. 2020. "The BBSome Assembly Is Spatially Controlled by BBS1 and BBS4 in Human Cells." *bioRxiv*: 2020.03.20.000091. https://doi.org/10.1101/2020.03.20.000091 (January 18, 2021).

Prevo, Bram et al. 2015. "Functional Differentiation of Cooperating Kinesin-2 Motors Orchestrates Cargo Import and Transport in C. Elegans Cilia." *Nature Cell Biology* 17(12): 1536–45. https://pubmed.ncbi.nlm.nih.gov/26523365/ (January 18, 2021).

Prevo, Bram, Jonathan M. Scholey, and Erwin J. G. Peterman. 2017. "Intraflagellar Transport: Mechanisms of Motor Action, Cooperation and Cargo Delivery." *The FEBS journal* 284(18): 2905–31. http://doi.wiley.com/10.1111/febs.14068 (February 13, 2019).

Pugacheva, Elena N. et al. 2007. "HEF1-Dependent Aurora A Activation Induces

Disassembly of the Primary Cilium." *Cell* 129(7): 1351–63. /pmc/articles/PMC2504417/?report=abstract (August 9, 2018).

Qiu, Ni et al. 2012. "Disruption of Kif3a in Osteoblasts Results in Defective Bone Formation and Osteopenia." *Journal of Cell Science* 125(8): 1945–57.

Rachel, RA et al. 2012. "CEP290 Is Required for Photoreceptor Ciliogenesis and Other Cilia Related Functions." *Cilia* 1(S1): P98. https://www.ncbi.nlm.nih.gov/pmc/articles/PMC3555976/ (January 18, 2021).

Ramsbottom, Simon A. et al. 2018. "Targeted Exon Skipping of a CEP290 Mutation Rescues Joubert Syndrome Phenotypes in Vitro and in a Murine Model." *Proceedings of the National Academy of Sciences* 115(49): 12489–94. https://www.pnas.org/content/115/49/12489 (July 12, 2019).

Reiter, Jeremy F., Oliver E. Blacque, and Michel R. Leroux. 2012. 13 EMBO Reports *The Base of the Cilium: Roles for Transition Fibres and the Transition Zone in Ciliary Formation, Maintenance and Compartmentalization*. EMBO Rep. https://pubmed.ncbi.nlm.nih.gov/22653444/ (January 15, 2021).

Rohatgi, Rajat, Ljiljana Milenkovic, and Matthew P. Scott. 2007. "Patched1 Regulates Hedgehog Signaling at the Primary Cilium." *Science* 317(5836): 372–76. https://pubmed.ncbi.nlm.nih.gov/17641202/ (April 22, 2021).

Rupik, Weronika. 2013. "Ultrastructural Studies of Cilia Formation during Thyroid Gland Differentiation in Grass Snake Embryos." *Micron* 44(1): 228–37.

Sánchez, Irma, and Brian David Dynlacht. 2016. "Cilium Assembly and Disassembly." *Nature Cell Biology* 18(7): 711–17. http://www.nature.com/articles/ncb3370 (November 3, 2018).

Sandrock, Kirstin et al. 2011. "Characterization of Human Septin Interactions." *Biological Chemistry* 392(8–9): 751–61. https://www.degruyter.com/view/j/bchm.2011.392.issue-8-9/bc.2011.081/bc.2011.081.xml (January 4, 2018).

Sang, Liyun et al. 2011. "Mapping the NPHP-JBTS-MKS Protein Network Reveals Ciliopathy Disease Genes and Pathways." *Cell* 145(4): 513–28. https://pubmed.ncbi.nlm.nih.gov/21565611/ (January 15, 2021).

Satir, P., L. B. Pedersen, and S. T. Christensen. 2010. "The Primary Cilium at a Glance." *Journal of Cell Science* 123(4): 499–503. http://jcs.biologists.org/cgi/doi/10.1242/jcs.050377.

Satir, Peter. 2017. "CILIA: Before and After." *Cilia* 6(1): 1–11.

Satir, Peter, and Søren Tvorup Christensen. 2007. "Overview of Structure and Function of

Mammalian Cilia." *Annual Review of Physiology* 69: 377–400. http://physiol.annualreviews.org (January 15, 2021).

Saudou, Frédéric. 2012. "A 'so Cilia' Network: Cilia Proteins Start 'Social' Networking." *Journal of Clinical Investigation* 122(4): 1198–1202.

Sayer, John A et al. 2006. "The Centrosomal Protein Nephrocystin-6 Is Mutated in Joubert Syndrome and Activates Transcription Factor ATF4." *Nature Genetics* 38(6): 674–81. http://www.nature.com/articles/ng1786 (July 11, 2019).

Schou, Kenneth Bødtker, Lotte Bang Pedersen, & Søren, and Tvorup Christensen. 2015. "Ins and Outs of GPCR Signaling in Primary Cilia." *EMBO reports*. http://embor.embopress.org/content/embor/early/2015/08/21/embr.201540530.full.pdf (July 6, 2018).

Schwarz, Nele et al. 2017. "Arl3 and RP2 Regulate the Trafficking of Ciliary Tip Kinesins." *Human Molecular Genetics* 26(13): 2480–92. https://www.ncbi.nlm.nih.gov/pmc/articles/PMC5808637/pdf/ddx143.pdf (February 13, 2019).

Sellin, Mikael E, Linda Sandblad, Sonja Stenmark, and Martin Gullberg. 2011. "Deciphering the Rules Governing Assembly Order of Mammalian Septin Complexes." http://www.molbiolcell.org/cgi/doi/10.1091/mbc.E11-03 (September 27, 2018).

Sharma, Neeraj et al. 2011. "Soluble Levels of Cytosolic Tubulin Regulate Ciliary Length Control." http://www.molbiolcell.org/cgi/ (November 15, 2018).

Shi, X., X. Zhan, and J. Wu. 2015. "A Positive Feedback Loop between Gli1 and Tyrosine Kinase Hck Amplifies Shh Signaling Activities in Medulloblastoma." *Oncogenesis* 4(11).

Shi, Xiaoyu et al. 2017. "Super-Resolution Microscopy Reveals That Disruption of Ciliary Transition-Zone Architecture Causes Joubert Syndrome." *Nature Cell Biology* 19(10): 1178–88. http://www.nature.com/doifinder/10.1038/ncb3599 (March 13, 2018).

Shida, Toshinobu et al. 2010. "The Major α-Tubulin K40 Acetyltransferase ATAT1 Promotes Rapid Ciliogenesis and Efficient Mechanosensation." *Proceedings of the National Academy of Sciences of the United States of America* 107(50): 21517–22. www.pnas.org/cgi/doi/10.1073/pnas.1013728107 (October 13, 2020).

Shimada, Hiroko et al. 2017. "In Vitro Modeling Using Ciliopathy-Patient-Derived Cells Reveals Distinct Cilia Dysfunctions Caused by CEP290 Mutations." *Cell Reports* 20(2): 384–96. https://www.sciencedirect.com/science/article/pii/S2211124717308598 (July 12, 2019).

Simons, Matias et al. 2005. “Inversin, the Gene Product Mutated in Nephronophthisis Type II, Functions as a Molecular Switch between Wnt Signaling Pathways.” *Nature Genetics* 37(5): 537–43. http://www.nature.com/naturegenetics (January 14, 2021).

Slaats, Gisela G et al. 2016. “MKS1 Regulates Ciliary INPP5E Levels in Joubert Syndrome.” *Journal of medical genetics* 53(1): 62–72. http://www.ncbi.nlm.nih.gov/pubmed/26490104 (July 12, 2019).

Smith, Ursula M. et al. 2006. “The Transmembrane Protein Meckelin (MKS3) Is Mutated in Meckel-Gruber Syndrome and the Wpk Rat.” *Nature Genetics* 38(2): 191–96.

Snow, Joshua J., Guangshuo Ou, Amy L. Gunnarson, M. Regina S. Walker, et al. 2004. “Two Anterograde Intraflagellar Transport Motors Cooperate to Build Sensory Cilia on C. Elegans Neurons.” *Nature Cell Biology* 6(11): 1109–13. https://www.nature.com/articles/ncb1186.pdf (February 13, 2019).

Snow, Joshua J, Guangshuo Ou, Amy L Gunnarson, Maria Regina, et al. 2004. *Two Anterograde Intraflagellar Transport Motors Cooperate to Build Distinct Parts of Sensory Cilia on Caenorhabditis Elegans Neurons*. https://cloudfront.escholarship.org/dist/prd/content/qt6737m19b/qt6737m19b.pdf?t=lnqgql (February 13, 2019).

Srivastava, Shalabh et al. 2017. “A Human Patient-Derived Cellular Model of Joubert Syndrome Reveals Ciliary Defects Which Can Be Rescued with Targeted Therapies.” *Human Molecular Genetics* 26(23): 4657–67. https://pdfs.semanticscholar.org/e2d8/fabdda29b783e0aa8dd656a6c4d4bd43630a.pdf (July 11, 2019).

Sugiyama, Noriyuki, Tadasuke Tsukiyama, Terry P. Yamaguchi, and Takahiko Yokoyama. 2011. “The Canonical Wnt Signaling Pathway Is Not Involved in Renal Cyst Development in the Kidneys of Inv Mutant Mice.” *Kidney International* 79(9): 957–65.

Sugiyama, Shinju, and Motomasa Tanaka. 2019. “Distinct Segregation Patterns of Yeast Cell-Peripheral Proteins Uncovered by a Method for Protein Segregatome Analysis.” *Proceedings of the National Academy of Sciences of the United States of America* 116(18): 8909–18.

Sun, Shufeng et al. 2019. “Three-Dimensional Architecture of Epithelial Primary Cilia.” *Proceedings of the National Academy of Sciences of the United States of America* 116(19): 9370–79.

Takao, Daisuke, and Kristen J. Verhey. 2016. “Gated Entry into the Ciliary Compartment.” *Cellular and Molecular Life Sciences* 73(1): 119–27.

Tammachote, Rachaneekorn et al. 2009. “Ciliary and Centrosomal Defects Associated with Mutation and Depletion of the Meckel Syndrome Genes MKS1 and MKS3.” *Human Molecular Genetics* 18(17): 3311–23. https://academic.oup.com/hmg/article-lookup/doi/10.1093/hmg/ddp272 (July 12, 2019).

Tanos, Barbara E. et al. 2013. “Centriole Distal Appendages Promote Membrane Docking, Leading to Cilia Initiation.” *Genes and Development* 27(2): 163–68. http://www.genesdev.org/cgi/doi/10.1101/gad.207043.112. (September 17, 2020).

Taschner, Michael, and Esben Lorentzen. 2016. “The Intraflagellar Transport Machinery.” *Cold Spring Harbor Perspectives in Biology* 8(10). /pmc/articles/PMC5046692/?report=abstract (January 18, 2021).

Tateishi, Kazuhiro et al. 2013. “Two Appendages Homologous between Basal Bodies and Centrioles Are Formed Using Distinct Odf2 Domains.” *Journal of Cell Biology* 203(3): 417–25. https://pubmed.ncbi.nlm.nih.gov/24189274/ (September 17, 2020).

Taylor, S. Paige et al. 2015. “Mutations in DYNC2LI1 Disrupt Cilia Function and Cause Short Rib Polydactyly Syndrome.” *Nature Communications* 6(1): 7092. http://www.nature.com/articles/ncomms8092 (February 13, 2019).

Tö, Janos et al. 2015. “TGF-β Signaling Regulates the Differentiation of Motile Cilia.” *CellReports* 11: 1000–1007. http://dx.doi.org/10.1016/j.celrep.2015.04.025http://dx.doi.org/10.1016/j.celrep.2015.04.025ThisisanopenaccessarticleundertheCCBYlicense (July 6, 2018).

Toropova, Katerina et al. 2019. “Structure of the Dynein-2 Complex and Its Assembly with Intraflagellar Transport Trains.” *Nature Structural and Molecular Biology* 26(9): 823–29. https://doi.org/10.1038/s41594-019-0286-y (January 18, 2021).

Valadares, Napoleão Fonseca, Humberto d’Muniz Pereira, Ana Paula Ulian Araujo, and Richard Charles Garratt. 2017. “Septin Structure and Filament Assembly.” *Biophysical reviews* 9(5): 481–500. http://www.ncbi.nlm.nih.gov/pubmed/28905266 (January 10, 2018).

Vuolo, Laura et al. 2020. “Cytoplasmic Dynein-2 at a Glance.” *Journal of cell science* 133(6). https://jcs.biologists.org/content/133/6/jcs240614 (January 18, 2021).

Wang, Guang et al. 2019. “Rab7 Regulates Primary Cilia Disassembly through Cilia Excision.” *Journal of Cell Biology* 218(12): 4030–41. https://pubmed.ncbi.nlm.nih.gov/31619485/ (December 29, 2020).

Wann, A. K.T., and M. M. Knight. 2012. “Primary Cilia Elongation in Response to Interleukin-1 Mediates the Inflammatory Response.” *Cellular and Molecular Life*

Sciences 69(17): 2967–77.

Wei, Yongbao et al. 2014. “MiR-223-3p Targeting SEPT6 Promotes the Biological Behavior of Prostate Cancer.” *Scientific Reports* 4: 1–8.

Westlake, Christopher J. et al. 2011. “Primary Cilia Membrane Assembly Is Initiated by Rab11 and Transport Protein Particle II (TRAPPII) Complex-Dependent Trafficking of Rabin8 to the Centrosome.” *Proceedings of the National Academy of Sciences of the United States of America* 108(7): 2759–64. www.pnas.org/cgi/doi/10.1073/pnas.1018823108 (March 30, 2021).

Wheway, Gabrielle, Liliya Nazlamova, and John T. Hancock. 2018. “Signaling through the Primary Cilium.” *Frontiers in Cell and Developmental Biology* 6: 8. http://journal.frontiersin.org/article/10.3389/fcell.2018.00008/full (January 16, 2019).

Williams, Corey L. et al. 2014. “Direct Evidence for BBSome-Associated Intraflagellar Transport Reveals Distinct Properties of Native Mammalian Cilia.” *Nature Communications* 5(1): 1–13. www.nature.com/naturecommunications (February 26, 2021).

Wingfield, Jenna L. et al. 2017. “IFT Trains in Different Stages of Assembly Queue at the Ciliary Base for Consecutive Release into the Cilium.” *eLife* 6.

Wloga, Dorota, Ewa Joachimiak, Panagiota Louka, and Jacek Gaertig. 2017. “Posttranslational Modifications of Tubulin and Cilia.” *Cold Spring Harbor Perspectives in Biology* 9(6). http://cshperspectives.cshlp.org/ (November 28, 2019).

Wood, J A et al. 1980. “Mutations Affecting Segment Number and Polarity in Drosophila.” *Geochim. cosmochim. Acta (in the press); Meteoritics* 287(2): 787–90.

Wu, Chien-Ting, Hsin-Yi Chen, and Tang K. Tang. 2018. “Myosin-Va Is Required for Preciliary Vesicle Transportation to the Mother Centriole during Ciliogenesis.” *Nature Cell Biology*: 1. http://www.nature.com/articles/s41556-017-0018-7 (January 23, 2018).

Xu, Qian et al. 2019. “Type I Collagen-Induced YAP Nuclear Expression Promotes Primary Cilia Growth and Contributes to Cell Migration in Confluent Mouse Embryo Fibroblast 3T3-L1 Cells.” *Molecular and Cellular Biochemistry* 450: 87–96. https://doi.org/10.1007/s11010-018-3375-z (February 20, 2019).

Young, R. W. 1967. “The Renewal of Photoreceptor Cell Outer Segments.” *The Journal of cell biology* 33(1): 61–72. /pmc/articles/PMC2107286/?report=abstract (February 26, 2021).

Zhou, Xia et al. 2014. “SIRT2 Regulates Ciliogenesis and Contributes to Abnormal Centrosome Amplification Caused by Loss of Polycystin-1.” *Human Molecular Genetics*

23(6): 1644–55. https://academic.oup.com/hmg/article/23/6/1644/736677 (October 13, 2020).

7. List of Abbreviations

ARL13B	ADP-ribosylation factor-like protein 13B
BBS	Bardel Biedl syndrome
BBSome	Bardet–Biedl syndrome complex
Blast	Blasticidin S
CCDC120	Coiled-coil domain-containing protein 120
CCDC68	Coiled-coil domain-containing protein 68
cDNA	complementary DNA
CEP123	Centrosomal protein of 123 kDa
CEP164	Centrosomal protein of 164 kDa
CEP170	Centrosomal protein of 170 kDa
CEP290	Centrosomal protein of 290 kDa
CEP83	Centrosomal protein of 83 kDa
CEP89	Centrosomal protein of 89 kDa
CP110	Centriolar coiled-coil protein of 110 kDa
DAPI	4',6-diamidino-2-phenylindole
DMSO	Dimethyl sulfoxide
DNA	Deoxyribonucleic acid
DYNC2	Cytoplasmic dynein 2
EFHC1	EF-hand domain-containing protein 1
EGFP	Enhanced Green Fluorescent Protein
EHD1	Eps15 homology domain 1
FBF1	Fas-binding factor 1
G0	Exit of G1
G1	First gap phase

G2	Second gap phase
GFP	Green Fluorescent Protein
Gli	Zinc finger protein
HEF1	Enhancer of filamentation 1
HEK293	Human embryonic kidney cells 293
INPP5E	Phosphatidylinositol polyphosphate 5-phosphatase type IV
KIF17	Kinesin-like protein KIF17
KIF24	Kinesin-like protein KIF24
KIF2a	Kinesin-like protein KIF2a
KIF3A	Kinesin-like protein KIF3A
KIF7	Kinesin-like protein KIF7
LRRC45	Leucine rich repeat containing protein 45
MAP4	Microtubule-associated protein 4
MKS	Meckel syndrome
MKS1	Meckel syndrome 1
MKS3	Meckel syndrome 3
mTOR	Serine/threonine-protein kinase mTOR
NEK2	Never in mitosis A-related kinase 2
ng	Nanogram
nM	Nanomolar
NPHP	Nephronophthisis
NPHP1	Nephronophthisis-1
ODF2	Outer dense fibre protein 2
PBS	Phosphate-buffered saline
PCNT	Pericentrin

PIPKI	Phosphatidylinositol 4-phosphate 5-kinase type-1 gamma
PLK1	Polo-like kinase 1
pM	Picomolar
Rab11	Ras-related protein Rab-11A
Rabin8	Rab-3A-interacting protein
RNA	Ribonucleic acid
S	Synthesis
SCLT1	Sodium channel and clathrin linker 1
SDS-page	sodium dodecyl sulphate–polyacrylamide gel electrophoresis
siRNA	Small interfering RNA
SSTR3	Somatostatin receptor type 3
Sufu	Suppressor of fused homolog
TCHP	Trichoplein keratin filament-binding protein
TGF	TGF-beta receptor
TMEM67	Transmembrane protein 67
Tre3G	Tetracycline repressor controlled promoter
TTBK2	Tau-tubulin kinase 2
WDR11	WD repeat-containing protein 11
µg	Microgram
µM	Micromolar

Acknowledgement

I would like to thank my supervisor, Dr Gislene Pereira, for giving me the chance to concentrate on my doctoral studies. She provided me a nice research environment and supported me growing up an independent scientist. I have little doubt we have great scientific and social relationships throughout my PhD life.

I am grateful to my TAC members Dr Oliver Fackler and Dr Elmar Schiebel for suggesting me good scientific advice.

I would like to appreciate all of the members of Pereira's group for your friendship and kindness. Especially, Dr Bahtiyar Kurtulmus supported me mammalian cell culture experiments and nice suggestion about my PhD project. Dr Rafael Duenas Sanchez gave me good ideas for my study. Astrid Hofmann helped a lot of my German language problems and was the best chatting partner next to my desk. Cheng Yuan discusses well our project each other.

I am glad to thank Dr Annett Neuner from ZMBH for getting ultra-structure primary cilia images by electron microscope, Dr Holger Lorenz from the ZMBH Imaging facility for sharing and helping STED microscopy, Dr Monika Langlotz from the ZMBH FACS facility for cell sorting, Dr Ulrike Engel from Heidelberg University Nikon imaging centre for supporting Live-cell imaging, Dr Kathryn Anderson from Memorial Sloan-Kettering Cancer Center for sharing KIF7 antibody and Dr Tomas Holstein from COS for sharing RT-PCR machine.

I deeply thank Hannah Lee from Heidelberg University for proofreading my thesis.

I strongly appreciate Dr Shoji Hata from Tokyo University for giving me ideas to improve my project.

I would like to thank HBIGS for my financial support and for giving me lots of chance to join academic lectures and social events.

I would like to thank my parents Taro and Shizuka, and my younger sister Hanako for encouraging me from far away from Germany.

I show full of thankfulness for Jin Meuhua (Mika) offering a nice apartment and maintenance of my flat.

I finally thank all my friends in Heidelberg, especially from the Japanese scientist community (Toshiki, Shotaro, Masafusa, Soh, and Yuki).